

https://dspace.org/

The non-explosive mechanisation of the South African gold mine stoping operation

Dunn, Paul Gregory

2015-01-20
http://hdl.handle.net/10539/16622

Downloaded from a DSpace repository. https://dspace.org/

THE NON-EXPLOSIVE MECHANISATION OF THE SOUTH AFRICAN GOLD MINE STOPING OPERATION

Paul Gregory Dunn

A dissertation submitted to the Faculty of Engineering, University of the Witwatersrand, in fulfilment of the requirements for the degree of Master of Science in Engineering

Johannesburg, 1989

I declare that this dissertation is my own, unaided work. It is being submitted for the degree of Master of Science in Engineering at the University of the Witwatersrand, Johannesburg. It has not been submitted before for any degree or examination in any other University.

P.G. DUNN

1st day of AUGUST 1989

I declare that this dissertation is my own, unaided work. It is being submitted for the degree of Master of Science in Engineering at the University of the Witwatersrand, Johannesburg. It has not been submitted before for any degree or examination in any other University.

P.G. DUNN

1st day of AUGUST 1989

SYNOPSIS

The research described in this dissertation is an investigation into the non-explosive mining of hard rock, using a slot-based, mining method. The motivation for undertaking this study has arisen from the need to mechanise and improve the effectiveness and operational efficiency of the South African gold mining industry. This research was undertaken at the Technical and Development Services of the Anglo American Corporation of South Africa.

Slot-based mining consists of cutting slots in the stope face and breaking out the rock between the slots using mechanical methods. Three different slotting mechanisms have been investigated to determine their effectiveness in cutting hard rock: Dry abrasive waterjet cutting, slurry abrasive waterjet cutting and diamond circular saws.

A number of designed factorial experiments have been carried out on surface, using dry abrasive and slurry abrasive waterjet cutting equipment, to determine the relationship between the relevant cutting parameters. Pressure, orifice size, abrasive mass flow ratio and exposure have been identified as having the greatest influence on cutting performance, as measured by depth of cut.

Overall, slurry abrasive waterjet cutting is more than twice as efficient as dry abrasive cutting, in terms of nozzle power and depth of cut achieved.

Diamond circular saws have been empirically tested underground in quartzite, to arrive at approximate cutting costs. The tests to date indicate that the diamond circular sawing of quartzite underground is both practically and economically viable.

As a slotting tool diamond circular saws are far superior to abrasive waterjet cutting, both in terms of cutting rate and costs.

In conjunction with the slotting of hard rock, a breaking device is required to remove the rock between the slots. To date, conventional barring techniques have achieved breaking rates of up to 1 m^3/h, in fractured rock conditions. Further research is required to find a suitable non-explosive breaking device to liberate hard unfractured quartzite.

A computer based evaluation package has been developed to financially evaluate the introduction of non-explosive mining into the conventional mining infrastructure. This package highlights the considerable financial benefits associated with a slot-based mining system. This potential increase in financial return constitutes the main motivation and justification for continuing the development of slot-mining into a production mining system.

ACKNOWLEDGEMENTS

The work described in this thesis forms part of the research and development programme of Technical and Development Services (T&DS), Anglo American Corporation. I would like to thank this organisation for allowing me to submit these studies for this degree.

The author wishes to acknowledge all those persons who have, directly or indirectly, assisted in the preparation of this dissertation.

In particular to my supervisors, Dr O Fenn (Projects Manager, T&DS) and Professor H R Phillips (University of the Witwatersrand) for their guidance and assistance during the preparation of this dissertation.

The invaluable work carried out by the Mining and Boring Research Section of T&DS is much appreciated. Thanks also to the Operations Research Department and to Mrs G Visser for typing the dissertation in its various forms.

Finally, special thanks to my parents for their encouragement and support through the early years and to my wife, Lin for her encouragement and support throughout the course of this study.

CONTENTS **Page**

TITLE PAGE		(i)
DECLARATION		(ii)
SYNOPSIS		(iii)
ACKNOWLEDGMENTS		(v)
CONTENTS		(vi)
LIST OF TABLES		(xi)
LIST OF FIGURES		(xiii)
1.	**INTRODUCTION**	1
1.1	**Mechanised Non-Explosive Stoping**	1
1.2	**The Mining Engineering Challenge**	3
1.3	**Benefits of Mechanised Non-Explosive Mining**	9
1.4	**Disadvantages of Mechanised Non-Explosive Stoping**	11
1.5	**Slotting Systems**	13
1.6	**Breaking System**	17
2.	**PREVIOUS WORK CARRIED OUT INTO NON-EXPLOSIVE MINING**	18
2.1	**Rockbreaking by Cutting**	19
2.1.1	Drag bit rockcutter	19
2.1.2	Radial rock slotter	23
2.1.3	Diamond sawing	25
2.1.4	Abrasive entrained waterjet cutting	29
2.1.5	Laser cutting	34
2.2	**Rockbreaking by Reef Drilling**	35
2.2.1	Reef boring	37
2.2.2	Stope Coring	38

CONTENTS (Continued)

		Page
4.2	Slurry Cutting Work	76
4.3	Diamond Circular Saw Work	77
5.	PROPERTIES OF THE TEST MATERIALS USED	79
5.1	Mineralogy of Norite	80
5.2	Mineralogy of Quartzite	83
6.	RESULTS AND DISCUSSIONS	86
6.1	Dry Abrasive Waterjet Cutting	87
6.1.1	Prediction formula for the depth of cut achieved with a dry abrasive entrained waterjet	87
6.1.2	Determination of Quartzite/ Norite (Q/N) ratio	91
6.1.3	Non linear effect of mass flow ratio (MFR) on cut depth	99
6.1.4	Recycling of iron based abrasives	101
6.2	Slurry Abrasive Waterjet Cutting	106
6.2.1	Slurry-Jet Experiment No.1 - initial investigation	106
6.2.2	Slurry-Jet Experiment No.2 - further investigation	108
6.2.3	Slurry-Jet Experiment No.3 - maximum cut depth achievable	112

CONTENTS **Page**

TITLE PAGE		(i)
DECLARATION		(ii)
SYNOPSIS		(iii)
ACKNOWLEDGMENTS		(v)
CONTENTS		(vi)
LIST OF TABLES		(xi)
LIST OF FIGURES		(xiii)
1.	**INTRODUCTION**	1
1.1	**Mechanised Non-Explosive Stoping**	1
1.2	**The Mining Engineering Challenge**	3
1.3	**Benefits of Mechanised Non-Explosive Mining**	9
1.4	**Disadvantages of Mechanised Non-Explosive Stoping**	11
1.5	**Slotting Systems**	13
1.6	**Breaking System**	17
2.	**PREVIOUS WORK CARRIED OUT INTO NON-EXPLOSIVE MINING**	18
2.1	**Rockbreaking by Cutting**	19
2.1.1	Drag bit rockcutter	19
2.1.2	Radial rock slotter	23
2.1.3	Diamond sawing	25
2.1.4	Abrasive entrained waterjet cutting	29
2.1.5	Laser cutting	34
2.2	**Rockbreaking by Reef Drilling**	35
2.2.1	Reef boring	37
2.2.2	Stope Coring	39

CONTENTS (Continued) Page

2.3	Rockbreaking by Impacting	41
	2.3.1 Swing hammer miner	42
	2.3.2 Impact hammer (ripper)	45
	2.3.3 Impact planer	48
2.4	Rockbreaking by Pressurising a Pre-Drilled Hole	49
3.	EXPERIMENTAL TEST SITE AND EQUIPMENT	60
3.1	Dry Abrasive Waterjet Cutting (up to 240 MPa)	60
3.2	Slurry Abrasive Waterjet Cutting (up to 40 MPa)	62
3.3	Diamond Circular Saw Cutting	63
3.4	Non-Explosive Breaking Equipment	67
3.5	Rig Design	67
4.	EXPERIMENTAL DESIGN AND PROCEDURE	70
4.1	Dry Abrasive Waterjet Cutting Work	70
	4.1.1 Design of the experiment	70
	4.1.2 Use of logarithms on depth of cut	70
	4.1.3 Determination of experimental error	72
	4.1.4 Investigation of the quartzite/norite (Q/N) ratio and low mass flow ratio (MFR)	73
	4.1.5 Recycling of iron based abrasives	75

CONTENTS (Continued) Page

4.2	Slurry Cutting Work	76
4.3	Diamond Circular Saw Work	77
5.	PROPERTIES OF THE TEST MATERIALS USED	79
5.1	Mineralogy of Norite	80
5.2	Mineralogy of Quartzite	83
6.	RESULTS AND DISCUSSIONS	86
6.1	Dry Abrasive Waterjet Cutting	87
6.1.1	Prediction formula for the depth of cut achieved with a dry abrasive entrained waterjet	87
6.1.2	Determination of Quartzite/ Norite (Q/N) ratio	91
6.1.3	Non linear effect of mass flow ratio (MFR) on cut depth	99
6.1.4	Recycling of iron based abrasives	101
6.2	Slurry Abrasive Waterjet Cutting	106
6.2.1	Slurry-Jet Experiment No.1 - initial investigation	106
6.2.2	Slurry-Jet Experiment No.2 - further investigation	108
6.2.3	Slurry-Jet Experiment No.3 - maximum cut depth achievable	112

CONTENTS (Continued) Page

	6.2.4	Slurry-Jet Experiment No.4 - stand-off distance experiment	114
	6.2.5	Slurry-Jet Experiment No.5 - investigation of the effect of angle of attack on depth of cut	116
	6.2.6	Slurry-Jet Experiment No.6 - cutting with quartzite abrasive	118
	6.2.7	Slurry-Jet Experiment No.7 - abrasive recycling and replenishing tests	123
	6.2.8	A depth of cut model for slurry cutting	136
6.3	**Diamond Saw Cutting**		137
	6.3.1	600 mm diameter blade	138
	6.3.2	800 mm diameter blade	140
	6.3.3	Comparison of 600 mm and 800 mm diameter blades	143
6.4	**Development of a Slot-Based Mining Method**		145
7.	**FINANCIAL EVALUATION OF SLOT-BASED NON-EXPLOSIVE MINING SYSTEMS**		150
8.	**CONCLUSIONS AND RECOMMENDATIONS FOR FUTURE RESEARCH**		159
8.1	**Dry Abrasive Waterjet Cutting (up to 240 MPa)**		159

CONTENTS (Continued) Page

8.2 Slurry Abrasive Waterjet Cutting (up to 40 MPa) 161
8.3 Diamond Circular Saw Cutting 163
8.4 Breaking Out of Rock Between the Slots 165
8.5 Computer Evaluations 166
8.6 Recommendations for Future Research 167

REFERENCES 169

APPENDICES 178

Appendix 1 178
Test Results and Experimental Parameters for the Abrasive Waterjet Cutting Testwork

Appendix 2 191
Abrasive Waterjet Cutting Test Sheet

Appendix 3 192
Derivation of a Model for Q/N Ratio (Dry Abrasive Waterjet Cutting)

Appendix 4 197
Statistical Analysis of Slurry Cutting Results

Appendix 5 204
Sieve Analyses for Abrasive Recycling Testwork

Appendix 6 208
A Typical Financial Evaluation of a Slot Based Non-Explosive Mining System

LIST OF TABLES

		Page
4.1	Experimental Variables and Values (dry abrasive cutting investigation)	71
4.2	Experiment Design (dry abrasive cutting investigation)	71
4.3	Analysis of Experiment Variance	72
4.4	Individual Measurements	73
4.5	Mean for a Slot	73
4.6	Experimental Variables and Values (Q/N ratio investigation)	74
4.7	Experimental Variables and Values (recycling of iron based abrasive)	75
5.1	Mineralogical Assemblage of Norite	82
5.2	Variations in the Measured Properties of Norite According to the Direction of Loading to the Foliation	82
5.3	Mineralogical Assemblage of Quartzite (tested on surface)	83
5.4	Mineralogical Assemblage of Quartzite Underground (President Brand 2 Shaft, 60/69 Stope)	85
6.1	Effect of Quartzite Block on Q/N Ratio	91
6.2	Descriptive Terms ("Low", "Middle" and "High")	92
6.3	Properties of Various Iron Based Abrasives	102
6.4	Related Significance of Mean Depth of Cut at the 95% Confidence Level	103
6.5	Experimental Variables and Values (Slurry Jet Experiment No 1)	106
6.6	Experimental Variables and Values (Slurry Jet Experiment No 2)	109

LIST OF TABLES (Continued)

		Page
6.7	Effect of Stand-Off Distance on Cut Depth for Those Pair of Trials Within Slurry-Jet Experiment No 2 for which Measured Values of The Mass Flow Ratio were Comparable	113
6.8	Experimental Variables and Values (slurry cutting using quartzite abrasive)	118
6.9	Comparison of 600 mm and 800 mm Diameter Blades	143
8.1	Typical Operating Parameters of Slotting Tools	160

LIST OF FIGURES

		Page
1.1	Total Labour Productivity in the Gold Mining Industry	4
1.2	Stope Workers per Metre of Stope Face and Stope Labour Productivity on South African Mines	4
1.3	Typical Fracture Zone Around a Stope Face	6
1.4	Qualitative Variation in the Corrosivity of the Underground Environment	6
1.5	Consequences and Benefits of Mechanised Non-Explosive Mining	10
1.6	Configuration of Slots for Cutting and Breaking Method	12
1.7	Configuration of Slots for Block-Cutting Methods	12
1.8	Dry Abrasive and Slurry Abrasive Waterjet Cutting Nozzles	14
1.9	Schematic Illustration of Abrasive Waterjet Cutting Systems	16
2.1	Diagram of a Drag Bit Cutting the Rock Illustrating the Components of the Bit Forces and the Optimum Jet Position	20
2.2	The Drag Bit Rock Cutter	20
2.3	The Boart Radial Rockslotter	24
2.4	Diamond Circular Saw	27
2.5	Diamond Wire Saw	27
2.6	Krasnoff Nozzle Arrangement	33
2.7	The Mining Principle of Boring or Coring Overlapping Holes	36
2.8	Typical Position of Reef Borer	36
2.9	Debex Stopecorer	40

LIST OF FIGURES (Continued) Page

2.10	Laboratory Drop Test Rig Results	40
2.11	The Swing Hammer Miner	42
2.12	The COMRO Impact Ripper	43
2.13	Results Achieved With the Impact Ripper	47
2.14	Longitudinal and Circumferal Notches in a Hole	47
2.15	Flow Industries Flowex Device	53
2.16	CSIR Water Gun (Cannon)	53
2.17	Two Sided Bullwedge Used in Conjunction with Hydraulic Impact Hammers	56
2.18	Setting Behaviour of Expanding Cements	56
2.19	Electron Beam Method of Mining	59
2.20	Dielectric Heating of Rock	59
3.1	General View of Surface Test Site Equipment	61
3.2	Slots Produced by Abrasive Waterjet Cutting	61
3.3	Slurry Abrasive Delivery System	64
3.4	Slurry Nozzle and Traverse Arrangement	64
3.5	Longyear 360 H35 Wall Saw Unit	65
3.6	Rig used to Support Longyear Machine	65
3.7	NPK H60 Hydraulic Impact Hammer	68
3.8	Bullwedging Operations Underground	68

LIST OF FIGURES (Continued) **Page**

5.1	A Photomicrograph of a Thin Section of Norite	81
5.2	Foliation and Weakness Planes of Norite	81
5.3	A Photomicrograph of a Thin Section of Quartzite	84
6.1	The Effect of Water Pressure on Depth of Cut in Norite	88
6.2	The Effect of Orifice Size on Depth of Cut in Norite	88
6.3	The Effect of MFR (Mass Flow Ratio) on Depth of Cut in Norite	88
6.4	The Effect of Exposure Time on Depth of Cut in Norite	89
6.5	The Effect of Water Pressure on Depth of Cut in Quartzite (Low MFR Model)	93
6.6	The Effect of Water Pressure on Depth of Cut in Quartzite (High MFR Model)	93
6.7	The Effect of Orifice Size on Depth of Cut in Quartzite (Low MFR Model)	94
6.8	The Effect of Orifice Size on Depth of Cut in Quartzite (High MFR Model)	94
6.9	The Effect of MFR on Depth of Cut in Quartzite (Low MFR Model)	95
6.10	The Effect of MFR on Depth of Cut in Quartzite (High MFR Model)	95
6.11	The Effect of Exposure Time on Depth of Cut in Quartzite (Low MFR Model)	96
6.12	The Effect of Exposure Time on Depth of Cut in Quartzite (High MFR Model)	96
6.13	Effect of MFR on Depth of Cut in Norite, Expressed as a Percent of the Maximum Depth of Cut Achieved in Norite	100

LIST OF FIGURES (Continued)

		Page
6.14	Effect of Cut Number (number of times abrasive has been re-used) on Depth of Cut in Norite	100
6.15	Photographic Analysis of the Degradation of Chilled Iron Shot	105
6.16	Photographic Analysis of the Degradation of Chilled Iron Grit	105
6.17	Effect of MFR on Depth of Cut in Norite (Second Exposure)	111
6.18	Effect of MFR on Depth of Cut in Norite (First Exposure)	111
6.19	Effect of Pass Number (Exposure) on Depth of Cut in Norite	115
6.20	Effect of Stand-Off Distance on Depth of Cut in Norite	115
6.21	Effect of Angle of Attack on Depth of Cut in Norite	119
6.22	Effect of MFR (Quartzite) on Depth of Cut in Norite	119
6.23	Effect of Cut Number (number of times the abrasive is re-used) on Depth of Cut, using Chromite Abrasive	125
6.24	Effect of Cut Number (number of times the abrasive is re-used) on Depth of Cut, using Quartzite Abrasive	125
6.25	Effect of Cut Number (number of times the abrasive is re-used) on Depth of Cut, using Iron Based Abrasive	128
6.26	E5 Iron Grit before Cutting (magnified 10 times)	128
6.27	E5 Iron Grit after 11 Cuts (magnified 10 times)	128
6.28	Effect of Abrasive Replenishment with Abrasive Recycling on Depth of Cut	134

LIST OF FIGURES (Continued)

		Page
6.29	Depth of Cut Modelled in Terms of Nozzle Power and Abrasive Flowrate	134
6.30	Schematic Illustration of Diamond Circular Saw Cutting Modes	137
6.31	Face Rig Developed Underground for Abrasive Waterjet Cutting	148
6.32	Stope Width Control Achieved using Slot-Based Mining (President Brand 2 Shaft, 60/69 Stope)	148
7.1	Effect of the Slot-Based Mining Methods on % Improvement in NPV Profits	152
7.2	Schematic Illustration of the NPV Evaluation Model, Developed for Slot-Based Mining	153

1.0 INTRODUCTION

One of the greatest engineering challenges facing the South African gold mining industry today, is the development of a *mechanised, non-explosive mining system*. The development of a non-explosive method of breaking the rock in the gold mines would represent a significant advance, given the restricting effects of blasting in terms of both the productivity of the stoping operation and rates of face advance. In this regard, the concept of "slot-mining", which consists of cutting slots in the stope face and breaking out the rock between the slots using mechanical methods, was identified as a method offering much potential.

An integrated non-explosive mining system, based on the slot-mining concept, is under development by Anglo American Corporation's Technical and Development Services (T&DS). Two slot-mining systems, based on a combination of leading edge and proven technology, are being evaluated, utilising abrasive water-jet cutting and diamond circular blade sawing.

This dissertation evaluates the practical advantages of slot-mining to the South African gold mining industry and discusses the results of the laboratory and underground test work carried out to date. It also highlights critical areas requiring further research and development.

1.1 Mechanised Non-Explosive Stoping

The discovery of the Main Reef Group of reefs on the farm Langlaagte in 1886 marked the opening of the richest and most *extensive goldfield in history*. Today, *more than one hundred* years later, as mining has progressed to depths approaching 4 km, South Africa has become the foremost mining country in the world, and gold mining has for many years formed the backbone of the country's economy.

However, the South African gold mining industry is currently in decline. First, the average grade has dropped from 13,5 grams per ton to about 5,16 grams per ton over the period 1970-1985, while the gold mined decreased from 1 000 tons in 1970 to about 606 tons in 1987.

Furthermore, and of equal concern, is the change in working costs. The working costs, expressed in rands per ton yield, have risen over the past 15 years at a rate that is twice the rate of the consumer price index. Examination of the working costs, in terms of cost per kilogram of gold mined, suggests that costs have increased at five times the consumer price index; so there is a very high cost inflation in the industry. The combined effect of decreasing grade and increasing cost is that the role of South Africa as a gold producer is reduced, both in terms of market proportion and in terms of competitiveness. In 1974 South Africa produced nearly 1 000 tons of gold per annum, which amounted to 70,6 per cent of the world's gold production, while in 1987 this dropped to 606 tons of gold or 44,2 per cent of the world's gold production.

As a result of the high cost inflation, South Africa now ranks only fifth among the major gold-producing countries of the world in terms of costs, after having been the lowest-cost producer for years.

To date, the effects of all these aspects were compensated for by the decrease in the value of the rand compared to other currencies, and the industry has been able to continue making an important contribution to the economy of the country. If the cost trend continues and the gold price in dollar terms remains stable, then only a sliding rand can secure the industry. However, the implications of such a development for the general economic development of the country are obvious.

The only way to maintain profits and ensure the long term future of the gold mining industry is through the large-scale application of mechanisation. The coal industry worldwide is a classic example which supports this argument; concerning gold mining, trackless mining is another example.

Stoping has been identified as the most obvious area for improvement by mechanisation. Nearly half of the total underground labour force is employed in stoping; it accounts for approximately 40% of a mine's working costs and the level of mechanisation in stopes is very low, the most significant change taking place more than fifty years ago when face scrapers were introduced to replace lashing, Figure 1.1. Although the tons produced per metre of stope face has increased from 170 t/annum in 1972 to nearly 400 t/annum in 1984, this improvement has been mainly attributable to the increase in the number of stope workers, Figure 1.2.

To maximise the benefit of mechanising the stoping operation, the use of explosives must be eliminated. It has long been recognised that the major drawback of conventional mining is that it imposes a cyclical nature on the mining operation. This restricts both productivity and rates of face advance and does not allow the most economic use of a very costly infrastructure. As a result, an alternative method of breaking the rock is required, if a significant advance is to be made to improve the efficiency of the mining operation.

1.2 The Mining Engineering Challenge

It is pertinent at this stage to reflect on the conditions prevailing in the South African gold mines, so that the mining and engineering challenge facing the industry, regarding the development of a mechanised non-explosive system, can be put into perspective.

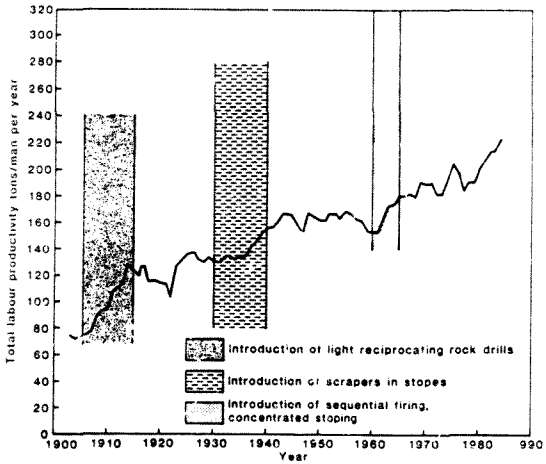


Figure 1.1 : **Total Labour Productivity in the Gold Mining Industry (after Wagner [1])**

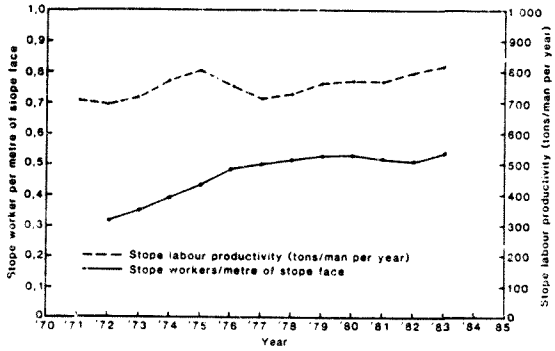


Figure 1.2 : **Stope Workers per Metre of Stope Face and Stope Labour Productivity on South African Mines (after Wagner [1])**

The main gold deposits, generally in the form of narrow tabular reefs that extend over many kilometres on strike and dip, are located along the rim of the elliptical Witwatersrand basin.

The reefs normally dip between 10° and 30° and are mined at depths approaching 4 km where the virgin rock temperature exceeds 60° C.

The tabular nature of the gold-bearing reefs, the irregular distribution of gold in the reefs, and the great depth at which most of the reefs are situated effect mining in many ways. The geometry of the reef bodies and their depth are very unfavorable from the point of view of rock stresses and heat flow. The phenomena resulting from rock stress are the most important in affecting the design of stoping methods and machines. High stresses occur in the rock ahead of the working faces. These cause extensive rock fracturing and results in difficult and hazardous mining conditions and the need for elaborate support measures.

The fractured condition of the face, shown schematically in Figure 1.3, has a major bearing on rockbreaking and rockhandling methods. Many fractures run into the rock above and below the stope, resulting in rough hangingwall and footwall conditions. Often there are parting planes near the reef, which makes control of the stope width difficult and increases the tendency for rockfalls from the hangingwall and the formation of steps in the footwall.

These facts make support of the hangingwall and rockhandling all the more difficult. Effective strata control is an essential prerequisite for successful stope-face mechanisation. Production delays arising from damage to equipment, through rockfalls and rockbursts, assume more serious proportions in highly mechanised stopes than in conventional stopes.

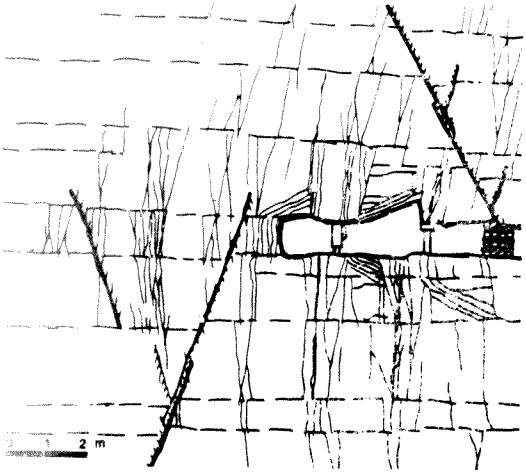


Figure 1.3 : Typical Fracture Zone Around a Stope Face

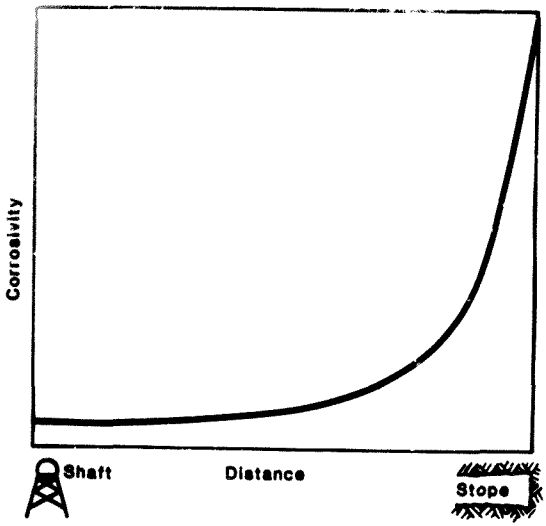


Figure 1.4 : Qualitative Variation in the Corrosivity of the Underground Environment

The tabular shape of the orebody promotes the flow of heat from the rock into workings, thereby creating an unfavorable thermal environment and the need for extensive mine cooling. The cooling of workings is one of the greatest problems in deep mining and new methods which introduce additional heat would aggravate the problem.

The restricted mining height in the stopes, together with the hard and abrasive nature of the rock being mined and the hot and humid environmental conditions that exist in stopes, has militated against large-scale mechanisation of stoping operations. In deep mining, there are many strong reasons for mining at the narrowest stope width feasible, which imposes limitations regarding equipment size. This is exacerbated by the need to provide clearance to ensure that machines operating in stopes do not become trapped as a result of elastic closure of the excavation, which at depth is quite considerable.

Materials used to construct equipment deteriorate in stopes at rates faster than in any other industrial environment. The rock contains a high proportion of quartz which is harder than nearly all the materials used in the construction of machines. Rock fragments of all sizes are present underground. These inevitably come in contact with moving surfaces, causing severe abrasion. The problem is compounded by corrosion.

It is well known that the underground environment is corrosive, but it is not commonly appreciated how much more corrosive it is at a stope face than elsewhere in a gold mine. Figure 1.4 illustrates how the corrosivity of the environment, caused by the accumulation of acids and salts in the mine water, increases toward the stope face. Corrosion products are soft and are removed rapidly by abrasion, thereby exposing fresh surfaces which in turn corrode rapidly. The common corrosion resistant materials are not abrasion resistant and the abrasion resistant materials are not corrosion resistant.

The extreme corrosion and abrasion which occurs in stopes constitute a major obstacle in achieving reliability of stoping equipment.

The influence of geological features such as parting planes, joints and faults is another important consideration in the design of methods and machines for stoping. The negotiations of faults imposes restrictions on mechanised mining systems. To accomplish this the mechanical system must be able to move up or down on a steep slope to reduce the amount of off-reef mining. The movement of equipment in stopes of restricted height is attended with various serious difficulties.

Finally, the depth at which the reefs are situated and the irregular distribution of gold in the reefs make mine planning and grade control difficult and favour mining methods that have a high degree of flexibility. Heavy mechanised mining systems do not have a high degree of flexibility because of their inability to be easily moved and serviced on a mine wide basis.

Mechanisation would be best served by concentration of the mining operation. However, this is difficult to achieve in tabular deposits of variable ore grade.

Although stoping has been identified as the most obvious area for improvement, against the abovementioned background it is not surprising that deep-level gold mining uses a low level of mechanisation, a low degree of face utilisation, and very labour intensive methods. Conditions prevailing in deep narrow stopes are such that only rudimentary machines such as rockdrills, scrapers and hydraulic props have been used to any significant extent. Furthermore, the time taken for these machines to develop and become fully accepted is testimony to the difficulty in developing equipment to work reliably and effectively in the stoping environment.

1.3 Benefits of Mechanised Non-Explosive Stoping

The introduction of a mechanised non-explosive mining system, to gold stoping, would undoubtedly represent a significant advance to the mining industry, as it offers many potential benefits. Most importantly, non-explosive mining can be continuous, thus allowing for higher rates of face advance. Staggered shifts would also become possible and would alleviate underground travelling and shaft congestion. In addition, because non-explosive mining methods produces less fines than conventional, it becomes practical for the waste rock to be sorted at the face and used as backfill, thereby reducing the amount of rock to be transported from the face. It is also possible that the reduction in fines will bring about an increase in gold recovery.

When used with backfill, non-explosive mining also results in improved strata and environmental control which would permit mining at greater depths and, moreover, working conditions could be vastly improved.

Cook et al [2], stated that a substantial financial return was realised when the "tramming width" was reduced by a factor of two and to compensate, so that the volume of rock milled was not decreased, the rate of mining was doubled. This reduction in tramming width can be achieved by either packing the waste in the back area or by reducing the stoping width. Reducing the effective stoping width and, therefore, the amount of gravitational energy released per unit area mined would improve strata control, Joughin [3]. Figure 1.5 summarises the consequences and benefits of any future mechanised non-explosive mining system.

In its efforts to develop a non-explosive mining system, the concept of "slot-mining" has been identified by T&DS as the method offering the most potential, Marlowe [5][6] Fenn [7].

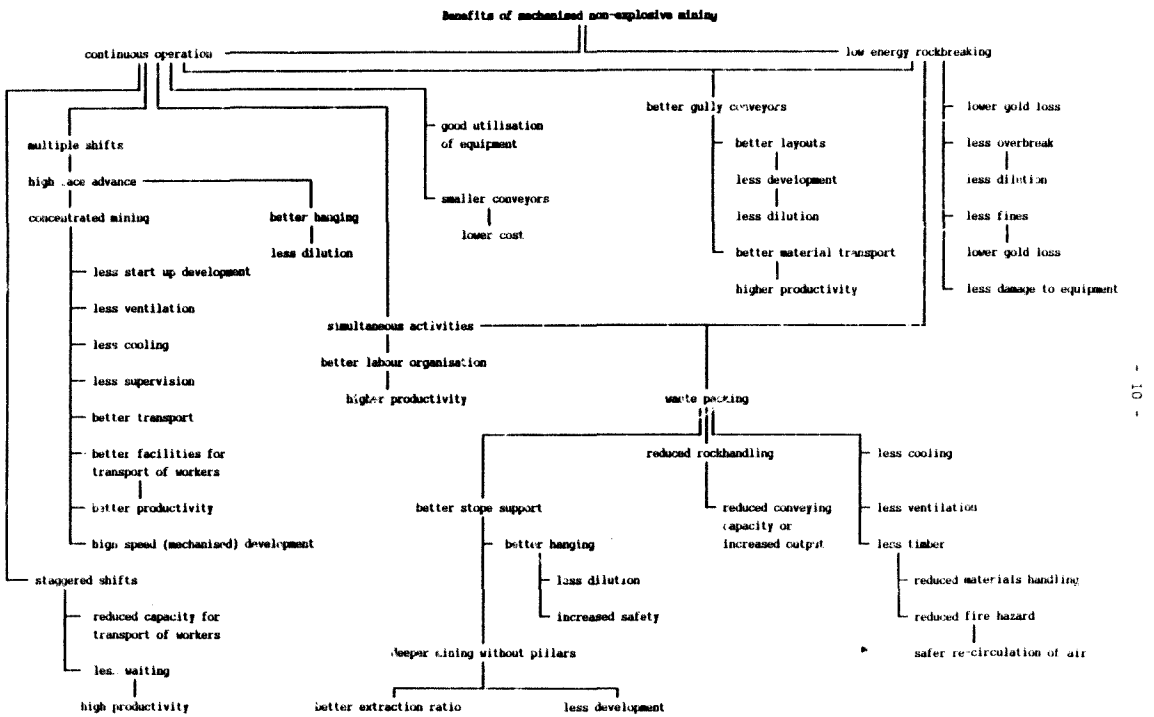


Figure 1.5 : Consequences and Benefits of Mechanised Non-Explosive Mining (after Haase et al [4])

The cutting of slots in the stope face, Figure 1.6, relieves the vertical stress acting on the rock, facilitating its removal from the face. Because of separation of the reef from the waste, slot-mining also allows the gold bearing reef to be selectively mined. This simplifies the waste packing operation and allows a high-quality waste to be packed. In addition, slotting results in smooth hangingwall and footwall conditions which improves support and stope width control.

1.4 Disadvantages of Mechanised Non-Explosive Stoping

As stated previously, rock stress related phenomena plays a major role in the design of mechanised stoping methods. It can be argued that the degree of fracturing about an excavation has played a predominant role in determining the degree of success of the mechanised stoping systems investigated to date (see Section 2).

Generally in stopes, the rock is very hard and strong and requires considerable energy to break. Methods such as impact breaking (ripping), at present under investigation by the Chamber of Mines Research Organisation (COMRO), takes advantage of the stresses ahead of the stope face to do most of the fracturing. However, where these fractures are absent and the rock is relatively unfractured, it is difficult to remove the rock. Such "hard patches" cannot be fully explained, but have been found to occur immediately ahead of a concentrated fracture zone, such as a shear fracture, a zone of closely spaced face parallel fractures or a joint, **Jager et al** [8]. The inability to mine hard patches at an acceptable rate constitutes a major obstacle to the implementation of impact ripping as a mechanised stoping method.

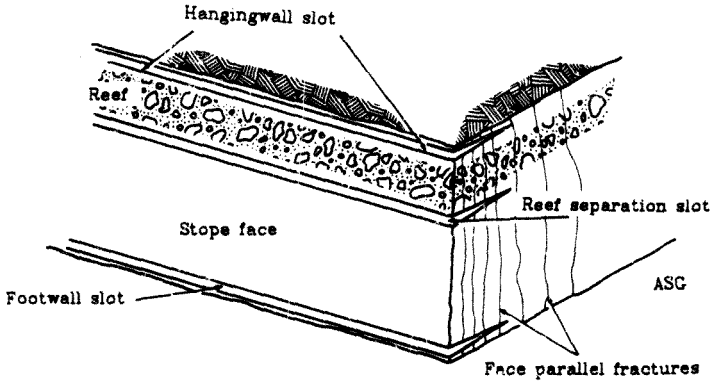


Figure 1.6 : Configuration of Slots for Cutting and Breaking Method

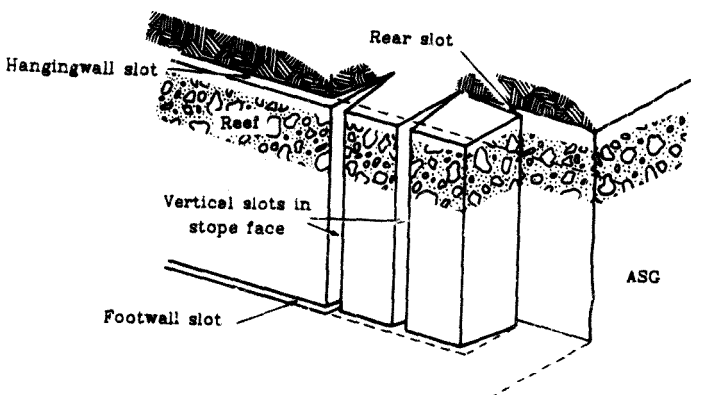


Figure 1.7 : Configuration of Slots for Block-Cutting

T&DS's slot-based mining system is not subject to the restraints imposed by the degree of fracturing inherent in the rock mass surrounding the excavation. Fractured rock is easily broken, while hard patches can simply be addressed by block-cutting, (Figure 1.7) or slashing the hard patch. Therefore, from a rockbreaking point of view, it can be considered to constitute a complete mining system, albeit in the development stage.

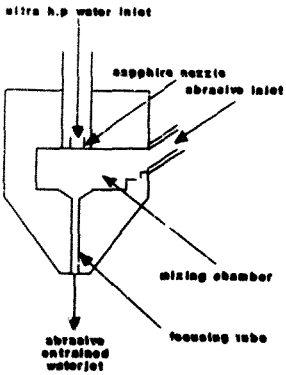
1.5 Slotting Systems

The current work under investigation by T&DS, can be divided into three areas:

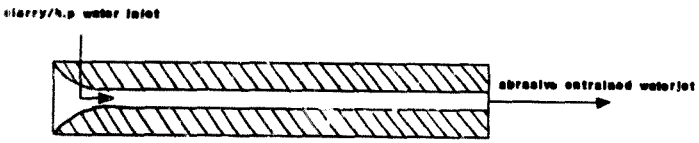
Ultra High Pressure Dry Entrained Abrasive Waterjet Cutting (>70 MPa)

Dry entrained abrasive waterjet cutting, referred to as dry abrasive cutting, has been investigated since 1985. Its basic operating principle is as follows; intensifiers or high pressure plunger pumps are used to pressurise the water up to 240 MPa, which is then expelled through a sapphire nozzle to form a coherent, high velocity waterjet. To increase the cutting capabilities of the jet, a dry abrasive is entrained into the waterjet, at the nozzle.

The waterjet and abrasive, which must be supplied in a dry form, are introduced into a specially designed abrasivejet nozzle, Figure 1.8, from separate feed ports. Here part of the waterjet's momentum is transferred to the abrasives, whose velocities rapidly increase. As a result of momentum transfer between water and abrasive, a focused, high velocity stream of abrasives exits the accelerator nozzle and performs the cutting action.



Dry Abrasive Waterjet Nozzle



Slurry Abrasive Waterjet Nozzle

NOT TO SCALE

Figure 1.8 : Dry Abrasive and Slurry Abrasive Waterjet Cutting Nozzles

High Pressure Slurry Waterjet Cutting (<70 MPa)

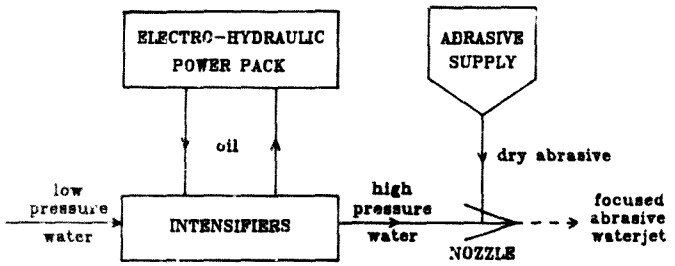
Due to claims that slurry abrasive waterjet cutting is a more efficient process than dry abrasive waterjet cutting, **Saunders** [9], it was investigated.

Although slurry abrasive waterjet cutting utilises an abrasive entrained waterjet to cut the rock, the abrasive/waterjet cutting technology of the system differs to that of the dry abrasive system. In the slurry cutting system the abrasive is injected into the water under pressure upstream of the nozzle, rather than entraining it into a high velocity jet downstream of the nozzle, as happens with the dry abrasive system. The abrasive and water are then accelerated together through a simple orifice arrangement, Figure 1.8.

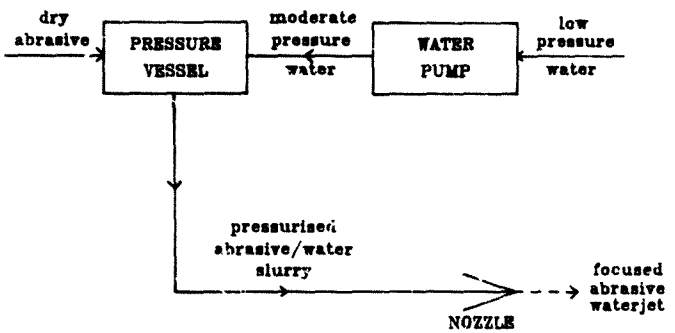
The cutting rate for both dry abrasive and slurry cutting is controlled by adjusting the abrasive feed rate, the jet stand-off distance (distance between the exit of the nozzle and the target material), the water pressure, the water flow rate, the abrasive parameters or the traverse speed. A schematic illustration of both abrasive waterjet cutting systems is presented in Figure 1.9.

Diamond Circular Saw Cutting

T&DS is also investigating diamond sawing as a means of cutting slots in the rock face. The diamond saw unit is capable of accommodating saw blades up to 1 000 mm in diameter and has a maximum power requirement far less than the abrasive waterjet slotting systems. The saw blade comprises of a steel centre or core, designed and heat treated to have a certain "tension" to ensure flatness and concentricity while cutting. Diamond impregnated segments are brazed to its periphery.



DRY ABRASIVE CUTTING



SLURRY ABRASIVE CUTTING

Figure 1.9 : Schematic Illustration of Abrasive Waterjet Cutting Systems

The segments comprise a bonding medium such as cobalt or bronze in which diamond particles are randomly distributed. The bonding medium (or matrix) has the job of anchoring the diamond particles thereby enabling them to perform the actual cutting.

Hence, diamond sawing relies on micro-indentation and grinding related phenomena to remove the rock. To ease constant efficient cutting, the bonding matrix must wear at the same rate as the diamond particles. The equipment utilised to date is described in Section 3.

1.6 Breaking System

With slot-based mining, a non explosive breaking system is required to remove the rock between the slots. Ideally a slot-mining system should be capable of effectively mining both fractured and unfractured rock, particularly when the hard-patch phenomenon is taken into account. To reduce the breaking time, an alternative to the cut-intensive block slotting or slashing method would be preferred.

At present, T&DS utilises a hydraulic impact hammer, of 200 J blow energy at 1 400 blows per minute, and conventional barring techniques to remove the fractured rock from the face.

To date, mechanical bullwedging and hydraulic pressurisation of pre-drilled holes (see Section 2.4), have shown potential for breaking hard, unfractured rock. Although these methods have potential, the breaking of hard patches has proved to be an intractable problem. Pending the development of a suitable rockbreaking technique, it is conceivable that slot-mining methods may be confined to the high stress environment. Hence, further development of the slot-based mining method is necessary before it can be applied to all South African gold mine conditions.

2.5 PREVIOUS WORK CARRIED OUT INTO NON-EXPLOSIVE MINING

Although non-explosive rockbreaking is used in other mining applications, such as quarrying and open-cut mines, this literature review has been confined to rockbreaking work directly related to deep-level gold mining. However, rockbreaking techniques used outside this area are mentioned for completeness.

Many different methods of breaking rock without the use of explosives have been proposed. Methods relying on chemical dissolution, fusion and vaporisation have not been found to be applicable to the underground mining industry for reasons of impracticability, cost, hazards to health, and energy limitations. As a result they have been excluded from this review.

Most practicable non-explosive rockbreaking methods depend ultimately on mechanical stresses to break the rock. Rock can be broken by pulling, bending, shearing, cleaving and indentation. Pulling is only possible by first drilling a hole, bending and shearing can only be achieved by first cutting slots and cleaving is achieved by first drilling holes which are then pressurised to cause breakage. The only direct method for continuous breaking is indentation. This can be in the form of roller cutting, drag bit cutting or impacting.

For the purpose of this review the methods have been split into; rockbreaking by cutting, rockbreaking by reef drilling, rockbreaking by impacting and rockbreaking by pressurising a pre-drilled hole.

2.1 Rockbreaking by Cutting

Economic assessments, **Cook et al** [2], have shown that substantial benefits would result from the use of an alternative method of rockbreaking which would permit the reef to be mined more selectively. With the view to the development of a continuous, selective mining process an investigation was made of most known methods of rockbreaking, **Cook et al** [10]. These included ultra high pressure water jets, mechanical wedging with or without impact, diamond sawing, roller bits, percussive tools, drag bits, various thermal methods such as jet piercing, lasers, electron beams and electrical techniques.

A drag bit method with a tungsten carbide tipped tool for cutting the rock, was selected as the most feasible of the techniques for developing a machine which could be made to mine selectively, under the conditions encountered in deep-level mining.

2.1.1 Drag bit rockcutter

Preliminary cutting investigations were carried out in a shaping machine and in a lathe with the aid of instrumented drag bits, to measure the cutting forces and tool wear in several types of rock for various cutting parameters, **Cook et al** [10].

These preliminary experiments showed that the force acting on the cutting tool consisted of two roughly equal components; the cutting force parallel to the direction of the movement of the tool relative to the rock and the penetrating force acting at right angles to the rock surface, Figure 2.1(a).

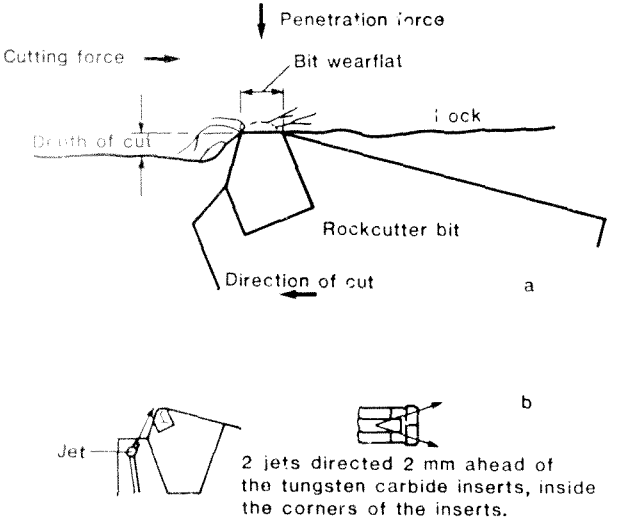


Figure 2.1 : Diagram of a Drag Bit Cutting the Rock Illustrating the Components of the Bit Force and the Optimum Jet Position (after Riemann [11]; Hood [12])

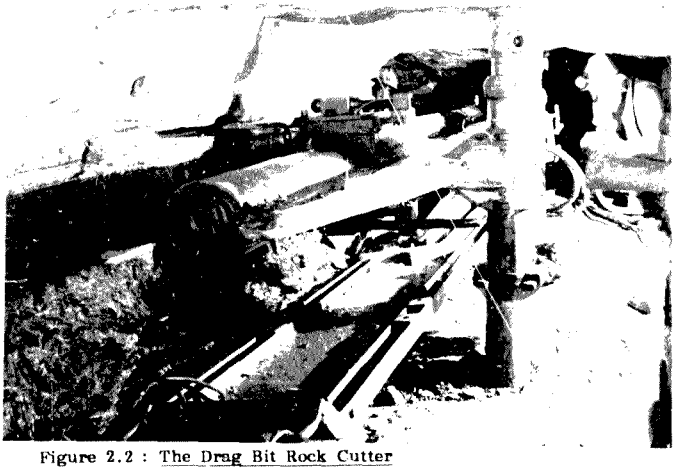


Figure 2.2 : The Drag Bit Rock Cutter

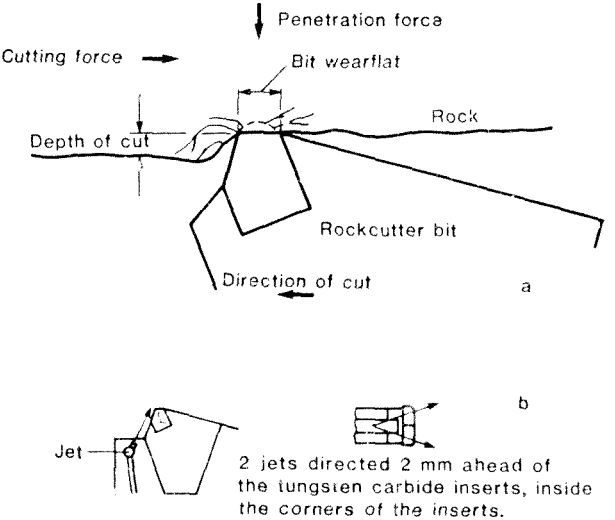


Figure 2.1 : Diagram of a Drag Bit Cutting the Rock Illustrating the Components of the Bit Force and the Optimum Jet Position (after Riemann [11]; Hood [12])

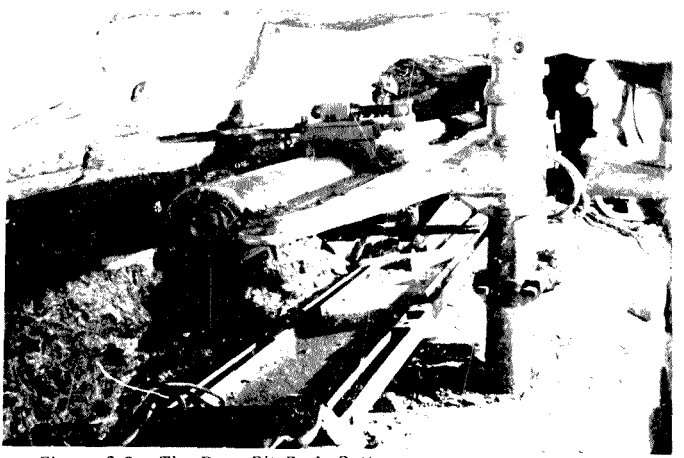


Figure 2.2 : The Drag Bit Rock Cutter

The cutting and penetrating forces on a tool were estimated to be of the order of 40 kN when making a cut 20 mm wide and 9 mm deep in hard rock. Wear on the tool was found to be moderate provided that cutting speed was less than 1,5 m/sec. Specific tool wear was less than 1 part of tungsten carbide in 25 000 parts of quartzite by weight when deep cuts, 2 mm or more, were made at speeds of less than 0,5 m/sec.

These results showed that it was possible to design a machine capable of mining 8 m³ per 6 hour shift; cutting for approximately half the time.

The first prototype underground rockcutting machine used a linear reciprocating cutting action. The testing of this and other similar rockcutting machines, showed that this design formed the basis of a feasible system of continuous selective mining, and revealed deficiencies in design which had to be overcome to yield a machine capable of mining at an economic rate. Further prototypes, Figure 2.2, were developed and trials established that rockcutting and waste packing constituted a practical method of stoping.

To combat high tool wear, the use of water jets to assist the cutting action of the drag bit was proposed. Preliminary tests were carried out by **Riemann** [11] to investigate the use of water as a means of cooling the bit during the cutting operation. It was anticipated that two benefits would be derived by applying a continuous waterjet to a bit while cutting rock. The first was that adequate cooling was expected to reduce the thermal damage to the bits. The second advantage was that a reduction of the mean and peak forces for a given depth of cut should decrease the mechanical load on the bit and thereby enhance the bit life.

Further work into the use of waterjets to assist drag bits, cutting in hard rock, was carried out by **Hood** [12]. He found that high pressure waterjets, directed immediately ahead of the bits while they were cutting norite (which had a compressive strength of approximately 250 MPa), significantly reduced the bit forces. Forces on the bit were found to be particularly sensitive to the point of impingement of the waterjets relative to the bits. The optimum configuration was found to be with two jets, one directed towards each corner of the bit and impinging on the rock approximately 2 mm ahead of the leading edge of the bit, Figure 2.1(b).

Experiments in which drag bit and high pressure waterjets were used to cut strong abrasive quartzites in the underground mining situation demonstrated a potential increase of up to five times the average depth of cut, due to reduction of the forces on the bit. The results from the underground tests showed that the life of the bit was improved by a factor of approximately two when waterjets were used.

Despite mining in excess of 60 000 m² **Joughin,** [13] the drag bit cutter was discontinued in 1978 due to poor labour productivity, excessive bit wear and the inability to mine hard, unfractured rock at an acceptable rate. In addition, the rockcutter consisted of heavy and bulky equipment which had to be staked to absorb the very high cutter reaction forces. In unfractured rock it had to be supplemented by a secondary rockbreaking method which resulted in far too complex a system. This caused incompatibility of the rockbreaking and rockhandling equipment which reduced labour productivity even further.

2.1.2 Radial rock slotter

The radial rock slotter developed by Boart International, Figure 2.3, was a device which utilised a compressed air powered rockdrill to slot the rock, **Bingham et al** [14]. It consisted of a pneumatically operated pivoting arm, which had a percussion hammer and tool mounted on it. The arm was mounted at a fulcrum point on the main frame and was able to pivot through an angle of 30-45°, depending on the cutting radius and the depth of cut.

The main frame of the slotter was mounted on a rail system by "V" shaped shoes and clamped to the rails by large diameter air thrusters. The machine was indexed (i.e. 18 mm on a 52 mm diameter bit) along the rails by pneumatic cylinders, which were also clamped to the rails by the air thrusters.

ence of indexing was achieved by clamping and
the air thrusters and operating the cylinders. Dur
the ...ting operation the machine was clamped to rails and on
released whilst indexing. By changing a spacer bracket, the cut could be located at any part of the face.

The principle of cutting using the rock slotter took into account the way rock fractures under impact and the forces generated, utilising these characteristics to produce rock removal rates significantly greater than could be achieved in the normal hole drilling process.

The angle of attack, bit diameter, thrust, index distance, power of the machine and type of rock were all interrelated and determined the rock removal rate. Balanced forces on the bit/rod system were essential to minimise bit jamming and reduce wear on the centraliser bushing.

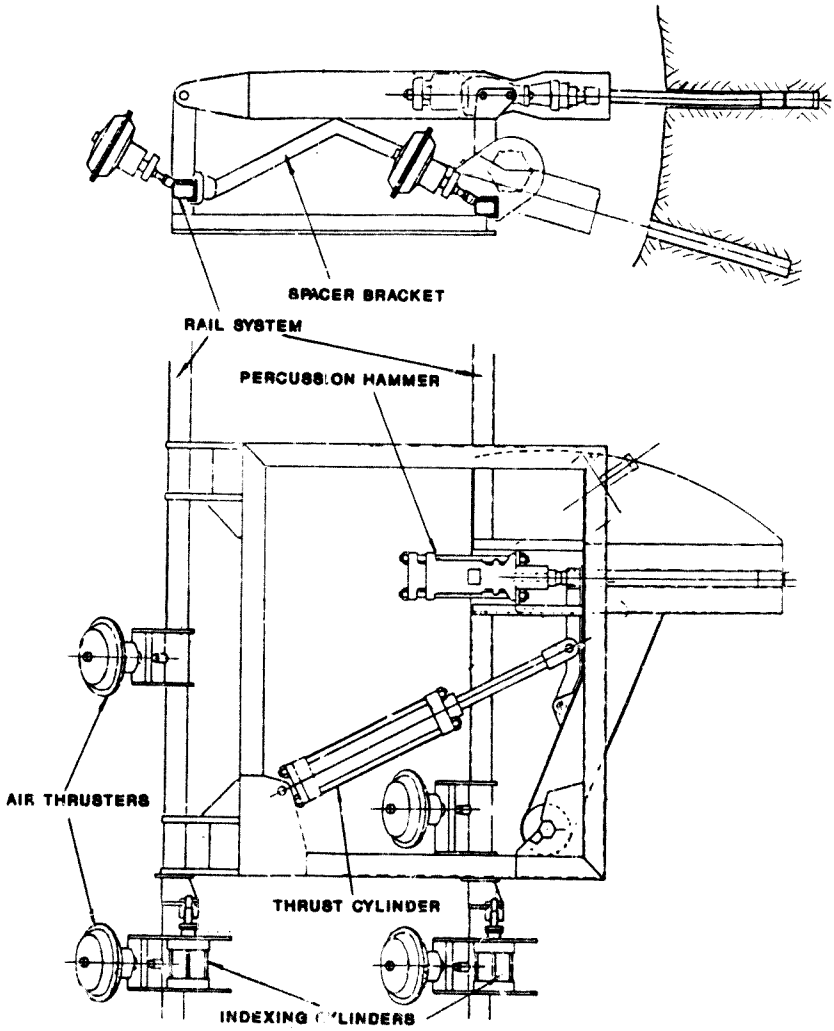


Figure 2.3 : The Boart Radial Rockslotter

The operating benefits of the radial rock slotter were as follows:

- ability to start a slot without the necessity of a free face
- cut a smooth profile, deep slot under unfractured rock conditions
- cut at any desired angle
- cut in either direction
- easily adapted to suit any conventional rock drill.

Slots of 600 mm depth were cut at an approximate cutting rate of 1 m^2/h, utilising the compressed air powered rockdrill. It was estimated at the time that slotting rates could be doubled with the introduction of oil hydraulic rockdrills.

The problem with the Boart rock slotter was that when it drilled through solid, unfractured ground the forces on the bit were balanced. However, when it entered fractured ground, the forces on the bit went out of balance causing unacceptable deviation and jamming of the bit. Hence this slotting tool would only be applicable to shallow gold mining where the fracture frequency ahead of the face is low.

2.1.3 Diamond sawing

Diamond sawing can be divided into two categories: circular saws and wire saws. Diamond chain saws do exist but are currently confined to cutting soft rock on a small scale, and as such, are not considered.

Diamond circular saws

Diamond circular saws have been extensively used worldwide for stone and concrete cutting in the quarrying and construction industries respectively. Their uses are well documented by **Tonshoff et al** [15], **Bienart** [16] **and Lutz** [17].

However, diamond saws have not been used on a large scale in the underground gold mining environment. **Hatch** [18] proposed the use of diamond circular saws in the gold and platinum industries, Figure 2.4. He concluded that diamond sawing would, at least, double present mining rates and that the costs were reasonable. In addition, **Hrtch** [18] proposed that a critical disadvantage of the technique was the system stability, on which the economic life of the saw may be dependant. This is relevant when you consider the mining environment is not conducive to a stable system.

One small scale application of diamond circular sawing in the gold mining industry, is the use of small circular saws for underground sampling of gold-bearing reefs, **Gouws** [19]. Although the operating costs of diamond saw sampling are higher than conventional chip sampling methods, this is offset by the advantages in accuracy.

In recent years, developments in saws and blade technology have continued to improve blade wear characteristics and cutting rates in hard rock. Improvements in the efficiency of driving diamond circular saw blades, has come mainly through the introduction of hydraulic rigs. In addition, investigations into the cause of diamond/matrix wear, by **Wright et al** [20] and others, have improved the blade wear characteristics so that the cutting operation is more cost effective.

Further innovations, such as the advent of polycrystalline diamond, as described by **Cullingworth** [21], and the laser welding of segments to the circular saw blade as opposed to brazing, **Schneider** [22], may further improve the economic viability of sawing in hard, abrasive rock formations.

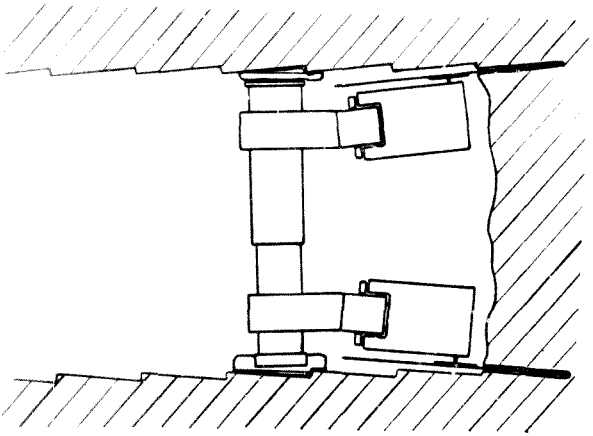


Figure 2.4 : Diamond Circular Saw (after Hatch [18])

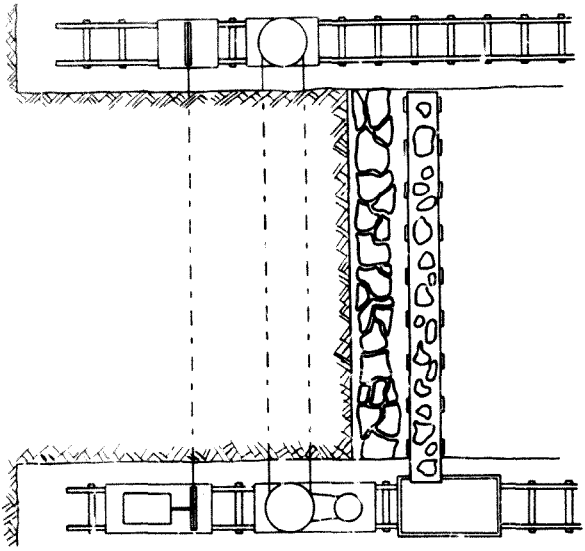


Figure 2.5 : Diamond Wire Saw (after Hatch [18])

Diamond Wire Saws

Hatch [18] also investigated the possibility of using diamond wire saws in the gold and platinum mining industries. He concluded that wire sawing was more promising than circular sawing because men and machinery are eliminated from the stope face.

Wire saws have been in existence since the late 60's and today are rapidly gaining acceptance in the dimensional stone cutting industry, Herbert [23] & Le Scanff [24]. A wire saw, Figure 2.5, is a device which pulls a taut wire across a rock face. When abrasive is impregnated into the wire, any material can be cut which has a hardness below that of the abrasive. Since diamond is the hardest of abrasives, all solid materials can be cut using diamond impregnated wire.

The success of diamond wire cutting is primarily dependant upon a properly designed wire. It has to be made of a material which has sufficient tensile strength to withstand the required tension and enough ductility to secure the diamond beads, which form the cutting elements of the diamond wire. Recent improvements in diamond technology have led to the development of the impregnated bead. The impregnated bead comprises a cylindrical hollow steel support surrounded by a diamond impregnated annulus, whose composition is similar to that of traditional diamond segments and with the diamond grit distributed evenly throughout the impregnated annular volume. This feature gives the tool a uniform cutting ability over its entire life, unlike the traditional electroplated beads used for cutting soft materials such as marble, which progressively lose their cutting ability as they wear.

It is claimed that wire cutting using diamond impregnated bead technology, is capable of cutting hard granites economically. Daniel [25], has reported cutting rates in granite and marble of up to 2,5 m^2/h and 7 m^2/h respectively.

Besides acceptable cutting rates, diamond wire sawing has the following benefits: It has the ability to cut the channel width only. This would result in a reduction in stoping width, effectively reducing the energy release rate, concomitantly alleviating the rockburst hazard. Strata control could be further enhanced by placing backfill virtually up against the working face, the result of eliminating men and machinery from the stope face.

2.1.4 Abrasive entrained waterjet cutting

It should be stated that the use of water jets as a mining tool in hard rock is a novel concept. Consequently there is very little literature available on this topic.

Lagesse [26] stated that waterjet cutting can be broken down into two categories, "destructive" and "precision cutting". The main destructive applications are the breaking of rock, coal, coke and other minerals or the removal of unwanted coatings on surfaces. In destructive waterjet cutting applications the emphasis is on the removal of as much material as possible and not the quality or depth of cut produced. Conversely, precision cutting is more concerned with the quality, depth and accuracy of cut and minimising the volume of material removed.

In conjunction with a slot-based mining system, the cut depth should be maximised whilst minimising the volume of rock removed. Hence, precision cutting is the only form of waterjet cutting addressed in this dissertation.

The high pressure waterjet, is an accepted cutting tool in a wide variety of industries.

Cutting applications include paper, cloth, wood, plastics, fibre glass and rocks of medium hardness, **Hashish** [27]. The disadvantages of cutting with water alone are that hard materials and rocks cannot be cut effectively. In addition, high power levels are needed for reasonable cutting rates in many applications.

During the 1960's, drilling fluids were pressurised from 69 MPa to 103 MPa by oil companies to generate fluid jets sufficient for augmenting rotary rock drilling. Although improvements in drilling rates and bit wear were reported, **Maurer** [28], pumping equipment that could operate at the pressures required was not believed to be available, **Pols** [29].

To increase waterjet cutting capabilities the introduction of abrasives into the waterjet stream has been investigated. In the 1970's abrasives such as sand and steel shot were added to the waterjets to assist drilling, proving increased drilling rates of 4 to 20 times those achieved in the same rock formations with conventional rotary drilling, **Wyllie** [30]. **Fair** [31], developed abrasive-jet drilling further and made some significant advances to the system. However the investigation was terminated in 1975, through high component wear associated with the abrasives and the associated costs involved. **Fair**, further concluded that abrasive-jet drilling would only be viable in the deeper two-thirds to three-fourths of deep holes, where conventional drilling rates are low.

More recently, **Baumann et al** [32] investigated the applicability of abrasive waterjets to assist road-heading machines in driving road-ways in the West-German coal industry. It was found by carrying out tests under preset conditions (abrasive mass flow 1 kg/min, cutting speed 1,5 m/min, water pressure 150 MPa and using quartz sand as the abrasive), that a 220% improvement in depth of cut was obtained, compared to using the waterjet in isolation.

From the 40 different abrasives tested, **Baumann et al** [32] identified a special corundum to be the most effective abrasive, yielding a 350% increase in depth of cut compared to the waterjet alone.

In addition, **Ihoobi et al** [33], researched abrasive waterjet assisted road-heading to excavate much harder rocks such as granite, andesite and rhydite. The authors conducted laboratory rock cutting tests with an abrasive waterjet, as a first step of development and produced a depth of cut formula:

$$H = K_1 \frac{We}{T.S} + K_2 \left[\frac{(Ga)}{(Gw)}\right]^n \frac{We}{T.S.}$$

where : K1 and K2: constants determined depending on the type of rock and abrasive
n: constant determined depending on the flowrate of water and abrasive.
We: *waterjet output power*
T: traverse rate
S: Stand-off distance
Ga: flowrate of abrasive
Gw: flowrate of waterjet

From the rock cutting tests carried out, the major conclusions were:

- the cutting effect of the waterjet only cannot be ignored
- the optimum flow rate of abrasive has a linear relationship to the waterjet flow rate
- the depth of cut shows a linear relationship to traverse rate and stand-off distance.

Tests to verify the
cutting and abrasive

JCI (Johannesburg C
the use of ultra high
cut underground qu
investigations were
Estates Gold Mine, Co

From the test-work ca
rates of up to 1,2
rates of up to 10 mm/
were also achieved.

However, problems in
pulse method called
and the development
that the cutting of
however, considerabl
potential of the resea

Fairhurst et al [35]
(Direct Injection Abr
a seven fold increas
input, has been clain
jet cutting over u
cutting, **Saunders** [3

A unique slurry cu
concentration slurry
has been patented,
system pressure w
accelerate together
acceleration process
exit flow consists of
of high density abra

Tests to verify the excavating effect of combined mechanical cutting and abrasive jet assistance have still to be carried out.

JCI (Johannesburg Consolidated Investments) have investigated the use of ultra high pressure abrasive entrained waterjets to cut underground quartzite, **Scott-Russell et al** [34]. Cutting investigations were carried out underground at Randfontein Estates Gold Mine, Cooke 1 Shaft and 16 Shaft.

From the test-work carried out underground, satisfactory cutting rates of up to 1,2 m^2/h were obtained. In addition drilling rates of up to 10 mm/sec utilising ultra high pressure water only were also achieved.

However, problems in breaking out the face, using a hydraulic pulse method called Flowex (see Section 2.4) proved ineffectual and the development program was terminated. It was concluded that the cutting of slots in hard rock had been a success, however, considerable development was required to transfer the potential of the research into a reliable production method.

Fairhurst et al [35] **& Saunders** [9] have developed the "Diajet" (Direct Injection Abrasive Jetting) slurry cutting system. Up to a seven fold increase in cutting performance, related to power input, has been claimed for high pressure slurry abrasive waterjet cutting over ultra high pressure dry abrasive waterjet cutting, **Saunders** [9].

A unique slurry cutting nozzle, Figure 2.6, in which a high concentration slurry is introduced within an annular water phase has been patented, **Krasnoff** [36]. Both phases are at full system pressure when introduced into the nozzle and they accelerate together towards the nozzle exit. Since the acceleration process in the nozzle is rapid and continuous, the exit flow consists of a high speed waterjet with an internal core of high density abrasive slurry.

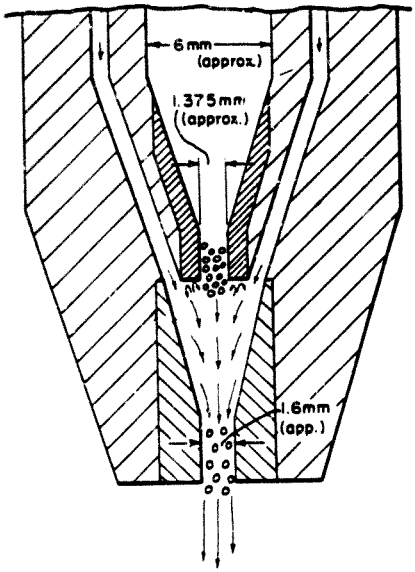


Figure 2.6 : Krasnoff Nozzle Arrangement

Krasnoff [37] claims an increase in efficiency over other abrasive waterjet cutting systems; however, this has still to be proven in practice.

The main disadvantages of slurry abrasive waterjet cutting, compared to dry abrasive cutting, is that it consumes relatively greater quantities of abrasive and water. Abrasive recycling to reduce the cost and quantities of abrasive required has been proposed, **Nakaya** [38].

Another method of reducing the abrasive and water consumption is to use a higher water pressure with a smaller orifice size. This maintains performance by using more nozzle power, but enables a lower abrasive and water flowrate to be used. To date most slurry cutting systems have operated up to 40 MPa water pressure. There are, however, systems available which operate up to 70 MPa, **Blocmfield** [39] **& Müller** [40].

2.1.5 Laser cutting

The use of high powered lasers to thermally weaken rock has been widely investigated **Carstens et al** [41] [42], **Mc Garry et al** [43] **and Jurewicz et al** [44]. These studies have predominantly involved the use of high concentrated laser power to form narrow cuts (kerf) in the rock as an aid to mechanical excavation. A comprehensive review of laser cutting has been compiled by **Maurer** [28].

Lasers produce intense electromagnetic radiation beams which melt and vaporise the rock. Melting is highly inefficient requiring large amounts of energy. Typically specific energies are of the order of 10 000 MJ/m^3. Removal of the molten rock from the face is also a problem.

In addition to creating a free face to promote breakage of the surrounding rock, kerf cutting with laser energy also weakens the rock in the vicinity of the cut through thermal cracking. This thermally degraded zone is important when lasers are used in conjunction with mechanical excavation techniques.

Besides the high energy requirements and high capital equipment costs associated with laser heating, lasers are highly sensitive to environmental conditions. **Carstens et al** [42], found that the laser transmission efficiency decreases rapidly as the relative humidity of the air increases. At a relative humidity of 10 percent, 30 percent of the laser power was absorbed by the air, while at a relative humidity of 100 percent nearly all the laser power was absorbed.

In the South African stoping environment the relative humidity is typically 85 percent, which would drastically reduce laser operating efficiency. **Carstens et al** [42], also found that in a typical rock drilling environment, laser beams lose up to 60 percent of their power to course dust.

Finally, lasers are delicate devices and further research would be needed to enable them to be suitably adapted to the unfavorable underground mining environment.

2.2 Rock Breaking by Reef Drilling

Additional rockcutting methods (referred to as reef drilling) investigated by the South African gold mining industry include; reef boring, investigated by Gold Fields of South Africa and COMRO, and stope coring which was carried out by De Beers. Both the boring and coring techniques comprise the removal of the gold bearing reef by boring or coring a series of overlapping holes in the plane of the reef from strike access tunnels (reef drives), Figure 2.7.



Figure 2.7 : The Mining Principle of Boring or Coring Overlapping Holes with Approximate Dimensions

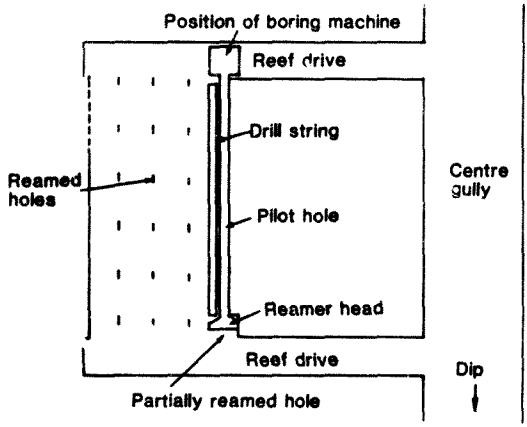


Figure 2.8 : Typical Position of Reef Borer

An additional benefit of these methods, is that by reducing the effective stoping width (typically around 600 mm), the amount of gravitational energy released by mining would be proportionally reduced. This parameter has been shown by **Joughin** [3] and other workers to be of great importance in minimising rockbursts. Furthermore, as drilling is carried out from reef drives, no person need enter the stope. As a result, the safety of the mining operation is greatly enhanced.

Jager et al [45], proposed that six distinct geological characteristics were likely to effect mining by reef drilling, namely:

- straightness and thickness of the reef
- incidence of faults and their throws
- type of rock and its mechanical properties
- presence or absence of parting planes adjacent to the reef
- dips of the reef and adjacent strata
- magnitude of the stress in the rock which is to be mined by drilling.

To minimise the loss of gold through inaccuracy in drilling and fault losses, panel lengths of 20 m were suggested for drilling applications.

2.2.1 Reef boring

Reef boring was based on conventional raiseboring technology. The reef boring machine was positioned in the upper of two drives, Figure 2.8. The initial stage of the operation was to drill a pilot hole in the plane of the reef from the drive in which the machine was positioned to another approximately 20 m on dip below it. The pilot hole, which was approximately 240 mm in diameter, served as a guide for the reaming head. The reaming head, or hole opener, comprised three rotary cutters which were pulled up the pilot hole by the machine, thus enlarging the hole to roughly 600 mm diameter.

The holes were drilled on 550 mm centres, which ensured some overlap and resulted in a continuous slot being formed and the maximum amount of reef being extracted, Figure 2.7.

Underground trials were conducted at Doornfontein and West Driefontein Gold Mines. At the West Driefontein test site, rock stress was found to have an adverse effect on the boring operation. **Jager et al** [45], observed the following stress phenomena during reef boring a shallow depth of roughly 1 240 m:

The sides of the pilot holes spalled quite markedly, which made it difficult to maintain the desired direction of the pilot hole and also to stabilise the cutters. Fracturing parallel to the sides of the pre-developed reef drives extended about one metre on each side of the drive. This allowed enough closure in the fracture zone during the reaming operation to prevent the reamer head from being extracted at the bottom drive. As a result it had to be pulled out at the top drive and transported to the lower drive. **Jager et al** [45], stated that the effect of stress would be accentuated at greater depths.

Adams [46], investigated the stress phenomena associated with reef boring and found it to be the fundamental cause of the problems responsible for poor cutter life. Cutter performance for both pilot bit and reaming cutters was poor.

In one case the cutter failed after 1,5 m of operation while an average cutter life was only 30 m. An attempt to alleviate the effect of stress on the excavation by backfilling the reamed holes with a cement grout, was unsuccessful.

The general conclusion reached from the above investigations was that conventional raiseborer technology cannot be applied to reef boring, particularly in a high stress environment.

2.2.2 Stope coring

In 1975 Debex developed the Stopecorer, a machine which utilised the reef boring concept, but which used diamond drilling as opposed to raiseboring technology to bore out the reef, **Conradi et al** [47]. Very simply the stope-corer comprised a hydraulically powered diamond core drill, 600 mm in diameter, that could propel itself up or down the hole it was drilling, Figure 2.9.

The core barrel consisted of thirty diamond impregnated segments set into the leading cutting edge. The large openings left by the trunnion mounting behind the bit, allowed rock to pass continuously through the openings. Two jacks (clamps) at the rear of the mole thrust upwards, locking the unit in position for drilling. Hydraulic rams thrust the drill head forward and at the end of the drilling stroke, the front clamp was extended and the rear two retracted. The next stage involved propelling the rear forward, ready to start the next cycle.

The drilling and walking cycles can be automated and remotely controlled, depth indicators were fitted for exact positioning the mole up the hole.

Work by **Jager et al** [45], showed that 80% reef recovery could be obtained in Carbon Leader and the Vaal Reefs, given the usual frequency of faults and maximum reef thickness of 30 cm. From this work, **Conradi et al** [47], proposed a concept of 60 cm diameter holes drilled a distance of 20 m, on reef.

Underground tests with the stope corer were carried out at Sallies and Vaal Reefs gold mines at depths of roughly 1 200 and 1 600 m respectively.

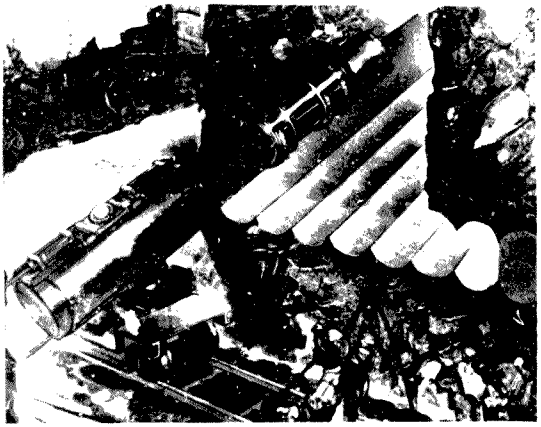


Figure 2.9 : Stopecorer Positioned in Hole

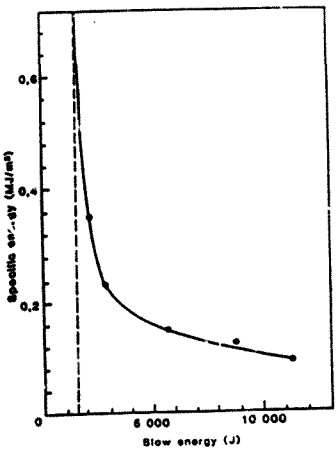


Figure 2.10 : Laboratory Drop Test Rig Results (after Haase et al [4])

During underground trials several problem areas were identified, the majority being related to how the rock reacted after coring, that is it either burst, disced or cored. When the rock spontaneously burst good drilling rates, typically 12 cm/min, were recorded. Discing, the most common occurrence, resulted in having to remove the rock manually from the core barrel. Progress was slow when discing occurred and, coupled with plastic closure and having to remove the machine away from the work face, resulted in re-drilling the gauge clearance. The procedure of opening an already drilled hole effectively reduced bit life.

Coring was not a serious problem during the underground trials as it only occurred very seldom at the start of a new panel. In unfractured rock conditions, however, coring could present a serious secondary rockbreaking and rockhandling problem.

Debex [48] claim to have solved the problems encountered during underground testing, through extensive equipment modifications. However, this has yet to be shown in practice.

2.3 Rockbreaking by Impacting

The idea of breaking hard rock deep underground by impacting, grew from knowledge of the rock conditions ahead of an advancing face, gained during the years of experimentation with rockcutters. Before that, it was believed that the rock ahead of the face was relatively solid, and that any fracturing observed at the free face was caused by the blasting process.

Observations of the rock ahead of the faces being advanced by rockcutting methods showed that a series of vertical fractures, parallel to the face, were propagated ahead of the face. The degree of fracturing and the distance between groups of fractures was dependant on the stress imposed on the rock by the overburden and the energy release rate determined by the stope geometry.

Impact breaking of solid rock confined by the surrounding rock would require such high blow energies as to make impact mining impracticable. However, the observation of rock fractures ahead of the face made impact breaking a possibility, but only at depths where the stress fracturing is appreciable.

Early research work set out to determine what hammer force would be required to break the rock effectively. Since fracturing in deep mines is generally spaced less than 500 mm apart, **Pickering et al (49)**, it was considered that an impact hammer would be required during mining operations to break through 0,5 m slabs of rock.

Tests were conducted in a drop test rig on blocks of norite, which had dimensions of 0,5 m x 0,5 m x 0,5 m. The results of these tests are presented in Figure 2.10. They show that the optimum hammer blow energy required under such conditions is approximately 4 000 J. Below this level the specific energy per unit volume of rock expended increases rapidly, while above it there are other considerations such as the size of the hammer which make increases in blow energy impractical.

Rapid rates of mining combined with good labour productivity can be obtained with rockbreaking by impacting. In addition, with narrow reefs, it is possible to sort and pack waste in the stope. Two approaches have been investigated: the swing hammer miner and impact rippers.

2.3.1 Swing hammer miner

The swing hammer miner was somewhat like a coal shearer in appearance, Figure 2.11. It was mounted on a conveyor and moved continuously while in operation. Six hammers pivoted in a rotor, swung outwards to strike the face as the rotor turned.



Figure 2.11 : The Swing Hammer Miner



Figure 2.12 : The COMRO Impact Ripper



Figure 2.11 : The Swing Hammer Miner

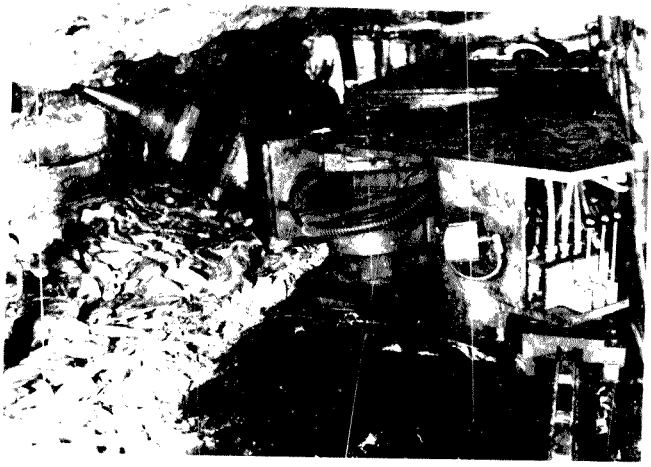


Figure 2.12 : The COMRO Impact Ripper

When the rock did not break, the hammers swung back, permitting the rotor to continue rotating, and allowing the hammers to regain their striking position during the remaining part of the revolution. It was hoped to achieve an instantaneous breaking rate of 2 m^2/hr.

In fractured ground the machine worked well using low blow energies, typically 500 joules at 18 blows per minute. However, **Joughin et al** [50], reported a number of features inherent in the machine that made it unattractive:

First, the angle of attack of the hammers was poor. When the hammers encountered a hard patch of rock that did not break readily, inclined fracture surfaces were formed. The configuration of the machine was such that the angle of attack became worse in relation to the inclined surfaces.

Thus, the ability of the hammers to break deteriorated just when the rock was most difficult to break. Secondly, the poor angle of attack lead to a very poor bit life, an order of magnitude less than that which could be acceptable. Thirdly, the machine was inherently mechanically complex and unreliable.

Bührmann [51] concluded that the mechanical reliability of the swing hammer miner was unacceptable and that rock excavation rate showed significant dependance on blow energy, power of the hammers and on fracture frequency of the rock. He also concluded that although the estimated cost of mining with swing hammer miners proved to be prohibitive, improvements in mining rate could be obtained by using two hammers of approximately 1 500 J blow energy.

With swing-hammer-impacting it was not possible to increase the blow energy very much without causing inordinate mechanical problems. Since it is possible to generate much higher blows more reliably and with more favourable angles of attack using impact rippers, it was decided not to pursue the swing hammer miner principle and to concentrate on impact rippers.

2.3.2 Impact Hammer (Ripper)

Of all the non-explosive mining systems investigated by COMRO, impact ripping, Figure 2.12, has been identified as being the most viable since it exploits the natural rock fracturing which occurs in deep mines around stope faces. When investigating other techniques it was found that either their rockbreaking rates were too slow or that the natural rock fracturing in fact rendered them non-functional.

Based on these findings, the development of a non-explosive impact ripping system, to determine the rate at which the rock could be broken, was initiated. The principle of impact ripping, consisted of a powerful impactor which is placed at a strategic point on a fractured face, and pieces of rock were knocked off the face.

The impactor was mounted on a highly articulated boom so that the machine operator could choose the impact point to take maximum advantage of the fractures.

Most of the rock was merely ripped off the face but some breaking was necessary to arrive at the desired stope width. The broken rock falls onto a reciprocating flight conveyor situated close to the face which removes the rock to the strike gulleys. The machine itself moves along the conveyor or guide rail in steps and rips off rock from the face to an approximate depth of 0,5 m in each pass.

Underground tests at Doornfontein Gold Mine were conducted at a depth of 2 700 m, where the energy release rate was between 10 and 30 MJ/m². As the hydraulic hammers on these machines were still under development, the blow energies were significantly less than the specified figure of 4 000 J, and varied between 2 400 and 2 700 J. The hammer operated at a frequency of 3 Hz.

The results achieved, Figure 2.13, were encouraging and where the rock was highly fractured, high rock-breaking rates were achieved. In moderately fractured rock, which comprised of approximately 63% of the rock broken, and slightly fractured rock, which comprised 20% of the rock broken, satisfactory breaking rates were obtained. Overall, an average rockbreaking rate of 9,5 m²/h was attained, **Spies et al** [52], which was encouraging given the relatively low blow energy of the hammer. Mining rates of greater than 10 m²/h could be possible with a hammer operating at a blow energy of 4 000 J and at a higher frequency, provided the energy release rate is not too low, **Pickering et al** [49].

Other advantages which became apparent during these underground trials were that impact ripping resulted in very few fines and relatively large fragments of rock being produced. When mining in reefs with narrow channel widths, it was possible to sort the waste from the reef and use it as backfill.

The main obstacles to impact ripping are: the achievement of acceptable component reliability and the extent to which rock will be consistently fractured in the mining situation.

Hammer reliability (currently around 45%) will have to be improved drastically to achieve high availability of the equipment.

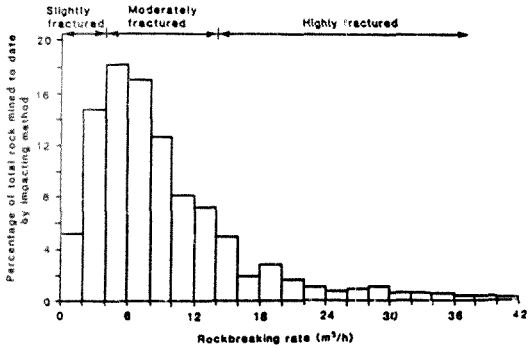


Figure 2.13 : Results Achieved with the Impact Ripper (after Spies [52])

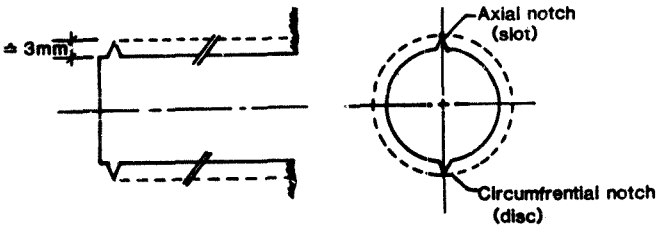


Figure 2.14 : Longitudinal and Circumferal Notches in a Hole

It is possible with the introduction of hydropower (using the hydro-static energy of the water head fed in columns down the shaft), that a more simple system will improve component life.

Unfractured rock that is too hard to break efficiently by impacting can be expected to occur intermittently in all mining environments. An auxiliary method of fracturing these hard patches is therefore required for effective mining by impact rock breaking (see Section 2.4). The method must be compatible with the environmental requirements which make continuous non-explosive rock-breaking desirable.

2.3.3 Impact Planer

Another impact rockbreaking system worth mentioning is the impact planer developed by COMRO from 1978 to 1983, Haase [53]. The impact planer was developed to overcome the problems of the deteriorating hammer attack angle of the swing hammer miner.

It consisted simply of two ballistic 2 000 J blow energy hammers which mined the rock similarly to the swing hammer miner. The only operational adjustments were height of the hammer, stand-off distance and driving speed.

Surface tests with this machine revealed several fundamental shortcomings associated with the hammer drive system. The output blow energy was far below target and the machine suffered from severe destructive vibrations.

Since the rectification of these problems would have required considerable redesign, the concept was abandoned in 1983.

2.4 Rockbreaking by Pressurising a Pre-drilled Hole

Rockbreaking by pressurising a pre-drilled hole is only discussed in the hard patch breaking context, as an aid to non-explosive mining. The reason for this is that burden spacings for "down-the-hole" non-explosive rockbreaking systems are generally small resulting in an impractical number of holes having to be drilled, to break out the entire stope face.

It requires approximately 0,4 MJ of energy to drill a 1 m long hole, 42 mm in diameter in quartzite, which is generally greater than the specific energy required by the non-explosive rockbreaking device. However, the technology of percussion drilling into rock is well developed and with the advent of hydraulic drills, the problems of drills stalling and jamming in closely fractured ground, due to inadequate rotational forces, have been largely overcome. "Down-the-hole", non-explosive rockbreaking systems are therefore conceptually acceptable.

It is desirable to break from a pre-drilled hole, as this breaks the rock in tension, which requires considerably less force to fracture the rock than would be required to break the rock in compression. Typically, the uni-axial tensile strength of quartzite is between 6% to 15% of the compressive strength.

Three important parameters have been identified which critically influence rockbreaking performance, Cudemann [54].

There is firstly the peak pressure which must at least exceed the tensile strength around the hole. If the peak pressure exceeds the compressive strength of the rock, crushing will be induced around the hole as the first step in the disintegration process.

This is not desirable, as it produces dust and blocks the driving medium from entering the developing cracks, and assisting in the disintegration process.

Non-explosive methods do not generally reach pressures which crush the rock, particularly since the underground quartzite is subjected to confining stresses from the overburden.

The second important parameter is the pressurisation time. For quasi-static pressurisation rates, typically two fractures develop, which does not necessarily mean that the rock will be dislodged. If pressurisation rates are increased, more fractures will develop because of inertia effects in the rock mass. It has been shown by **Blight** [55], that short pressurisation rates have an advantage over static pressurisation, because of 60% higher hoop stresses generated around the hole for the same driving pressures. This happens when pressurisation rates are fast in relation to the translational wave velocity in the rock.

The third important parameter is the length of the pulse, which is relevant for the disintegration of rock, since cracks propagate with speeds lower than those of transitional waves. Suitable ranges for the three critical parameters in order to induce multiple fracturing have been calculated for quartzite, **Brinkmann** [56].

Rock fracture conditions have an obvious influence on breaking performance. Although fractured rock will generally require lower energy input, some methods can actually be less effective in fractured rock, as it permits the dissipation of the applied energy through open cracks.

The effectiveness of breaking from holes can be improved if stress raisers are provided in the hole in the form of longitudinal or circumferal notches, Figure 2.14.

Non-explosive rockbreaking devices, based on the pressurisation of a pre-drilled hole, can be grouped into 3 sections. These devices are based on; the discharge of high pressure gas, fluid pressure and mechanical forces.

The following devices, based on gas pressure, involved inserting a tube into a pre-drilled hole which was held mechanically until the gas discharged.

The Armstrong, Cardox and Shockwave Breaker devices, which used compressed air, CO_2 and an exploding acetylene air mixture respectively, were systems which involved pressurising a pre-drilled hole by gas discharge.

The Armstrong air-breaker was able to store energy up to 0,23 KJ/cm^3 and had a rupture disc at the end of the steel tube which was designed to break at compressed air pressures, ranging between 68 to 103 MPa. **Souden** [57] investigated the Armstrong air-breaker and concluded that the main problem was that very straight holes had to be drilled to insert the tube. It was also found not powerful enough to break an acceptable burden in quartzite under all fracture conditions.

The Cardox breaker stored energy in the form of compressed CO_2 and the energy was released when the cartridge was ruptured by a small electrically ignited detonator. The peak operating pressure was around 260 MPa with a stored energy of 250 KJ. Ignition reliability, coupled with the fact that it broke poor burdens of only 150 mm in norite, made the device unattractive, **Clement** [58]. **Fenn** [59] confirmed these findings with four tubes failing to detonate and eight shooting out of the hole. The remaining four only broke an average of approximately 0,004 m^3 of rock per tube, during underground trials at West Rand Consolidated Gold Mine.

Fenn [59] also found the Cardox breaker to be highly dependant on hole straightness, and invariably the tubes could not be inserted to the required hole depth.

The Shockwave or Combustion Breaker was charged with 10% acetylene in air mixture at 20 MPa. On initiation, a shock wave was produced with pressures up to 1 500 MPa and rise times of 10 ms. The stored energy was approximately 0,55 KJ/cm^3. **Blight** [55] researched the device extensively and found the high energy storage was largely a result of the high temperatures generated during combustion. The inconsistent combustion process made testing of any nature difficult and even dangerous. To date, these difficulties have not been overcome. **Clement** [58] found that hole straightness was again the main problem with the Shockwave Breaker. In addition it was unable to break solid quartzite rock and could only break 300 mm burdens in fractured quartzite. **Joughin** [60], concluded that breaking rates were slow and costs were three times that of conventional blast mining.

The following devices, based on fluid pressure, have the potential for requiring less energy than gas driven methods since they do not operate with large volumetric expansions. This in some applications has the additional benefit of reduced fly rock.

The Flowex device, Figure 2.15, consisted of an accumulator of 6 litres capacity which was connected with a NW 38 hose via a quick release valve to a blast tube with a bore of 11 mm. This tube was inserted to a length of 200 mm into a 40 mm diameter water-filled hole, where it was mechanically sealed and locked. The water pulse from the accumulator, which was charged to 34 MPa, was released through two holes in the wall of the tube. Despite being reliant on hole geometry the Flowex device could also not break a burden of 100 mm in norite without notching, **Burrow et al** [61].

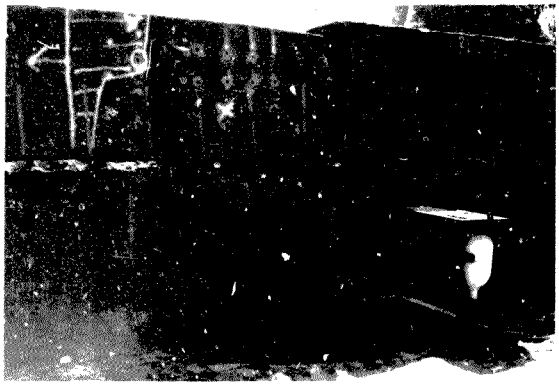


Figure 2.15 : **Flow Industries Flowex Device**

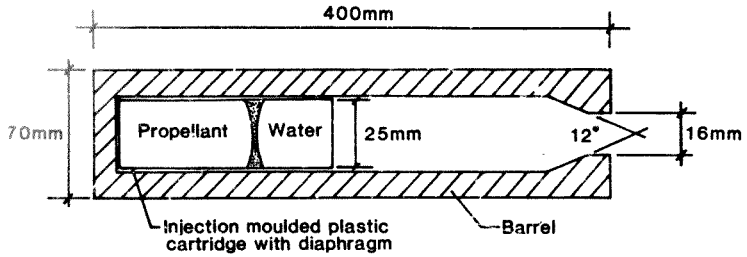


Figure 2.16 : CSIR Water Gun (Cannon)

The Boulder Buster, Essig Rockbreaker, CSIR water gun (Cannon), Figure 2.16, and COMRO water gun, all used a propellant cartridge of 10 g, 9,6 g, 9 g and 45 g of Ballastite respectively, in conjunction with water to fracture and break the rock.

The Boulder Buster could not break a burden of 100 mm in norite and was therefore inadequate, **Burrow et al** [61].

Fenn [59] tested the Essig rockbreaker underground at the West Rand Consolidated Gold Mine and found the device broke a negligible amount of rock and was particularly sensitive to hole geometry. In addition, the device was almost impossible to remove, if the rock was not broken.

Fenn [59] also tested the CSIR water gun at the West Rand Consolidated Gold Mine where it broke an average 0,01 m^3 of quartzite rock per shot. Unlike the Boulder Buster and Essig Rockbreaker the water gun is not a "down-the-hole" device and therefore does not rely on hole geometry. From the tests carried out by **Fenn** [59] it was found that water coupling (water filled holes) and discing of the holes enhanced breaking with the water gun and demonstrated the potential of a water cannon for breaking hard patches.

Based on the experience with the CSIR water cannon a more powerful water gun was developed by COMRO which had 250 ml of water entrained in a rubber sleeve and had a detachable front end to allow different nozzles to be used.

The propellant charge was far greater than that used in the Boulder Buster, Essig rockbreaker and CSIR water gun and enabled the device to have a stored energy of 250 KJ. A 250 mm burden in norite using a water filled hole was broken, **Burrow et al** [61].

The COMRO water gun along with other devices such as; Hydrex, Briggs water cannon and mechanical impact on water, have still to be investigated further, to determine their potential.

Mechanical methods can operate by static force generation in the hole or with intermittent pulsed force generation (dynamic).

The three methods discussed are the bullwedge which is a dynamic method and the Darda rocksplitter and Radial axial splitter, which are static methods.

The bull wedge, a conically shaped tool which is inserted into the hole and then driven in by an impact hammer has proved to be the most successful non-explosive hard patch breaking device tested to date, **Joughin** [60]. **Burrow et al** [61] also concluded that bull-wedging was the most viable hard patch breaking method to assist the impact ripper. In norite a burden of 150 *mm* at a hole distance of 200 *mm* could be broken with a blow energy of 500 J, **Burrow et al** [61]. The specific energy was 16 MJ/m^3 which was 60% higher than that of the COMRO water gun in a water-filled hole. Underground tests carried out by **Buckmaster** [62] at the Doornfontein Gold Mine, determined that a two sided wedge action, Figure 2.17, was more effective than the original conical shape due to the fact that it confined the stress in one plane. It was also proposed that an increase in blow energy would significantly enhance breaking. **Burrow et al** [61] confirmed this during comparative tests using 500 J and 80 J impact hammers. In addition, it was found that by notching the holes the specific energy for bull-wedging was reduced by approximately 15-25%, **Burrow et al** [61].

Both the Darda rocksplitter and radial axial splitter consisted of a feather and wedge assembly which was inserted into the hole and tensioned by a built-on hydraulic cylinder.

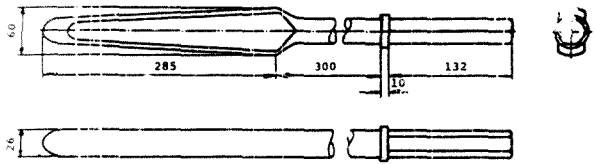


Figure 2.17 : **Two Sided Bullwedge used in Conjunction with Hydraulic Impact Hammer**

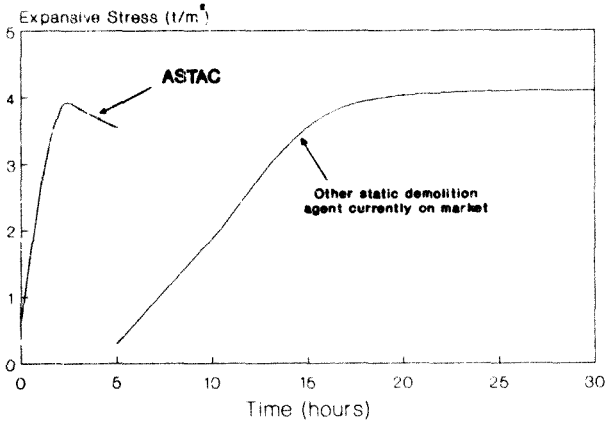


Figure 2.18 : **Setting Behaviour of Expanding Cements**

The Darda rocksplitter had an operating pressure of 50 MPa which resulted in a radial splitting force of approximately 1 MN, **Buckmaster** [62]. The Radial axial splitter had an additional function when compared to the Darda which enabled it to also induce a co-axial pulling force on the rock by reacting against the bottom of the hole, **Anderson et al** [63].

Both systems required a straight and round hole which gave practical difficulties and the feather and wedge assembly had to be greased which caused considerable wear with the unavoidable quartzite dust. Mechanical failures also occurred when the rock was not broken and the devices had to be retracted. For all these reasons the life of the units were short and operating costs were high.

Expanding solids have also been tried, which is a static method due to the long time involved. Special cement mixtures have been developed which generate tensile stresses up to 45 MPa when expanding in a hole, while in the process of hydration and crystallisation. **Burrow et al** [63] found that splotcrete (expanding cement) could break a burden of 200 mm in norite, however after 72 hours there was still fractured norite which could not be barred away. This was due to the "keying" action of the fractured blocks of norite.

Expanding cements may be suitable for pre-fracturing hard patches in quartzite, but only if setting times, presently around 16 hours, can be reduced. This limitation appears to have been overcome by a new product called Astac, which sets off after only 15 minutes, Figure 2.18. Further tests are required to prove the practical application and safety of such a method.

Thermal devices based on external heat sources, are suitable for spalling quartzite using thermal expansion as a full face operation. However, the high specific energy of spalling would require substantial power levels to achieve acceptable mining rates. These power levels could be provided by large gas torches and oxygen burners, but their heat input into the stope would be more than 40 times the geothermal heat flow, **Haase et al** [53]. Even when thermal methods are restricted to the cutting of narrow slots the cutting rate is too low to be of practical use.

One method of mining that has been proposed is the use of electron beams to weaken the rock and then removal of the rock by a ram and plow, Figure 2.19. Although the electron beams show great promise as a means of thermally weakening the rock, they do produce x-rays. This would mean a prohibitive amount of lead shielding would be required to protect personnel. Coupled with their high costs this precludes their use as a practical means of thermally weakening rock, **Fenn** [64].

Fenn [64] summarised the different thermal methods currently available for weakening rock and concluded that none of the techniques suited the problem of thermal weakening unfractured, confined quartzite. However, electrical methods are available now with much greater power capabilities. *Dielectric heating*, Figure 2.20, followed by dielectric breakdown and high current discharge has the potential to break certain types of rock, including quartzite. It operates by first heating the rock in a high frequency electro magnetic field between two electrodes, until a conducting path is generated between the electrodes. This path is then used for a high current discharge which shatters the rock. The principle of electrical energy conversion to heat rock internally warrants further investigation.

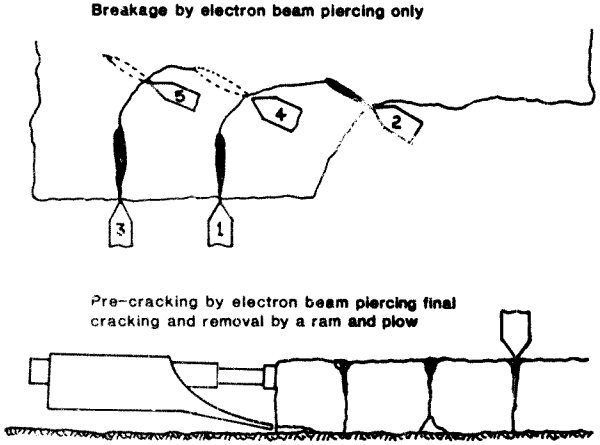


Figure 2.19 : Electron Beam Method of Mining

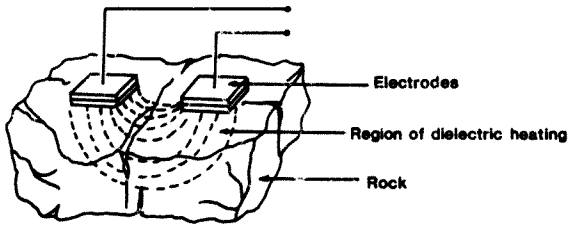


Figure 2.20 : Dielectric Heating of Rock

3.0 EXPERIMENTAL TEST SITE AND EQUIPMENT

The dry abrasive waterjet cutting, slurry abrasive waterjet cutting and diamond circular saw equipment used during surface and underground cutting experimentation is contained in this section. The equipment used during the breaking investigation is also covered.

The test materials, namely; norite and quartzite are described in detail in Section 5, with the design of the experimentation contained in Section 4.

3.1 Dry Abrasive Waterjet Cutting (Up to 240 MPa)

The dry abrasive waterjet cutting, factorially designed experiments were located at the T&DS Surface Test Site, President Steyn Gold Mine.

The equipment consisted of the abrasive waterjet nozzle and traverse mechanism, the high pressure water pumping units, water filtering units and abrasive delivery system, Figure 3.1.

Up to four ADMAC Model 40 DQ high-pressure intensifier pump units were used at once. The diesel-hydraulic power module supplied pressurised hydraulic fluid to drive the intensifier pumps and a separate electro-hydraulic power pack supplied pressurised hydraulic fluid to the linear tracker traverse mechanism. Each intensifier pack was powered by a 160 kW diesel engine and was capable of supplying 19 l/min at 241 MPa.

The dry abrasive nozzle assembly was mounted vertically above the norite test blocks on a hydraulically driven traverse mechanism. The traverse unit was mounted on a wheeled gantry enabling it to be positioned over each norite or quartzite block.

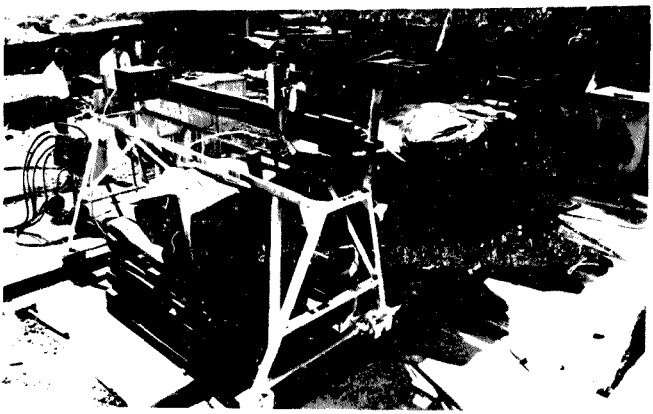


Figure 3.1 : General View of Surface Test Site Equipment

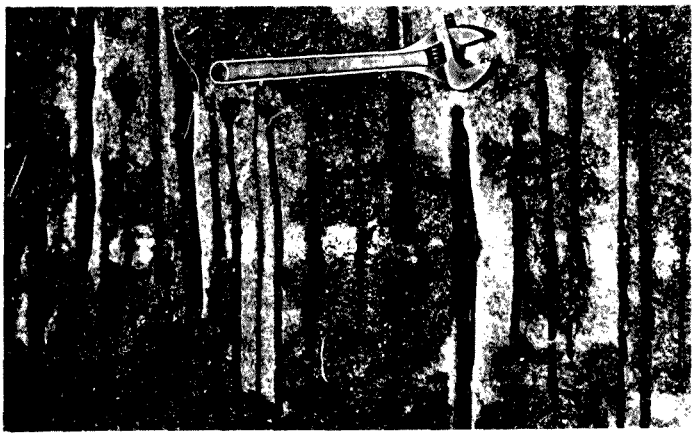


Figure 3.2 : Slots Produced by Abrasive Water Jet Cutting

Two abrasive waterjet nozzle assemblies were used for the tests. One had a volumetric capacity of 20 l/min, which was used for the small (0,89 mm) water orifice tests and the second had a capacity of 100 l/min which was used for the remaining medium (1,4 mm) and large (1,8 mm) water orifice tests.

The high pressure large waterjet orifice test cases called for all four pump units to operate simultaneously. This required 300 l/min of water filtered to 20 microns at a minimum pressure of 450 kPa.

In addition, similar intensifier based dry abrasive waterjet cutting equipment has been investigated underground by T&DS.

The equipment consists of the following four main components:

- electro-hydraulic power module
- intensifier pump unit
- linear tracker
- nozzle assembly

The hydraulic power module supplies pressurised hydraulic fluid to drive the intensifier pumps and power the linear tracker. The four double acting intensifiers provide 13 l/min of ultra high pressure water at 240 MPa to the nozzle.

Figure 3.2 illustrates the slots produced by abrasive waterjet cutting.

3.2 Slurry Abrasive Waterjet Cutting (up to 40 MPa)

As with the dry abrasive equipment the factorially designed experiments carried out with the slurry equipment were located at the T&DS Surface Test Site.

The equipment used to traverse the nozzle and filter the water was the same as that used during the dry abrasive surface test work. The water pressure was generated by a fixed displacement Jetin water pump, capable of delivering 130 l/min at 55 MPa.

The abrasive delivery system, Figure 3.3, consisted of five major components:

- electrically driven water pump
- air driven suction pump
- abrasive hopper with mesh screen
- high pressure storage vessel
- clear plastic catch pot vessel

The operation of the abrasive delivery unit is controlled by manually operated valves which enable three functions to be carried out:

- backwashing or flushing of the high pressure vessel
- charging of the high pressure vessel
- cutting

This abrasive delivery system injects the abrasive into the high pressure water line upstream of the nozzle arrangement. Figure 3.4 shows the slurry nozzle and traverse arrangement during the cutting operation.

3.3 Diamond Circular Saw Cutting

Preliminary underground test work was carried out at President Steyn 1A Ventilation Shaft, 30/41 Crosscut West and subsequently at President Brand 2 Shaft, 60/69, Gold Mines.

The saw used during the experiments was a Longyear 360-H35 hydraulic wall saw, Figure 3.5

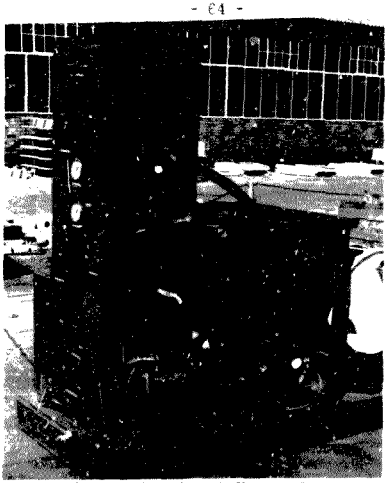


Figure 3.3 : Slurry Abrasive Delivery System

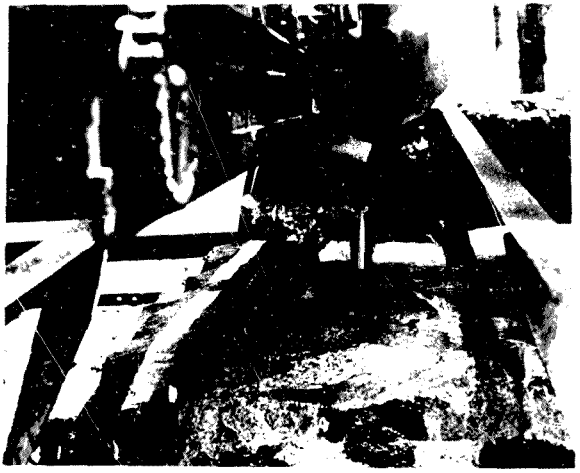


Figure 3.4 : Slurry Nozzle and Traverse Arrangement

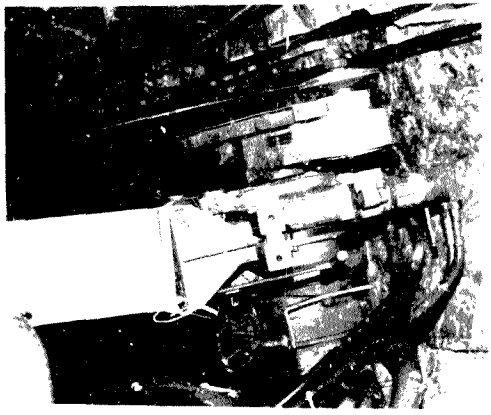


Figure 3.5 : Longyear 360 H35 Wall Saw Unit

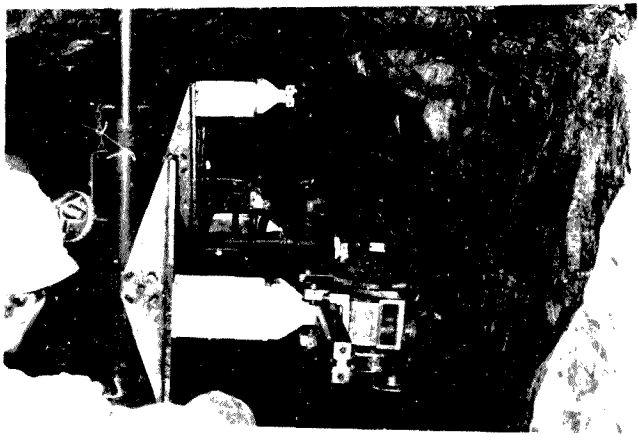


Figure 3.6 : Rig Used to Support Longyear Machine

The saw blade was powered by a Volvo hydraulic motor with a maximum operating pressure of 35 MPa and rotation speed of between 500 and 1 550 rpm.

Traversing of the saw was achieved by using a rack and pinion system, the pinion being powered by a Danfoss OMM32 hydraulic motor capable of delivering consistent saw traverse rates as low as 100 mm/min.

The maximum recommended blade diameter for this unit was 1 350 mm for standard cutting conditions and 1 050 mm for flush cutting.

Hydraulic power to the saw was supplied by a 55 kw Breuninghaus power pack, especially modified by the T&DS Engineering Hydraulic Workshops to supply separate and independent feeds to the blade rotation motor and the saw traverse motor respectively.

The support rig used during these underground trials was the one initially designed for a GDM 30 H Walcut diamond saw tested previously on surface, suitably modified to support the Longyear machine, Figure 3.6.

The rig allowed a number of slots to be cut in a crosscut sidewall before repositioning of the whole structure was required.

The blades used during the initial test work were referred to as the 600/JKM and 800/JKM blades.

The JKM matrix was manufactured by Boart Diamond products for use by the mining industry (e.g. core splitting of quartzite samples), but had not been previously utilised on large diameter blades.

The JKM matrix was made up mainly of a cobalt/bronze alloy.

The impregnated diamonds were of the type SDA 100A + with a coarseness ranging from 25 to 35 US mesh

3.4 Non-Explosive Breaking Equipment

After the slots have been made in the stope face, the breaking method most commonly employed was to remove the broken rock by conventional barring or pointed moils utilising an NPK H60 Hydraulic Impact Hammer, Figure 3.7. This has been successful in highly fractured ground, but in low fractured ground or hard patches it has been found to be ineffectual.

In an attempt to break this type of rock condition in tension, to reduce the specific energy required by the breaking method, two different breaking systems have been investigated; Flowex and Bullwedging. The Bullwedging operations underground is illustrated in Figure 3.8. Both systems utilise a pre-drilled hole and are described in detail under Section 2.4.

3.5 Rig Design

One of the key areas associated with a non-explosive slot based mining system is that of rig design. To date, development has been confined to a captive rig system as part of the abrasive waterjet cutting projects. Figure 3.8 shows the rail which is made up of 2 m rail sections articulated at the joint, so that the rails can move 7 degrees in any direction. Upon the rail, a traverse car moves the nozzles along the rock face. The traverse car consists simply of an electric motor which rotates a drive cog through an hydraulic gearbox. The cog in turn moves the traverse car along a fixed chain which runs the full length of the face. The horizontal support arms enable the rig to be incremented forward by 1 m before a new line of hydraulic props has to be installed.

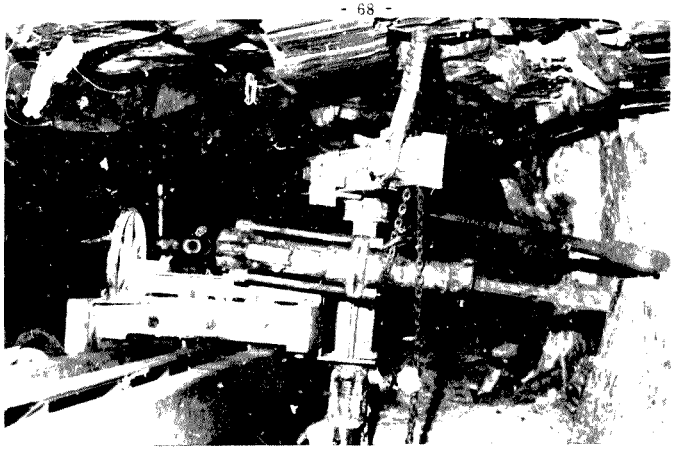


Figure 3.7 : NPK H60 Hydraulic Impact Hammer

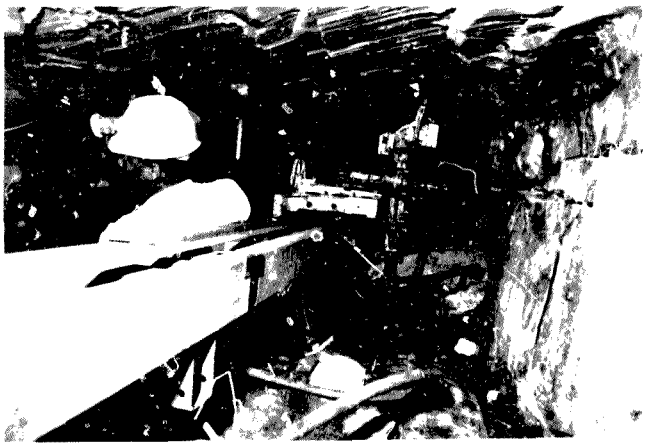


Figure 3.8 : Bullwedging Operation Underground (200 J Blow Energy at 1 400 Blows per Mi...

The advantages of a captive rig system is that it gives better control in following the reef plane and once set up, the cutting cycle is continuous with no further set up time required. It is not clear, as yet, whether a captive rig system would be suitable in conjunction with diamond circular saw cutting. The reason is that rig stability is of a paramount importance when sawing with a diamond impregnated blade. It may be conceivable that a non-captive rig would be preferable, however more work is required in this area.

4.0 EXPERIMENTAL DESIGN AND PROCEDURE

4.1 Dry Abrasive Cutting Work

4.1.1 Design of the experiment

The original design laid out was arranged to involve five variables concerning the operation of the dry abrasive unit and a sixth variable being the block of norite. Since it was felt that 81 runs (slots) would be a practically suitable number to undertake, a one-ninth partial replicate of a 3^6 factorial design was proposed. This meant examining 6 variables at 3 levels each. The experimental design, with test values, is given in Tables 4.1 and 4.2 and the results are presented in Appendix 1.

However, after it was discovered that the larger two sizes of chromite could not be obtained in sufficient quantity or quality to conduct the entire test programme it was agreed to continue with only one abrasive size for the whole series of tests. The nett results of this alteration to the design was a one-third replicate of a 3^5 experiment.

It was decided to take measurements at four positions along each slot and to record the depth achieved after 10 minutes, 20 minutes and 30 minutes spent slotting per metre of slot. These measuring times correspond to 1, 2 and 3 passes at 100 mm/min traverse rate, 2, 4 and 6 passes at 200 mm/min and 4, 8 and 12 passes at 400 mm/min. The results from the 81 run experimentation are contained in Section 6.1. An example of the test sheet used is supplied in Appendix 2.

4.1.2 Use of logarithms of Depth of Cut

It was noted that at high values of Depth of Cut more variability was present in the data, and, as such, values recorded for deeper cuts would be seen as more important than they should.

Table 4.1 : Experimental Variables and Values (Dry Abrasive Cutting Investigation

VARIABLE	VALUES			
1. Pressure	241	172	138	MPa
2. Orifice Diameter	0,89	1,40	1,80	mm
3. Traverse Rate	100	200	400	mm/min
4. Abrasive Mass Flow Ratio	0,10	0,15	0,20	
5. Abrasive Size	700	1 000	1 400	µm

Table 4.2 : Experiment Design (Dry Abrasive Cutting Investigation)

PRESSURE (MPa)	DIAMETER (mm)	WATER FLOW (l/min)	POWER (kW)	ABRASIVE FLOW (kg/min)			LENGTH OF CUT
				R=0,10	R=0,15	R=0,20	
241	0,89	18,1	73	1,9	2,7	3,6	0,5
	1,40	44,8	180	4,4	6,7	8,9	1
	1,80	74,6	300	7,5	11,1	14,9	1
172	0,89	15,4	44	1,5	2,3	3,1	0,5
	1,40	38,1	109	3,7	5,7	7,6	1
	1,80	63,0	181	6,3	9,4	12,5	1
138	0,89	13,8	32	1,3	2,1	2,7	0,5
	1,40	34,1	79	3,3	5,1	6,8	1
	1,80	56,5	130	5,6	8,4	11,3	1

The standard deviation between the recorded cut depths at the four measurement points was calculated for each slot, as well as the mean for each slot. A regression analysis revealed that a highly significant relationship (probability that relationship does not exist <0,0001) exists between the standard deviation and the mean, the equation of prediction being best modelled by:

Standard Deviation of a Slot Depth = 2,092 + 0,045 x Mean of the Slot Depth.

In these circumstances it is indicated that the logarithm should be used as the statistic to be analysed. Accordingly the standard deviation between the logarithms of cut depth at the four measurement points was calculated for each slot, and the corresponding regression analysis showed no significant relationship.

Therefore, use of the logarithm of Depth of Cut as the dependent variable satisfies one of the underlying assumptions of the Analysis of Variance, (i.e. normal and independent distribution of errors).

4.1.3 Determination of experimental error

There are two components of experimental error (variability) present in the data: 1) the variability between measurements within a slot and 2) the variability between slots which cannot be explained by the effects considered to be significant.

The following Analysis of Variance table may be drawn up to identify the sources of variability in logarithms of Depth of Cut:

Table 4.5 : Analysis of Experiment Variance

SOURCE	DEGREES OF FREEDOM	SUM OF SQUARES	MEAN SQUARE
Model (i.e. Explained by Operating Parameters)	19	158,0	8,316
Between Slots Error	223	4,5	0,020
Within Slots Error	729	2,7	0,004
TOTAL	971	165,2	0,170

From this table it may be calculated that the variance within a slot should be estimated as 0,004 and the residual variance between slots should also be estimated as 0,004 (since the mean square for between slots error represents 4 x variance between slots + variance within slots).

Thus any one logarithm of measurement of Depth of Cut would be subject to a variance of 0,008, and the average logarithm of four measurements for a slot would be subject to a variance of 0,005.

The following tables (Tables 4.4 and 4.5) for 95% confidence limits, may then be drawn up, based on these estimates of standard error:

Table 4.4 : Individual Measurements

DEPTH OF CUT (mm)	LOWER CONFIDENCE	UPPER CONFIDENCE
100	84	120
200	167	239
300	251	359
400	334	478
500	418	598
600	502	718

Table 4.5 : Mean for a Slot

DEPTH OF CUT (mm)	LOWER CONFIDENCE	UPPER CONFIDENCE
100	87	115
200	174	230
300	260	346
400	347	461
500	434	576
600	521	691

4.1.4 Investigation of the quartzite/norite ratio and low mass flow ratio

Use of Untransformed Values of Q/N Ratio

From the previous 81 run experimental programme, it was shown that it is necessary to use logarithms of the depth of cut as the statistic to be analysed. It was therefore considered necessary to test whether the logarithm of the Q/N ratio may be the statistic to be analysed.

The standard deviation between the recorded cut depths at the four measurement points was calculated for each slot, as well as the mean for each slot. A regression analysis revealed that no significant relationship (probability that relationship does not exist <0,6985) exists between the standard deviation and the mean. This result indicates that it is not necessary to transform the Q/N ratio data to logarithms for the analysis, and the untransformed data may be analysed.

The design investigating the effect of mass flow ratio and Quartzite/Norite (Q/N) ratio on depth of cut was arranged to encompass the values shown in the following table:

Table 4.6 : Experimental Variables and Values

VARIABLE		VALUES		
Pressure	(MPa)	138	186	228
Orifice Diameter	(mm)	0,89	1,26	1,63
Mass Flow Ratio	(kg/kg)	(0,025) 0,05	0,10	0,20

The original experiment was based on 3 variables at 3 levels giving a full 3^3 factorial design, and hence 27 runs (or slots). After preliminary investigation of the results it was thought that an investigation of a lower mass flow ratio was of interest, and a further 9 runs (at 3 levels of pressure and 3 levels of orifice) were carried out at the 0,025 mass flow ratio.

In order to maintain balanced sets of data and incorporate the 0,025 mass flow ratio data, the 0,20 mass flow ratio data had to be ignored for the secondary analysis. Hence two Q/N ratio models were derived, one for higher mass flow ratios and the other for lower mass flow ratios (see Appendix 3).

4.1.5 Recycling of iron based abrasives

The following tests were designed, using the dry abrasive intensifier based equipment, to demonstrate whether abrasives could cut, be screened, dried and then re-used (i.e. recycled). Both quartzite and chromite were both found not to be amenable to recycling as they were reduced to dust (< 300 μm) after the first cut. Therefore recycling of the abrasives was only carried out for the five best performing iron based abrasives.

Table 4.7 presents the independent variables used throughout the recycling experiments, together with the error levels within which they were maintained.

Table 4.7 : Experimental Variables and Values

VARIABLE	ACTUAL VALUE	UPPER LIMIT	LOWER LIMIT	RROR
Water Pressure (MPa)	241	253	229	± 5
Abrasive Flow Rate (kg/min)	1,2	1,26	1,15	± 5
Traverse Rate (mm/min)	75	79	71	± 5
Standoff (mm)	30	36	24	± 20
Cut Time (mins)	7	7,35	6,7	± 20
Orifice Diameter (mm)	0,81	-	-	-
Focus Tube I.D. (mm)	3,2	3,8	3,2	± 15
Norite Target Block	HOMOGENOUS			
Abrasive	VARIATIONS COMPENSATED BY CHECK ANALYSIS			± 2 max

A 25 kg sample of the abrasive was used and recycled until less than 4 kg remained. The method of retrieval involved collecting the spent abrasive with a magnet, washing through a 300 micron screen and drying. To quantify the size fraction changes occurring in given size bands, a sieve analysis was carried out on the new material and the dried spent abrasive, before it was returned to the system. To assess the repeatability of sieve analysis, two check analyses were carried out.

A visual analysis of the rate of degradation for each abrasive was obtained by successive quartering of the bulk sample to achieve a representative 1.0 gm sample, which was subsequently magnified and photographed.

4.2 Slurry Cutting Work

Since there was very little experience with the Diajet equipment, it was decided to carry out a relatively small factorial experiment, at only 2 levels of each of 4 factors so as not to commit large amounts of time and money before knowing something of the equipments characteristics. This became known as Slurry-Jet Experiment No. 1 and after further experimentation into lower abrasive mass flow ratios and high stand-off distances (Slurry-Jet Experiment No. 2) several other slurry jet experiments were conducted. They are all listed below:

Slurry-Jet Experiment No 1 - Initial experimentation into slurry cutting

Slurry-Jet Experiment No 2 - Further experimentation into slurry cutting

Slurry-Jet Experiment No 3 - Maximum cut depth achievable

Slurry-Jet Experiment No 4 - Effect of jet stand-off distance on cut depth

Slurry-Jet Experiment No 5 - Effect of jet impingement angle on cut depth

Slurry-Jet Experiment No 6 - Determination of the cutting ability of quartzite

Slurry-Jet Experiment No 7 - Abrasive recycling and replenishing tests

Each slurry-jet experiment had some specialised procedure or setting and these are given under the respective slurry jet experiment numbers in Section 6.2.

For each of the tests there was a unique control sheet (Appendix 2) stating values of all the variables specific to that test case. Once the supervisor was satisfied that the variables were set within the limits specified, (Appendix 1), a cut was made across the block.

Formal analyses of mean cut depths were carried out using a computer program. Initial analyses were done with the natural logarithms of the mean cut depths, since it was found that the standard deviation of the cut depth values was, in general, proportioned to the mean (this had also been true for cut depth values from experiments with the dry abrasive equipment). In such circumstances, analysing the logarithms of the depths enables statistically significant effects to be singled out from the general run of non-significant effects.

Where possible the tests were confounded using two separate norite blocks. Confounding is a mathematical technique for dealing with restricted experimental block sizes in large designed experiments. It results in the confusing of some parameter interactions with the effect of the different experimental blocks.

The results obtained during the slurry-jet experimentation are given in Section 6.2.

4.3 Diamond Circular Saw Work

To determine the feasibility of cutting slots in underground quartzites, using a diamond impregnated circular saw blade, a test programme was initiated underground at President Steyn 1A Ventilation Shaft, 30/41 crosscut west. The aim of this test programme was to determine approximate blade costs which could then be used to carry out a preliminary financial evaluation of a diamond saw based slot mining method.

It was initially proposed that a 3-level experiment be carried out, modelled on the experiments used for the abrasive waterjet cutting projects, in which the three variables would be the peripheral blade speed, the blade traverse rate and the depth of cut.

However, shortly after starting this test programme it was discovered that this test philosophy was not suitable for diamond saw blades. In contrast to abrasive water jets, where parameters can be varied independently and still yield meaningful results, the characteristics of the matrix composition virtually eliminates certain variations if one is to stay within the "cutting range" of a specific blade. Hence, a different approach was necessary.

This new approach involved sawing to the maximum possible depth at all times and adjusting the blade peripheral speed and the blade traverse rate, so as to ensure optimum cutting rates. This approach proved successful, with an appropriate set of cutting parameters being determined. It must be kept in mind that the main objective of these initial tests was to determine approximate sawing costs in underground quartzite, therefore, this empirical approach is justified.

During the underground test work carried out at President Steyn 1A Ventilation Shaft, the saw blade jammed occasionally. One of the reasons proposed for this, was the effect of stress on the rock around the blade and the possibility that rock closure may be the cause of blade jamming. It was therefore decided to cut in the high stress panel beside the dry abrasive cutting project at President Brand 2 Shaft to determine the causes of blade jamming.

The results obtained during the diamond circular saw investigations are presented in Section 6.3.

5.0 PROPERTIES OF THE TEST MATERIALS USED

Repeated attempts to obtain quartzite in the unfractured state and in the large size of specimens required for testing, proved unsuccessful. **Fenn** [65], also found difficulty in obtaining large pieces of unfractured quartzite and concluded that an alternative test material would have to be found.

As with **Fenn** [65], a gabbro norite quarried in the Rustenburg, Transvaal area was identified as a suitable alternate test material. The gabbro norite used, is a very hard and abrasive, course grained, igneous rock which has similar properties to those of quartzite.

Quartzite has uniaxial compressive strength values ranging from 150 MPa to 300 MPa; 250 MPa being a representative mean value. The uniaxial compressive strength of quartzite, using a 10 mm diameter ball to indent the rock specimen, is found to be related to the quartz content of the rock, ***Joughin*** [50]. A relatively consta. strength value of about 20 kN is measured when the rock has a quartz content below 75%. An average value for the indentation strength of norite, which has less than 2% quartz is 28 kN. The Moh's hardness of quartzite with a quartz content of approximately 75%, typically of that found in gold mines, is 6-7.

The overall Moh's hardness of the plagioclase felspars and chiopyroxene, the major constituents of norite, is 5-6. Therefore the major difference between the two rock types is that, although they are rocks of essentially similar strengths, quartzite is a far more abrasive material.

Except where some limited tests were carried out in quartzite to determine a quartzite/norite cutting ratio, all surface tests were carried out in gabbro norite blocks.

5.1 Mineralogy of Norite

The mineralogy of 3 samples of norite (A,B and C), determined by thin section, examination and analysis is given in Table 5.1. The samples were taken from three norite blocks (A,B and C), which were used for the 81 run experimentation, see Section 6.1.1.

The rock is best classified as gabbro norite, a plutonic type, commonly associated with differentiated igneous intrusions. The specimens of norite were found to be medium grained and consist essentially of plagioclase type feldspar and of pyroxene. Plagioclase grains are generally well developed, exhibit stubby lathe-shaped or rounded dimensions, and range from 1 to 4 mm in size, the majority being approximately 2.5 mm. The composition of the plagioclase, as determined by extinction angles of twinned crystals, corresponds to that of labradorite.

Norite exhibits a foliation resulting from many of the lath shaped minerals having settled with their long axes sub parallel to each other. A photomicrograph of a thin section is shown in Figure 5.1. This horizontal layering of the grains present in norite gives it a horizontal foliation which is a plane of weakness. Fenn (65), carried out mechanical strength tests on cores orientated at three mutually perpendicular directions, Figure 5.2. Direction Y was perpendicular to the foliation and directions X and Z were parallel to the foliation, perpendicular to one anotner.

The variation in the mechanical properties of norite as a result of the foliation is shown in Table 5.2. At a 95% confidence level, there is no statistically significant difference in the mechanical properties measured in the three mutually orthogonal directions. Therefore it can be concluded that norite can be classed as being relatively homogeneous.



Figure 5.1 : A Photomicrograph of a Thin Section of Norite

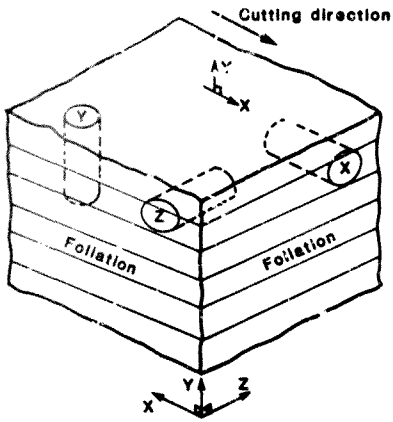


Figure 5.2 : Foliation and Weakness Planes of Norite

Table 5.1 : Mineralogical Assemblage of Norite

SAMPLE NUMBER	ESTIMATED ABUNDANCES OF MINERAL COMPONENTS (Vol.%)						
	Plag.	Orthop.	Clinop.	Myr.	Qtz.	Opq.	Amp.
A	65	17	12	4	1	t	1
B	65	17	13	3	1	t	t
C	66	16	12	5	1	t	t

Abbreviations used in Table 5.1:

Plag. - plagioclase
Orthop. - orthopyroxene
Clinop. - clinopyroxene
Myr. - myrmekite (fine quartz, feldspar intergrowths)
Qtz. - quartz (occurring as discrete grains)
Apaq. - opaques (consisting of ilmenite, magnetite, chalcopyrite and pyrite)
Amp. - amphibole
t. - trace

Table 5.2 : Variations in the Measured Mechanical Properties of Norite According to the Direction of Loading to the Foliation, (after Fenn [65])

MEASURED PROPERTY	NUMBER OF SAMPLES	DIRECTION OF APPLIED STRESS		
		PERPENDICULAR TO FOLIATION (Y)	PARALLEL TO FOLIATION (X)	PARALLEL TO FOLIATION (Z)
Uniaxial Compressive Strength (MPa)	4	203,0 ± 16,9	188,0 ± 45,6	185 ± 21,2
Uniaxial Tensile Strength (MPa)	4	15,0 ± 2,25	13,8 ± 2,72	12,5 ± 2,76
Uniaxial Tensile Strength (MPa)	4	75,5 ± 4,3	74,8 ± 4,8	71,7 ± 6,4

* The standard error of the mean quoted is as a 95% confidence level.

However, care was taken to ensure that the blocks used in the experimental programme were identically orientated in such a way that all the cutting tests were carried out perpendicular and parallel to the foliation as illustrated in Figure 5.2.

5.2 Mineralogy of Quartzite

The mineralogy of the quartzite blocks used on surface to determine the quartzite to norite cutting ratio (see Section 6.1.2) is given in Table 5.3. Three blocks (A,B and C) were used for the surface tests and when they are rigorously classified, fall into the lithic graywacke field. The term "graywacke" implies that the conglomerate rock consists of pebbles cemented together by a matrix content greater than 15%. The term lithic implies the presence of rock fragments such as shale, schist and chert. However, these rocks are generally referred to as quartzites. A photomicrograph of a thin section is shown in Figure 5.3.

Table 5.3 : Mineralogical Assemblage of Quartzite (Tested on Surface)

SAMPLE NUMBER	CLAST TYPES						MATRIX							
	M	qz* P	chert	comp**	shale	fs	qz	ser	clay	chl	py	bi	mt	Ti-ox
A	54	11 1	2	1	2		9	9	4	4	2	-	t	t
B1	37	9 6	10	10	3		10	5	2	t	2	-	-	-
B2	43	26 3	6	-	3		6	5	4	4	t	-	-	-
C	40	7 1	2	-	5		8	21	-	14	t	2	-	-

* M = monocrystalline
P = polycrystalline

** Various combinations of ser + clay, qz + ser, ser + qz + clay, etc. have all been lumped under a single heading "composite". These clasts are often schistose in nature.

Abbreviations used in Table 5.3 :

comp.	-	composite (ser/qz/cla[illegible])
qz.	-	quartz
ser.	-	sericite
fs.	-	feldspar
chl.	-	chlorite
py.	-	pyrite
bi.	-	biotite
mt.	-	magnetite
Ti-ox	-	Ti-oxides
t.	-	tr[illegible]e

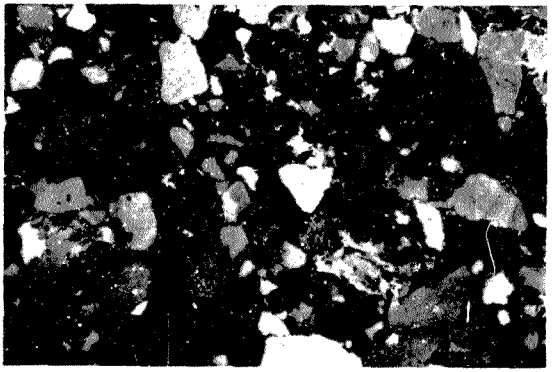


Figure 5.3 : A Photomicrograph of a Thin Section of Quartzite (tested on surface)

To compare the mineral composition of quartzite underground with that of the blocks of quartzite tested on surface, samples of Hangingwall (H), Footwall (F) and Reef (R) were taken in 60/69 *stope, President Brand 2 Shaft.* Three positions of the panel were sampled and analysis was carried out by thin section, Table 5.4.

Table 5.4 : Mineralogical Assemblage of Quartzite Underground (President Brand 2 Shaft, 60/69 Stope)

SAMPLE NUMBER	CLASTS						MATRIX						
	Quartz Mono.	Poly.	Chart	Comp-osite*	Pyro.	Chlorite.	Ser.	Chlr.	Qtz.	Py.	Ti.	Sph.	Zr.
Top-H	80	3	t	13	1	5	<1	t	1	<1	-	-	-
Top-R	32	50	10	-	7	t	-	t	<1	1	-	-	-
Top-F	80	<1	1	-	14	<1	-	t	3	-	t	t	-
Middle-H	89	5	2	-	1	t	1	t	2	t	-	-	t
Middle-R	45	15	-	15	14	-	2	t	-	7	2	-	t
Middle-F	86	1	1	-	8	<1	-	t	2	1-2	-	-	-
Bottom-H	78	5	2	4	6	<1	-	t	4	t	t	-	-
Bottom-R	58	17	8	5	1-2	t	<1	-	2	t	-	-	t
Bottom-F	80	3	3	<1	9	t	2	t	3	t	-	-	-

* Lithic fragments comprising mainly fine-grained quartz and sericite; clay and sericite; minor chert and carbonate and recrystallised volcanic material.

Abbreviations used in Table 5.4 :

mono. - monocrystalline
poly. - polycrystalline
pyro. - pyrophyllite
chlorit. - chloritoid
ser. - sericite
chlor. - chlorite
qtz. - quartz
py. - pyrite
ti. - titanium-oxides e.g. rutile, leucoxene
sph. - sphene
zr. - zircon
t. - trace

6.0 RESULTS AND DISCUSSIONS

The results from the surface and underground test work have been divided into four sections, namely: dry abrasive waterjet cutting, slurry abrasive waterjet cutting, diamond circular sawing and slot-based mining development underground.

The results of the designed factorial experiments carried out on surface using the dry abrasive and slurry abrasive cutting equipment, are presented predominantly in graphical form using data abstracted from tabulated results, Appendix 1. These results have been analysed using **SAS (Statistical Analysis System) Language** [66], prior to the graphs being fitted to the data (see Sections 6.1 and 6.2). To improve the clarity of some of the graphs, only the mean depth of cut values have been plotted instead of the four depths of cut measurements taken, Section 4.

It was considered unlikely that there would be significant high order interactions between the designed factors in the case of these practical experiments under industrial conditions. This meant that the high order interaction mean squares could be used to obtain an estimate of the residual error variance i.e. no actual replication of individual experiments was carried out.

According to **Brownlee** [67], high order interactions between factors are a "very rare occurrence" in industrial experiments.

The results, using the diamond circular saw equipment have been analysed empirically and are contained in Section 6.3. In parallel to the research carried out on surface and underground, development of the slot-based mining method has been undertaken and the results achieved to date are summarised in Section 6.4.

6.1 Dry Abrasive Waterjet Cutting

The test programme (see Section 4.1) for the 81 run experimentation, investigated the influence of pressure, orifice size, abrasive mass flow ratio (MFR) and exposure time on depth of cut. **Hashish** [68] has also identified abrasive type and particle size as having a large influence on depth of cut. Chromite due to its availability and low cost, associated with good performance, was chosen as the test abrasive throughout the 81 run experimentation. **Hashish** [69], also found that for rock cutting, the particle size of an abrasive should be as large as possible to maximise depth of cut. AFS 31 (American Foundry Size 31) chromite of 700 μm nominal particle size, was the largest size available in sufficient quantities, and was used throughout the test programme.

From the 81 tests carried out, Figures 6.1 to 6.4 were obtained (only the mean data points from Appendix 1 have been plotted). As expected the depth of cut increases with increasing pressure, orifice and exposure time but in each case, levels off at high values. For pressure and orifice size this is probably due to the decrease in efficiencies of the waterjet orifice and hydraulic components as pressure or water flowrate increases.

Increasing the exposure increases the depth of cut but reduces significantly as the effect of stand-off distance and jet friction with the sides of the slot, become more prominent with greater depth.

6.1.1 Prediction formula for the depth of cut achieved with a dry abrasive entrained waterjet

Based on the data obtained from the above experimentation a depth of cut model was derived.

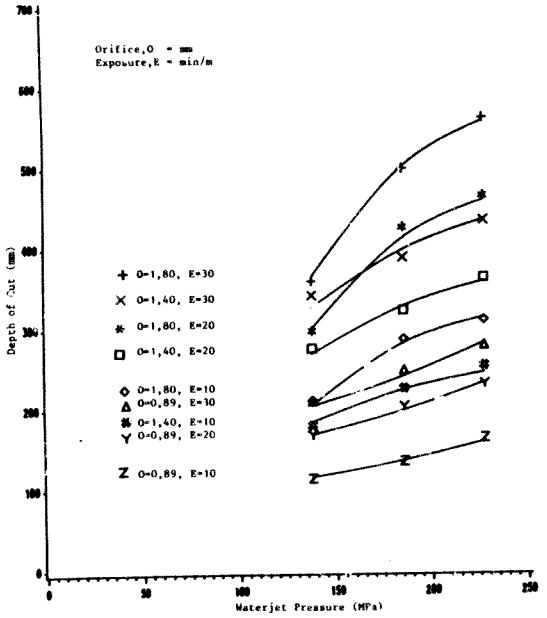


Figure 6.1 : The Effect of Water Pressure on Depth of Cut in Norite

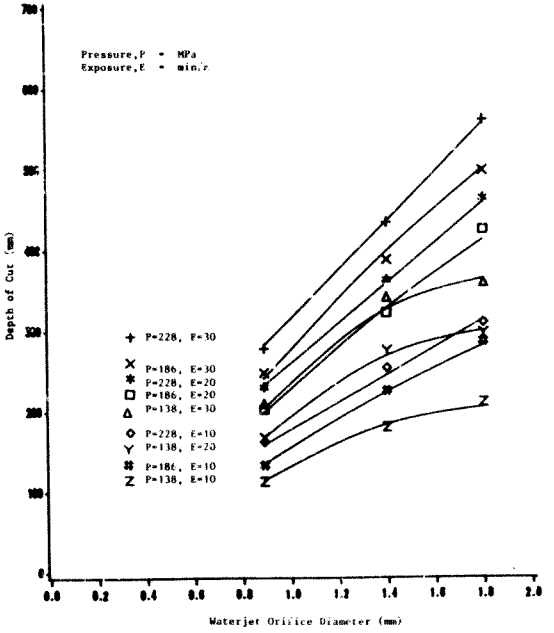


Figure 6.2 : The Effect of Orifice Size on Depth of Cut in Norite

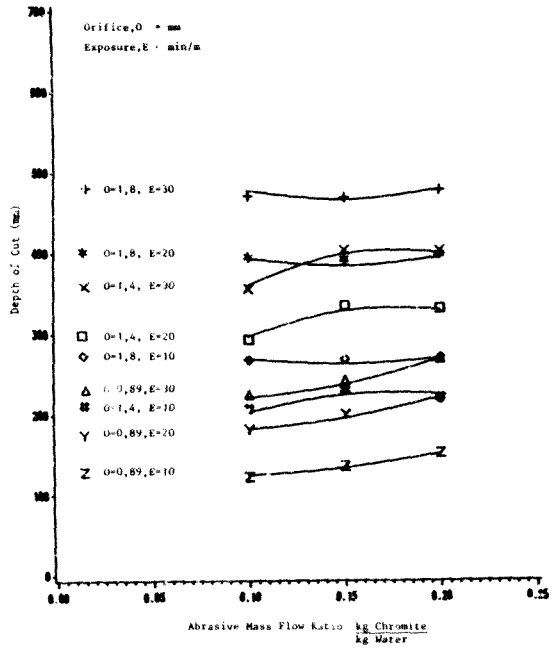


Figure 6.3 : The Effect of MFR on Depth of Cut in Norite

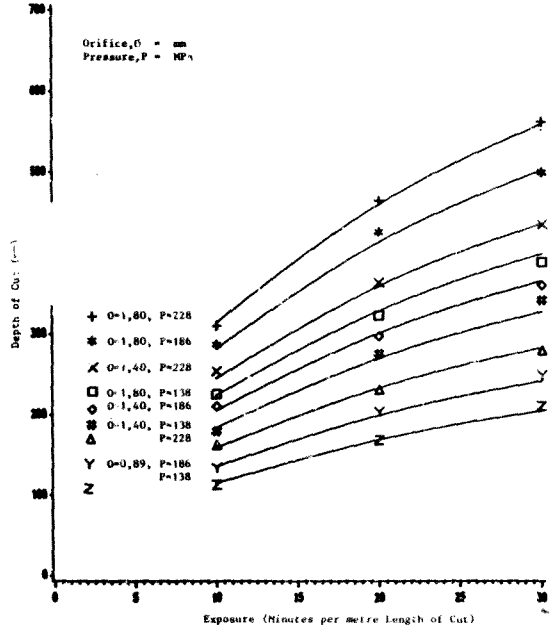


Figure 6.4 : The Effect of Exposure Time on Depth of Cut in Norite

This model represents the best fit to the data and contains all the main effects and interaction effects discovered to be significant in affecting the natural logarithm of depth of cut.

Depth of Cut Model

$$
\begin{aligned}
\ln(\text{Depth of Cut}) = {} & 5{,}600 \text{ (Mean for Experiment)} \\
& +0{,}173\ P - 0{,}055(P^2 - 2/3) \\
& +0{,}334\ O - 0{,}137(O^2 - 2/3) \\
& +0{,}053\ R \\
& -0{,}025\ T \\
& +0{,}287\ E - 0{,}094\ (E^2 - 2/3) \\
& +0{,}024\ P.O - 0{,}051(P^2 - 2/3)O \\
& +0{,}044\ P.(O^2 - 2/3) \\
& -0{,}020\ P.R \\
& -0{,}048\ O.R + 0{,}075(O^2 - 2/3)(R^2 - 2/3) \\
& -0{,}062\ (O^2 - 2/3)(T^2 - 2/3) \\
& +0{,}047\ R.(T^2 - 2/3) \\
& -0{,}030\ T.E.
\end{aligned}
$$

where P,O,R,T, and E take the values -1,0 or 1, according to the following correction equations for real variables:

Pressure, P (MPa) = $-3{,}026 + 0{,}0101\ \text{Pressure} + 0{,}000033\ \text{Pressure}^2$

Orifice, O (mm) = $-2{,}007 + 0{,}604\ \text{Orifice} + 0{,}5925\ \text{Orifice}^2$

Mass Flow Ratio, R (kg/kg) = $-3{,}000 + 20{,}0\ \text{Ratio}$

Traverse Rate, T (mm/mm) = $-2{,}333 + 0{,}015\ \text{Traverse} - 0{,}0000167\ \text{Traverse}^2$

Exposure, E (min/m of rock) = $-2{,}000 + 0{,}10\ \text{Exposure}$

For a given waterjet pressure, orifice diameter, traverse rate, exposure time and abrasive mass flow rate the model computes the natural logarithm of the depth of cut that such a system would achieve in norite. It can also be used as a analytical tool to predict the actual depth of cut the equipment would achieve at different operating parameters.

6.1.2 Determination of quartzite/norite (Q/N) ratio

For the determination of depth of cut in quartzite mass flow ratios of 0,05, 0,10 and 0,20 were investigated. The predicted depth of cut in norite was obtained from the depth of cut model, which was conducted at mass flow ratios of 0,1, 0,15 and 0,20. Since the mass flow ratios for both sets of experiments are similar then a good prediction for the Q/N ratio may be obtained (for the range of mass flow ratios considered).

The mean Q/N ratio was found to be 1,063, Table 3.1. That is, an increased mean depth of cut of 6,3% in quartzite. The 95% confidence limits for the overall Q/N ratio is 1,063 ± 0,218 which means that the depth of cut in norite is not significantly different from that of quartzite.

Table 6.1 : Effect of Quartzite Block on Q/N Ratio

QUARTZITE BLOCK	MEAN Q/N RATIO FOR BLOCK
A	0,964
B	1,093
C	1,132
Overall Mean	* 1,063 ± 0,218
* At the 95% confidence limit	

The two different models for Q/N ratio, from Appendix 3, were applied to the depth of cut model derived from the earlier experimentation and a series of graphs obtained, Figures 6.5 to 6.12 (only the mean data points from Appendix 1 have been plotted).

The effect of the following parameters for low and high mass flow ratios (MFR's) were modelled:

Waterjet pressure	(Figures 6.5 and 6.6)
Orifice diameter	(Figures 6.7 and 6.8)
Abrasive MFR	(Figures 6.9 and 6.10)
Exposure time	(Figures 6.11 and 6.12)

Due to the effect of mass flow ratio, the set of curves obtained are generally higher for the high mass flow ratio than for the low mass flow ratio. The low MFR = 0,025 and the high MFR = 0,20.

In the following discussion the meaning of the descriptive terms "low", "middle" and "high" (or "large") are as shown by Table 6.2.

Table 6.2 : Descriptive Terms ("Low", "Middle" and "High")

VARIABLE	VALUES		
Pressure MPa	138	186	228
Orifice mm	0,89	1,26	1,63
Exposure min/m	10	20	30
Descriptive term	Low	Middle	High or Large

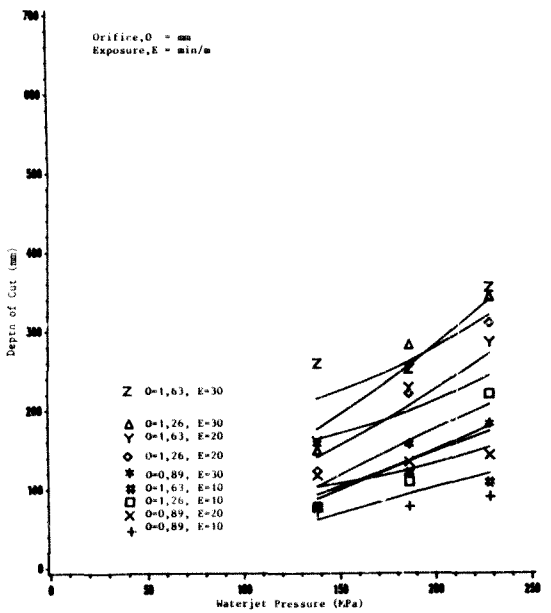


Figure 6.5 : **The Effect of Water Pressure on Depth of Cut in Quartzite (Low MFR Model)**

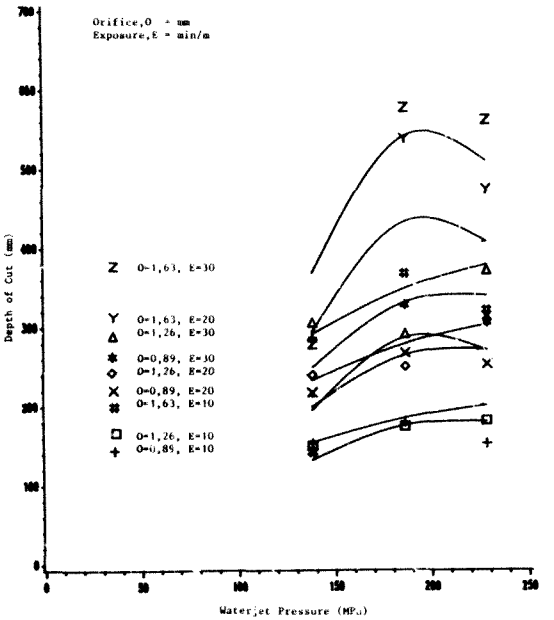


Figure 6.6 : **The Effect of Water Pressure on Depth of Cut in Quartzite (High MFR Model)**

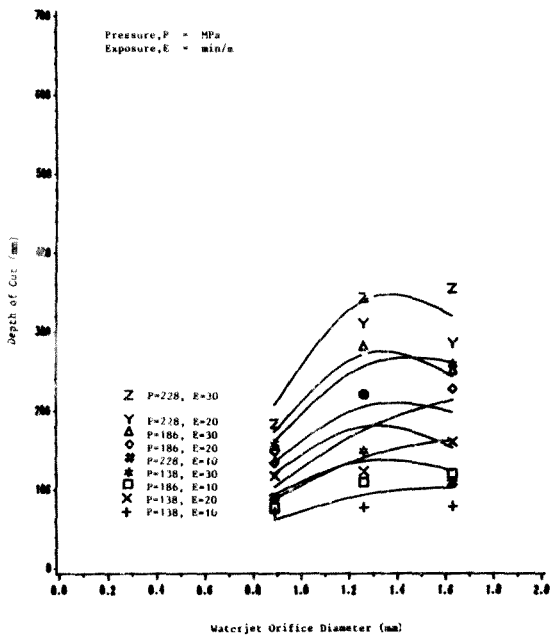


Figure 6.7 : The Effect of Orifice Size on Depth of Cut in Quartzite (Low MPR Model)

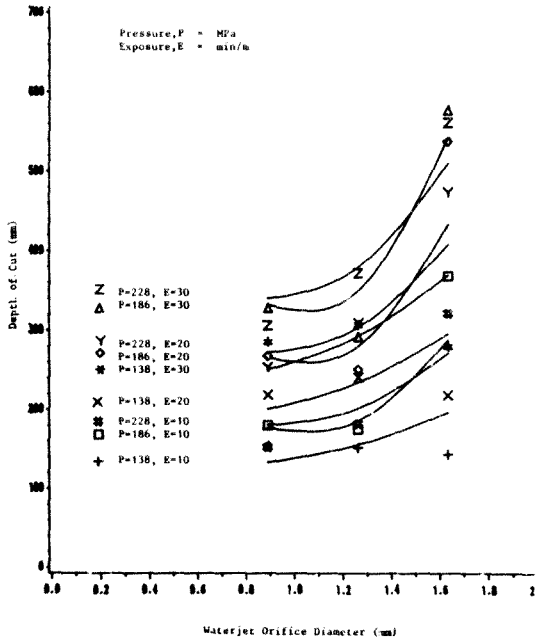


Figure 6.8 : The Effect of Orifice Size on Depth of Cut in Quartzite (High MPR Model)

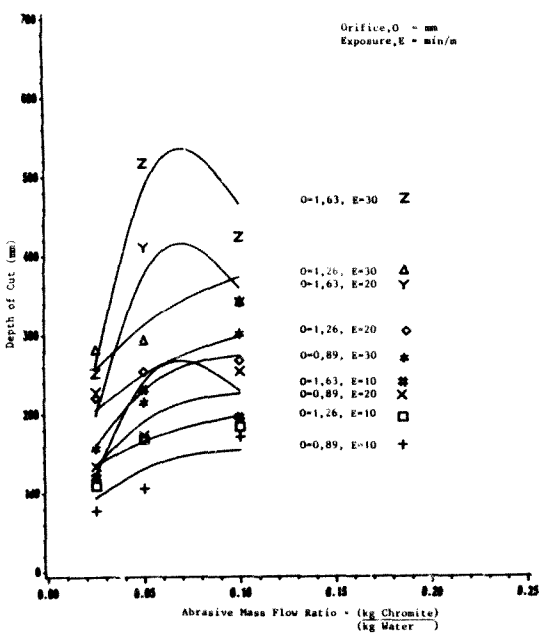


Figure 6.9 : The Effect of MFR on Depth of Cut in Quartzite (Low MFR Range, Pressure = 196 MPa)

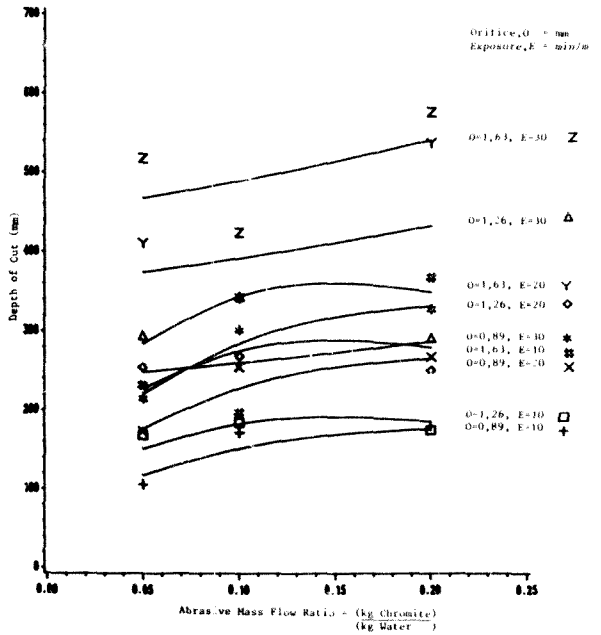


Figure 6.10 : The Effect of MFR on Depth of Cut in Quartzite (High MFR Range, Pressure = 196 MPa)

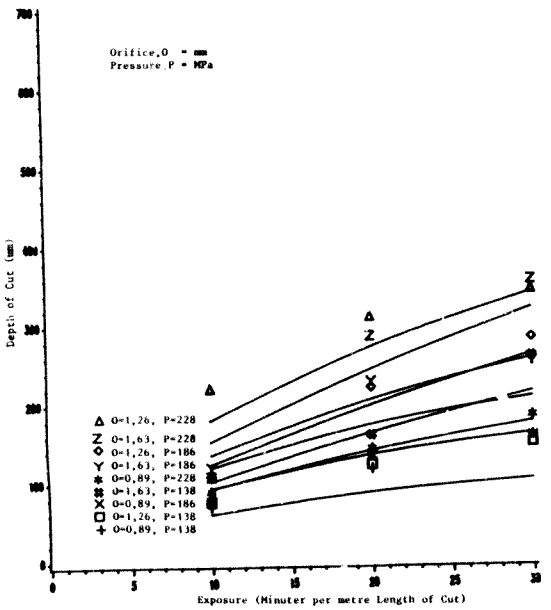


Figure 6.11 : The Effect of Exposure Time on Depth of Cut in Quartzite (Low MFR Model)

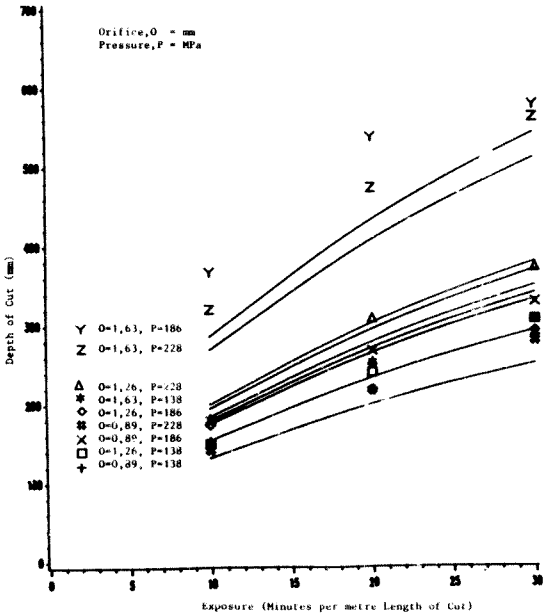


Figure 6.12 : The Effect of Exposure Time on Depth of Cut in Quartzite (High MFR Model)

Effect of Waterjet Pressure (Figures 6.5 and 6.6)

For the low MFR model increasing the pressure increases the depth of cut. At the low and middle orifices and for a fixed exposure time, the effect appears to be almost linear. At the high orifice diameter the effect is more marked when increasing from the middle to the high pressure.

For the high MFR model, increasing the pressure from the low value to the middle value increases the depth of cut. Increasing the pressure from the middle to the high value gives a decrease in the depth of cut at the high orifice diameter, and either a small increase or no increase in the depth of cut is observed at the low and middle orifice diameters.

Effect of Orifice (Figures 6.7 and 6.8)

For the low MFR model (Figure 6.9) at the low pressure, increasing orifice diameter gives an increase in depth of cut. The rate of increase of depth of cut increases with exposure time. (See the bottom, second from bottom and fourth from bottom curves, Figure 6.9).

At the middle and high pressures, increasing the orifice diameter from 0,89 to 1,26 mm increases the depth of cut, but then increasing the orifice diameter from 1,26 to 1,63 mm either reduces the depth of cut or it remains unchanged.

For the high MFR model (Figure 6.10) at the low and high pressures, increasing the orifice diameter gives an increase in the depth of cut, this increase being more marked by increasing the orifice diameter from the middle to high diameter.

A similar effect is found to occur at the middle pressure, except that the increase in depth of cut obtained by increasing the orifice diameter from the low to the middle diameter is small, and then increasing to the large orifice diameter gives a very marked increase in the depth of cut.

Effect of Abrasive Mass Flow Ratio (Figures 6.9 and 6.10)

The low and high MFR models overlap in the mass flow ratio range of 0,05 to 0,10 (see Appendix 3). Therefore it is here that a direct comparison of the two models can be made.

At the high orifice diameter the depth of cut is found to increase linearly with ratio according to the high MFR model, but with the low MFR model the depth of cut decreases with ratio in the 0,05 and 0,10 range.

Apart from this difference the graphs are quite similar in the 0,05 to 0,10 ratio range, with depth of cut decreasing with decreasing ratio, and the order of the curves being similar.

In the high MFR model the curves are fairly flat, and in the low MFR model the curves are found to be more steeply sloping. This shows that the effect of ratio on depth of cut becomes more marked at the lower (0,025 to 0,05) range.

When deciding on a choice of models then the obvious distinction should be made between the high and low MFR models. When deciding on a choice of model for a "middle" MFR then either model may be chosen.

Effect of Exposure (Figures 6.11 and 6.12)

For both mass flow ratios, increasing the exposure time from 10 to 20 to 30 minutes per metre length of slot increases the depth of cut.

Generally the rate of increase of depth of cut increases with pressure and orifice diameter (the curves are generally steeper). However for the high MFR model, increasing the pressure from 186 MPa to 228 MPa, at the large orifice diameter decreases the depth of cut (see the top two curves, Figure 6.8).

For the low MFR model, the middle orifice diameters gives a greater depth of cut than the larger orifice diameter at the middle and high pressures (see the top four curves, Figure 6.7).

The high MFR model (Figure 6.8) generally has steeper curves than the low MFR model (Figure 6.7) showing that the effect of exposure is more marked at the high mass flow ratios.

Both the low and high MFR models show steeper curves with increasing orifice and pressure, showing that the effect of exposure is more marked at higher orifice diameters and pressures.

6.1.3 Non linear effect of mass flow ratio (MFR) on cut depth

By expressing the depth of cut using chromite abrasive, achieved at various mass flow ratios (0,025, 0,05 and 0,1), as a percentage of the maximum depth of cut achieved at the highest mass flow ratio (0,2), Figure 6.13 is obtained. The curve is of the type $y=100 - Ae^{-Bx}$ and was fitted to the observations by the method of least squares.

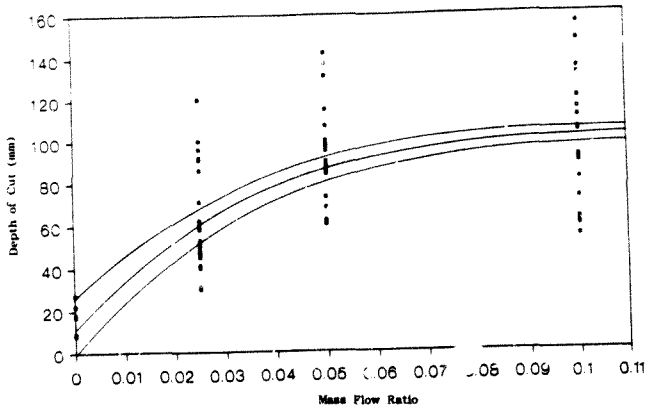


Figure 6.13 : **Effect of MFR on Depth of Cut in Norite, Expressed as a Percent of the Maximum Depth of Cut Achieved in Norite**

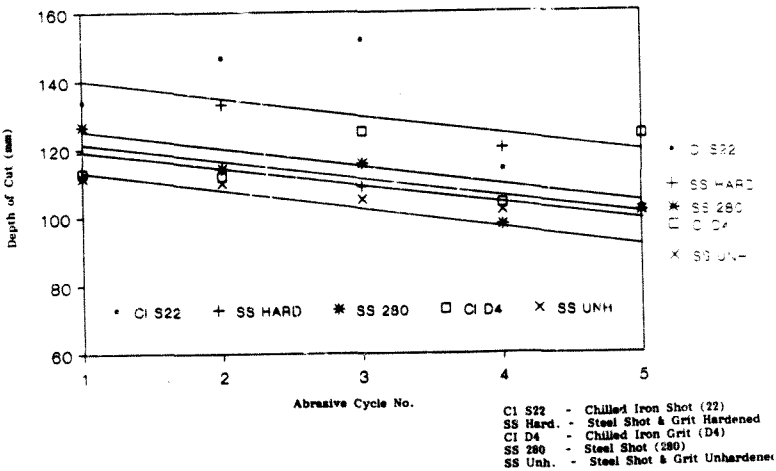


Figure 6.14 : **Effect of Cut Number (number of times abrasive has been re-used) on Depth of Cut in Norite**

For the purpose of evaluation, from a practical context, the expected cut-depth with a mass flow ratio of 0,075 kg/kg is 95% of the maximum, and there is only a 1 in 40 chance that this figure is as low as 91%. There is also a 1 in 40 chance that the figure is as high as 99%.

There seems little point in using an abrasive mass flow ratio above 0,075 for dry abrasive cutting, because above this figure the curve flattens out and small improvements in depth of cut are achieved by large increases in MFR. This is later substantiated from the findings of the slurry abrasive work (see Section 6.2.2).

6.1.4 Recycling of iron based abrasives

On observation of the shot blasting process at the T&DS workshops, the use of iron based abrasives, as cutting abrasives was proposed. It was found that their performance was better than that of chromite and in addition appeared to be amenable to recycling, as in the shot blasting process.

A test programme (Section 4.1.5) was initiated to evaluate the effect of recycling abrasives on depth of cut.

Six iron based abrasives were tested during the experimental programme:

- chilled iron shot 22
- steel shot 280
- chilled iron grit D4
- steel shot and grit (water quenched)
- steel shot and grit (as produced)
- steel shot mixture (110 and 280)

The properties of the various iron based abrasives are given in Table 6.3 and their respective mean depths of cut are presented in Table 6.4. The steel shot mixture and the chilled iron shot 22 are the worst and best performers respectively. The remaining abrasives, although not showing a significantly different mean depth of cut, form two significantly different groups (B and C). As a result of the poor cutting performance of the steel shot mixture (110 and 280), it was decided to dismiss this abrasive for the recycling tests.

Table 6.3 : **Properties of Various Iron Based Abrasives**

SUPPLIER	ABRASIVE NAME	BULK DENSITY g/ml	WEIGHTED MEAN SIZE μm	CRYSTAL TYPE	PARTICLE SHAPE	GENERAL CLASSIFICATION
WELLAMBIE ABRASIVES	CHILLED IRON SHOT 22	4,03	850,2	CUBIC	SPHERICAL SUB-SPHERICAL	* SHOT
WELLAMBIE ABRASIVES	CHILLED IRON GRIT D4	3,84	890,6	CUBIC	ANGULAR SUB-ANGULAR	* GRIT
STANDARD BRASS	STEEL SHOT AND GRIT (WATER QUENCHED)	3,90	831,7	CUBIC	5% SPHERICAL SUB-SPHERICAL 95% ANGULAR	GRIT
STANDARD BRASS	STEEL SHOT AND GRIT (AS PRODUCED)	3,90	790,0	CUBIC	5% SPHERICAL SUB-SPHERICAL 95% ANGULAR	GRIT
THOMAS FOUNDRY	STEEL SHOT 280	4,72	872,1	CUBIC	SPHERICAL SUB-SPHERICAL	SHOT

*PHOTOGRAPHIC ANALYSIS CARRIED OUT (SEE FIGURES 6.14 AND 6.15).

Table 6.4 : Related Significance of Mean Depth of Cut at the 95% Confidence Level

ABRASIVE	MEAN DEPTH OF CUT (mm)	SIGNIFICANCE
Steel Shot Mixture (110 and 280)	105,9 ± 15,0	A
Steel Shot & Grit (as produced)	115,9 ± 16,2	B
Steel Shot & Grit (water quenched)	120,0 ± 12,6	B
Chilled Iron Grit D4	134,4 ± 10,2	C
Steel Shot 280	138,1 ± 9,6	C
Chilled Iron Shot 22	148,7 ± 12,0	D
Abrasives with the same letter are not significantly different in terms of mean depth of cut at the 95% confidence level.		

The most desirable properties of an abrasive are large particle size and high density, **Splaine et al** [70]. A spherical shaped abrasive, by virtue of the fact that maximum mass is contained within minimum surface area, therefore ameliorates these characteristics. From the photographs of abrasive degradation and observed depths of cuts, there exists a correlation between "roundness value" for an abrasive and its depth of cut, although further work will be required in this area before actual values can be concluded.

The sieve analysis is presented in Appendix 5 and the depth of cut results are given in Table 3, Appendix 1. The analysis implies that the mean particle size of the abrasive reduces with successive cutting cycles, although the standard deviation of the mean suggests there is a great deal of variation about this value.

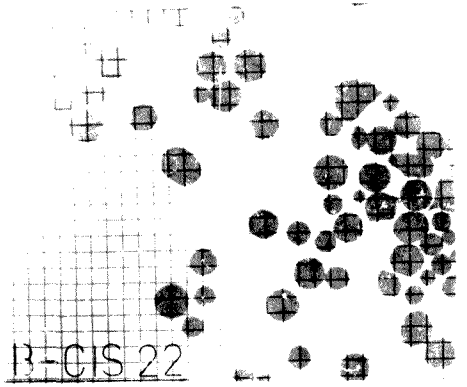
From Appendix 5, it can be shown that this loss in mean particle size of an iron based abrasive is equivalent to 15,9 microns per cutting cycle. From the kinematic model, **Splaine et al** [70], the loss in depth of cut, due to loss in mean particle size, may be determined. This value is calculated as 3,2% loss in depth of cut per cutting cycle.

By grouping all the data for the depths of cut together and assuming that the rate of reduction in depth of cut per cycle is the same for each iron based abrasive, the composite suggests a 99% significant reduction in depth of cut of 3,4 mm (2,8% ± 1,8%) per cutting cycle, as illustrated in Figure 6.14. This equates closely to the value calculated from the kinematic model, **Splaine et al** [70]. Hence, the reduction in depth of cut appears to be explained by the reduction in mean particle size of the abrasives.

Although all five abrasives were photographically analysed, only two series of photographs are included in the text since they are representative of the two major classifications of abrasive investigated, namely shot and grit, Figure 6.15 and 6.16 respectively.

With reference to Figure 6.15 and 6.16, chilled iron shot 22 and chilled iron grit D4 respectively, the greater rate of degradation of the chilled iron shot 22 is evident. These observations of abrasive degradation are consistent with the larger size particles abrading over successive cycles to produce smaller size chips.

When considering particle shape, it has been found that spherical or sub-spherical particles degrade at a lesser rate than angular particles, which themselves tend eventually to sub-spherical shapes. It would appear therefore that the minimum generation rate of fines is associated with spherical particles.



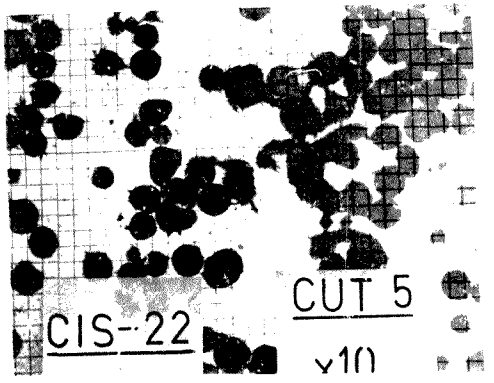
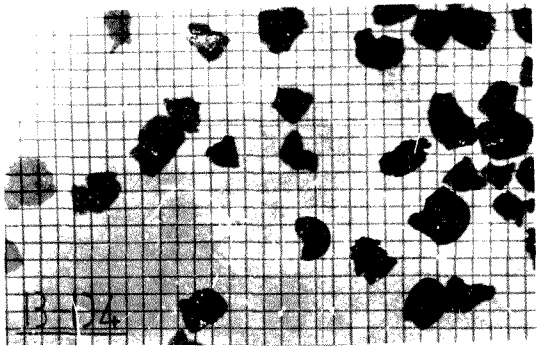


Figure 6.15 : Photographic Analysis of the Degradation of Chilled Iron Shot



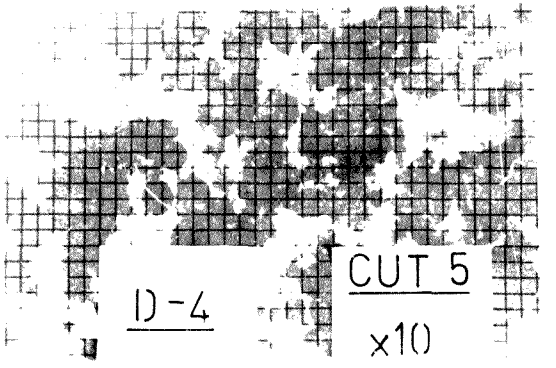


Figure 6.16 : Photographic Analysis of the Degradation of Chilled Iron Grit

6.2 Slurry Abrasive Waterjet Cutting

As mentioned in Section 4.2, the slurry-jet experiments were split into 7 separate sections. As a result, the specialised procedure, along with the results of each experiment and discussion are contained separately for each slurry jet experiment number. All results obtained during the slurry jet experimentation are contained in Appendix 1.

6.2.1 Slurry-Jet Experiment No 1 - initial investigation

Table 6.5 shows the chosen factors with their selected levels.

Table 6.5 : Experimental Variables and Values (Slurry-Jet Experiment No 1

	Symbol	Low Value	High Value
Pressure	A	20 MPa	39 MPa
Orifice Diameter	D	2,4 mm	2,8 mm
Mass Flow Ratio	C	0,2 kg/kg	0,4 kg/kg (nominal)
Stand-off Distance	B	20 mm	100 mm

The resulting 16 trials were confounded in 2 blocks of 8 trials each, each block of 8 trials being carried out in a different block of norite. The confounded effect was AxBxCxD.

In each trial, 2 passes were executed within the slot for that trial, to determine an estimate of the effect of exposure time on cut depth. Four measurements of the depth of cut were made after each pass within each slot of the experiment.

Table 1, Appendix 4, shows the results of the initial analysis for the cut depths after one exposure (or pass). The effects of single factors and interactions that were significant at least at the 95% level, are shown below :-

Main effect	A	Pressure
Main effect	C	Mass Flow Ratio
Main effect	D	Orifice
Interaction effect	AxD	Pressure x Orifice
Interaction effect	BxD	Stand-off x Orifice

Table 2, Appendix 4, shows the results of the initial analysis for the cut-depths after two exposures (again using natural logarithms). The significant effects are shown below :-

Main effect	A	Pressure
Main effect	C	Mass Flow Ratio
Main effect	D	Orifice
Interaction effect	AxD	Pressure x Orifice
Interaction effect	AxBxD	Pressure x Stand-off x Orifice

The above two lists are very similar and, since the 3-factor interaction AxBxD incorporates the 2-factor interactions which appear, AxD and BxD, and also two of the main effects, A and D, Tables 3 and 4, Appendix 4, are presented in identical format.

Tables 3 and 4, Appendix 4, show the behaviour of three main factors (excluding Mass Flow Ratio) and their interactions in terms of the appropriate mean depth of cut, for the first and second exposures respectively.

Also shown is the main effect of each of the four factors in the design, for each of the respective exposures. These numbers show the effect on the depth of cut of increasing from the low o the high setting, and whether or not each effect is found to be significant.

Since the main effect C (Mass Flow Ratio) did not interact significantly with any of the other factors, only its main effect is shown.

The effect of Mass Flow Ratio, when averaged over the two exposures, was a reduction in cut-depth of only 6,4% for a reduction in Mass Flow Ratio of 50% from the high value to the low value. This suggested that it may be possible to use lower abrasive flow rates without losing too much depth of cut, as had been the case with the dry abrasive waterjet cutting.

The effects and interactions involving Pressure and Orifice diameter were more or less as expected, from experience gained during the dry abrasive work, and Tables 3 and 4, Appendix 4 quantify the behaviour of the Slurry-Jet equipment for the factor ranges examined.

The only equivocal results that emerged were those related to Stand-off distance. It would be expected that cut-depths would fall off with increasing Stand-off distance, but examination of Table 3, Appendix 4, shows several instances of this expectation being reversed.

The net effect over the whole of Tables 3 and 4, Appendix 4, is a positive value of 5,2 mm (increase) in cut depth for an increase in Stand-off distance from 20 mm to 100 mm (although, from Tables 1 and 2, Appendix 4, this amount is not statistically significant even at the 75% level).

6.2.2 Slurry-Jet Experiment No 2 - further investigation

Following the previous discussion, it was decided to run a second, similar factorial experiment, with the same factors but at different levels for Mass Flow Ratio and Stand-off distance, as shown in Table 6.6.

Table 6.6 : Experimental Variables and Values (Slurry-Jet Experiment No 2)

	Low Value	High Value
Pressure	20 MPa	39 MPa
Orifice Diameter	2,4 mm	2,8 mm
Mass Flow Ratio	0,075 kg/kg	0,15 kg/kg(nominal
Stand-off Distance	100 mm	400 mm

The 16 trials were again confounded in the same 2 blocks of norite, 8 trials in each. Again, 2 passes were executed in each slot, and four measurements of cut depth were made after each of the two passes.

Preliminary study of the results from the completed experiment showed that the intended values of Mass Flow Ratio had not been achieved in 5 out of the 16 trials. This resulted in the "loss" of 4 out of 8 paired comparisons between low and high values of Mass Flow Ratio. Even worse, 2 out of the "lost" 4 paired comparisons had their "low" and "high" values reversed from the designed values. It was concluded that there was some instability in the control of Mass Flow Ratio at these new, low settings of the control valves.

The net result of these actual values of Mass Flow Ratio was that the experimental design (as achieved) was no longer balanced and symmetrical, such that the formal analysis of results by computer program should not be carried out, even for the effects of the other factors in the experiment.

Ad hoc, manual methods were devised to extract useful conclusions in respect of Mass Flow Ratio at these new, low values, and Stand-off distance at these new, high values.

(i) Effect of Mass Flow Ratio on Cut Depth

Mean cut depths (for the 2nd exposure) were plotted against Mass Flow Ratio achieved and are shown in Figure 6.17 with different symbols for each of the four combinations of Pressure and Orifice diameter (only the mean data points have been plotted).

Equivalent data from the first slurry-jet experiment was then added to the graph. It can be seen that curves of the type $y = A(1-e^{-Bx})$ can be fitted to each of the four sets of symbols on the graph, thus providing a coherent picture of the effect on cut-depth of Mass Flow Ratio over the whole range of that factor in both the first and second experiments.

The regression of depth of cut against Mass Flow Ratio indicates an approximate abrasive to water Mass Flow Ratio of 0,15 kg/kg to obtain 90% of the maximum depth of cut achievable at a given setting. This is twice the figure required by dry abrasive cutting and with flowrates of approximately 60 l/min this could mean as much as 4 times the abrasive consumption.

For completeness, a similar graph to that in Figure 6.18 was constructed for cut depths against Mass Flow Ratio for values after the 1st exposure, Figure 6.18. Figure 6.18 shows the same, coherent patterns as those in Figure 6.17, with, of course, reduced cut depths (only the mean data points have been plotted).

(ii) Effect of Stand-off distance on Cut Depth

Of the 8 possible paired comparisons between low and high Stand-off distances, 4 were found to have very similar values of actual Mass Flow Ratio. These 4 pairs were used to estimate the effect on cut depth of increasing the Stand-off distance from 100 mm to 400 mm.

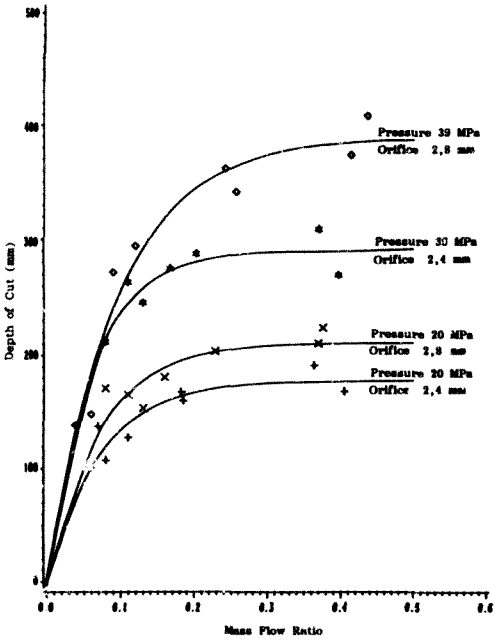


Figure 6.17 : Effect of MFR on Depth of Cut in Norite (second exposure)

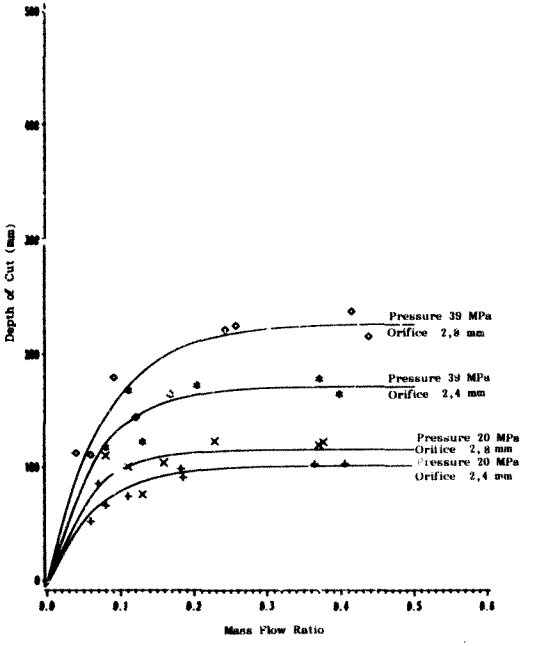


Figure 6.18 : Effect of MFR on Depth of Cut in Norite (first exposure)

The "raw" effect in each paired case (expressed as % reduction in cut depth) was adjusted to allow for the small difference between the nominally identical Mass Flow Ratios by reference to the curves in Figures 6.17 and 6.18. The results of these comparisons are shown in Table 6.7, for both first and second exposures. The overall mean reduction in cut depth was 20,2% for the 8 observed values, corresponding to an increase in Stand-off distance of 300 mm.

The practical advantages of this phenomenon with regards to slotting an irregular face underground are obvious when optimisation of depth of cut and hence advance rate is at a premium. Problems which are being experienced at present, in maintaining a low Stand-off distance underground with the dry abrasive cutting equipment would be greatly reduced when utilising slurry abrasive cutting.

6.2.3 Slurry-Jet Experiment No 3 - maximum cut depth achievable

These tests were conducted with the aim of determining the ultimate cut depth achievable with the slurry jet equipment, given that cutting time was no object.

The tests were started with a 2,8 mm diameter nozzle, nominal 30 MPa pressure, 2 turns each of the valves controlling mass flow ratio, 100 mm/min traverse speed, and with chromite abrasive cutting Norite Face A.

Twenty-four passes were completed in this slot, the tests being stopped when no increase in mean depth was recorded between successive passes.

Table 6.7 : **Effect of Stand-Off Distance on Cut Depth for those Pairs of Trials within Slurry-Jet Experiment No 2 for wt : Measured Values of the Mass Flow Ratio were Comparable**

TRIAL NO	ORIFICE DIAMETER (mm)	PRESSURE (MPa)	MASS FLOW RATIO (kg/kg)	EXPOSURE	STAND-OFF (mm)	CUT DEPTH (mm)	% DIFFERENCE IN CUT DEPTH		
							RAW	ADJUSTMENT FOR MASS FLOW RATIO	NET EFFECT
16	2,4	20	0,071	1	100	87,5			
							-37	+5	-32
14	2,4	20	0,064	1	400	55,0			
7	2,4	39	0,114	1	100	169,5			
							-27	-3	-30
5	2,4	39	0,128	1	400	123,0			
2	2,8	20	0,110	1	100	112,5			
							-18	-1	-19
9	2,8	20	0,115	1	400	92,5			
3&13	2,8	39	0,068	1	100	146,6			
							-21	+8	-13
11	2,8	39	0,062	1	400	115,5			
16	2,4	20	0,071	2	100	138,8			
							-26	+5	-21
14	2,4	20	0,064	2	400	103,0			
7	2,4	39	0,114	2	100	265,0			
							-7	-3	-10
5	2,4	39	0,128	2	400	246,8			
2	2,8	20	0,110	2	100	180,5			
							-15	-1	-16
9	2,8	20	0,115	2	400	152,8			
3&13	2,8	39	0,068	2	100	205,9			
							-28	+9	-20
11	2,8	39	0,062	2	400	147,8			

OVERALL MEAN -20,2%

When the mean cut depth was plotted against pass number (see Figure 6.19) it was noted that, although the mean cut depth of pass No 24 was not greater than that of pass No 23, the trend of the last few passes was still significantly increasing. The following procedure was used to estimate a value for the ultimate cut depth. It was noted that the curve in Figure 6.19 was of type $y = A(1-e^{-Bn})$, where y = cut depth and n = pass number.

By rearranging this equation and taking natural logarithms, regression of ln(A-y) against pass number should yield a linear correlation whose slope is equal to B and whose intercept is ln(A). Since A was not known beforehand, a search was made for a value of A, from which to subtract each observed value of y, such that the fitted line had an intercept whose antilog was equal to A. That value of A was then the estimate of the ultimate cut depth, with confidence limits derived from the standard error of the intercept.

Estimated Ultimate cut depth = 986 mm with Upper 95% limit = 1 100 mm and Lower 95% limit = 873 mm

6.2.4 Slurry-Jet Experiment No 4 - stand-off distance experiment

The results from Slurry-Jet Experiment No 2 indicated that increasing the stand-off distance from 100 mm to 400 mm resulted in a loss of cut depth of about 20%. This was a much smaller reduction than had been expected in the light of earlier work with the dry abrasive equipment. More tests were done, at greatly increased stand-off distances, to investigate this matter further.

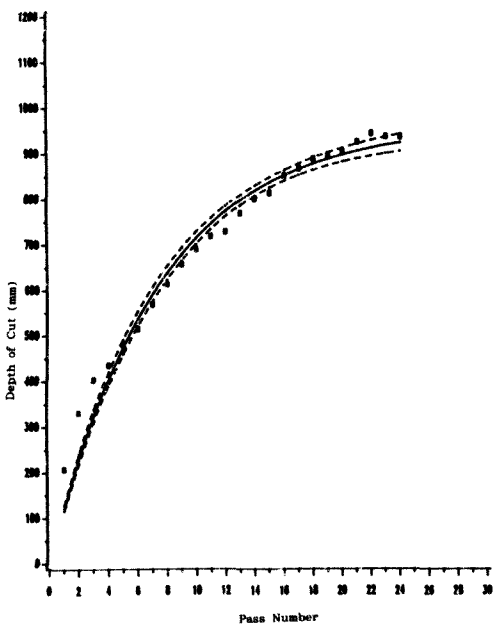


Figure 6.19 : Effect of Pass Number (Exposure) on Depth of Cut in Norite

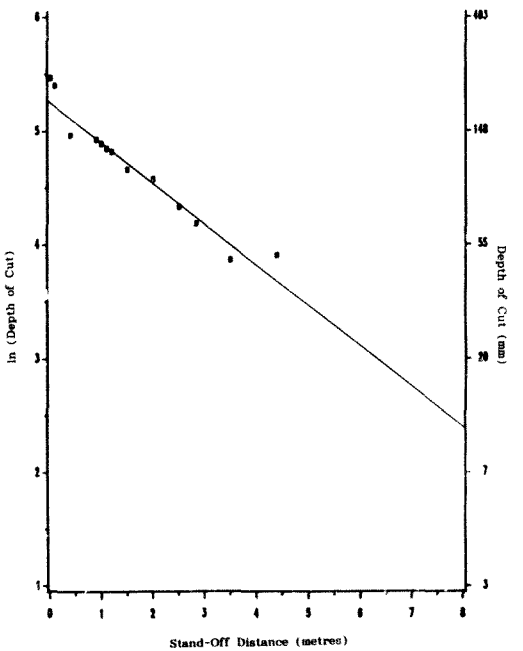


Figure 6.20 : Effect of Stand-off Distance on Depth of Cut in Norite

The greatest distance tried was 4,44 metres from the nozzle exit to the rock face. These tests were done with a 2,8 mm nozzle, 38 MPa pressure, 2 turns of the valves controlling mass flow ratio, 100 mm/min traverse speed, and with chromite abrasive cutting Norite face A.

The resulting mean depths of cut were significantly (99,9%) correlated negatively with stand-off distance and the natural logarithms of the mean depths were even better correlated with stand-off distance; consistent with a model of the form $y = Ce^{-Dx}$, where y = cut depth and x = stand-off distance. Figure 6.20 shows a plot of ln(cut depth) against stand-off distance, with the least-squares fitted line shown. The implied constants in the above model are C = 197,7 and D = 0,364 when x is measured in metres and y is given in millimetres. The inferred loss of cut depth by increasing the stand-off distance from 100 mm to 400 mm with this model is only 10,3%.

At the maximum stand-off distance tested, the mean cut depth was still 50 mm and, if the fitted model is extrapolated, it indicates that, even at 8 metres stand-off, there should be a measurable cut depth of about 10 mm.

6.2.5 Slurry-Jet Experiment No 5 - Investigation of the effect of angle of attack on depth of cut

The angle of attack investigation was conducted at fixed values of pressure, stand-off distance, abrasive mass flow ratio and nozzle orifice. The abrasive used was chromite and equal numbers of slots were cut into two different faces of a norite block. The angles which were used in the experiment were varied between -60° and +60°.

The object of the analysis was to find which angle of attack gave the biggest depth of cut. It was expected that with increasing angle, depth of cut would increase up to a maximum and then decrease. A quadratic model of the form :

$$DOC = A + B \times Angle + C \times Angle^2$$

was postulated, where

DOC is the Depth of Cut in mm,

A is the intercept value (i.e. the depth of cut at 0°),

B is the coefficient of Angle,

C is the coefficient of the square of Angle,

Angle is the value of the angle in degrees. A positive value indicates a leading angle and a negative value indicates a trailing angle.

Table 5, Appendix 4, shows the results of a regression analysis modelling the above using the SAS computer package.

The results show that the best estimate of the postulated model is:

$$DOC = 222,54 + 0,6894\ Angle - 0,0266\ Angle^2.$$

Differentiating with respect to Angle and setting the result equal to zero gives an estimate of the angle for maximum depth of cut:

$$\frac{d(DOC)}{d(Angle)} = 0,6894 - 2(0,0266)Angle$$

$$= 0 \text{ (Equate to zero)}$$

$$Angle = \frac{-0,6894}{-2(0,0266)}$$

$$= 12,96°$$

Expressed in terms of degrees, the 95% confidence limits for the angle of maximum cut depth (12,96° ± 3,3°) are 9,7° and 16,3°.

The model is found to be highly significant (>99,9%), and the values of the parameter estimates (i e. the intercept, and the coefficients of Angle and Angle²) are found to be significantly different from zero (>99,9%).

Figure 6.21 shows a plot of the data points with the model and 95% confidence limits superimposed.

Using approximate estimates of the confidence limits of the value of the angle for maximum cut depth, the angle for maximum depth of cut was not found to be significantly different between the two norite faces used.

6.2.6 Slurry-Jet Experiment No 6 - cutting with quartzite abrasive

A factorial experiment was carried out at 2 levels of 3 factors. The chosen factors and their selected levels were as follows :

Table 6.8 : Experimental Variables and Values (Slurry Cutting using Quartzite Abrasive)

	Symbol	Low Value	High Value
Standoff Distance	A	20 mm	100 mm
Mass Flow Ratio	B	0,09 kg/kg	0,15 kg/kg(nominal)
Orifice Diameter	C	2,4 mm	2,8 mm
Water pressure was kept constant at 39 MPa.			

The resulting 8 trials were confounded in 2 blocks of 4 trials each, each block of 4 trials being conducted in a different block of norite. The confounded effect was A x B x C.

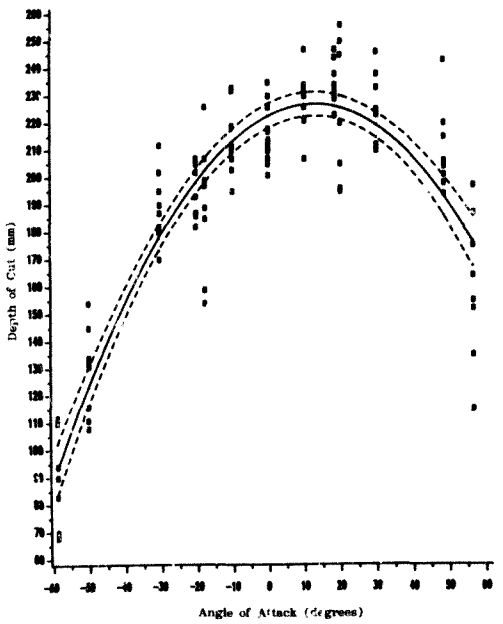


Figure 6.21 : Effect of Angle of Attack on Depth of Cut in Norite

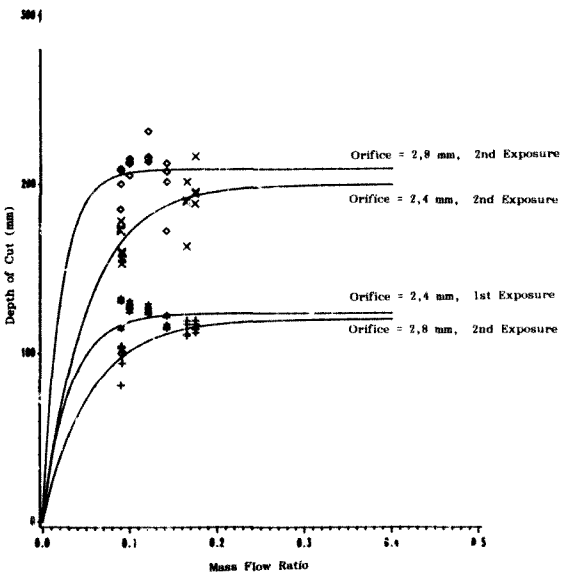


Figure 6.22 : Effect of MFR (Quartzite) on Depth of Cut in Norite

In each trial, 2 passes were executed within the slot for that trial, to determine an estimate of exposure time on depth of cut. Four measurements of the depth of cut were made within each slot after each pass.

Yates analysis of logarithms of cut depth data

Previous experience has shown that it is sensible to undertake the analysis using the logarithms of the depth of cut data.

Table 6 and Table 7, Appendix 4, show the results of the Yates analysis of the data, for the first and second exposures respectively.

The main effects and interactions that were found to be significant at least at the 95% level were found to be the same for both the first and second exposure, and are shown below:

Main effect	B	Ratio
Main effect	C	Orifice
Interaction effect	BxC	Ratio x Orifice

The effect of Stand-off (A) was not found to be significant.

Tables 8 and 9, Appendix 4, show the behaviour of two main factors (excluding Stand-off) and their interactions in terms of the appropriate mean depth of cut, for the first and second exposures respectively. Also shown is the main effect of each of the three factors in the design, and whether or not each effect is found to be significant.

Since the main effect A (Stand-off) and its interactions were not found be be significant, only its main effect is shown in the tables.

Though the effect of mass flow ratio was found to be significant, its actual effect in terms of depth of cut was 6,81 mm and 14,44 mm for the first and second exposure respectively, giving an overall effect of only 10,63 mm when averaged over both exposures.

The mean mass flow ratio for the low and high ratios respectively was 0,093 and 0,151. Therefore for an increase in mass flow ratio of 0,058 (62,4% of the low ratio value) the average depth of cut increased by only 7,2%. This suggests that low mass flow ratios may be used without losing too much depth of cut. The type of behaviour just discussed is similar to that which was found with chromite abrasive.

The effect of stand-off distance, when averaged over both exposures, was found to be a positive value of 2,13 mm in depth of cut, suggesting an increase in depth of cut with stand-off. This apparently contradictory result should be of little concern as the effect was not found to be significant even at the 80% level. Again this behaviour was exhibited by chromite abrasive.

The effect of Orifice, when averaged over both exposures, was found to be a positive value of 22,81 mm. This, expressed as a percentage change in depth of cut obtained with the low orifice setting, is an increase of 16,0% in the depth of cut.

Cut depths were plotted against mass flow ratio using different symbols for each combination of orifice and exposure, Figure 6.22. It has been seen previously for chromite abrasive (Slurry-jet Experiment No's 1 and 2) that curves of the type $y=A(1-e^{-Bx})$ generally describe this type of data well.

The best fitting curves were generated, using the SAS NLIN procedure for each orifice/ exposure combinations, and superimposed on the same graph.

It can be seen that the shape of the curves at low mass flow ratios is not well estimated as there is no data in this region, and if no previous evidence for this type of model existed then it would probably be rejected. Generally the data is only present on the graph where the curves have started to flatten out, and the effect of mass flow ratio appears to be small in the region covered by the data. The range of mass flow ratio is from approximately 0,09 to a range of ured to the chromite data which nge in mass flow ratio from approximately 0,04 to 0, of 0,40.

A comparison of the quartzite mass flow ratio model with the chromite mass flow ratio model shows that the quartzite curves generally flatten out at lower mass flow ratios (approximately 0,1 kg/kg) than the chromite curves (approximately 0,15 kg/kg).

Therefore the maximum dependency due to mass flow ratio is approached earlier for quartzite than for chromite abrasive.

This implies that the effect of mass flow ratio will only be large over a small range of low mass flow ratios for quartzite, but for chromite it will be a large effect over a bigger range.

To estimate the overall quartzite/chromite abrasive cutting ratio a standard analysis of variance was performed. This gave an overall mean figure of 73.0% and a variance between the slots of 31,25. The 95% confidence of the mean of 73% are 60,4% and 85,6%.

6.2.7 Slurry-Jet Experiment No 7 abrasive recycling and replenishing tests

Recycling of abrasives with slurry-jet cutting

The specialised procedure for carrying out the abrasive recycling tests was to fully charge the slurry cutting unit with a specified amount of abrasive. After each cut the abrasive was collected, dried and weighed and a particle size analysis conducted on a quartered sample. To facilitate the collection of abrasive, a cowling was fitted around the nozzle. Successive cuts were carried out until the specified amount of abrasive was exhausted.

The slurry recycling tests were conducted at fixed values of pressure, stand-off distance and nozzle orifice, Table 14 (Appendix 1). The abrasive mass flow ratio control valve was fixed at two turns, but the actual mass flow ratios were different for each abrasive. They were approximately 0,08, 0,19 and 0,28 for quartzite, chromite and iron grit E5 abrasives respectively. Five cycles were undertaken for each of chromite and quartzite abrasive, and eleven cycles for iron grit E5 abrasive. All the slots were cut in one norite face.

Chromite Abrasive

A linear regression modelling depth of cut against cut number showed that depth of cut significantly (>99,9%) decreased with increased recycling. However a plot of the data indicated that it had a curve in it, and a statistical test which was conducted found the curve to be highly significant (>99%). The nature of the curve was such that the decrease in depth of cut became less each time the abrasive was recycled.

It was hypothesised that with increasing recycling the depth of cut would tend towards some positive depth of cut value rather than towards zero depth of cut. As a consequence a model of the form :

$$DOC = A + Be^{(C \times Cutno)}$$

was postulated, where :

DOC is the depth of cut in mm,
A is a constant which the depth of cut approaches at high cut number (i.e. the assymptote),
B is the coefficient of the exponential term,
C is the coefficient of Cutno, which is expected to be negative,
Cutno is the cut number, or number of recycles.

The SAS NLIN procedure produced the output shown in Table 10, Appendix 4, which shows the best estimate of the model as being :

$$DOC = 51,04 + 197,69e^{-0,7719\ Cutno}$$

Figure 6.23 shows a plot of the data and the above model and the sieve analysis is contained in Table 6, Appendix 5.

As Cutno becomes large then the exponential term reduces to zero. The best estimate of the depth of cut at large cut number is therefore 51,0 mm. The computer printout shows that the 95% confidence limits are 33,5 mm and 68,6 mm.

Though the model was found to be highly significant (>99,9%), these estimates should be treated with caution as there is no data at high cut number to confirm our results, and the results are reliant on the belief of a non-zero assymptote.

Quartzite Abrasive

A linear regression model showed that depth of cut decreased significantly (>98%) with an increase in cut number. Table 11, Appendix 4, shows the computer output from the regression, giving the following model :

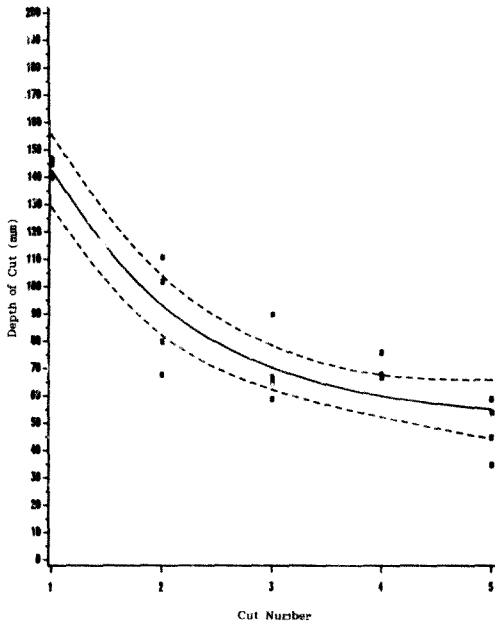


Figure 6.23 : Effect of Cut Number (number of times the abrasive is re-used) on Depth of Cut in Norite Using Chromite Abrasive

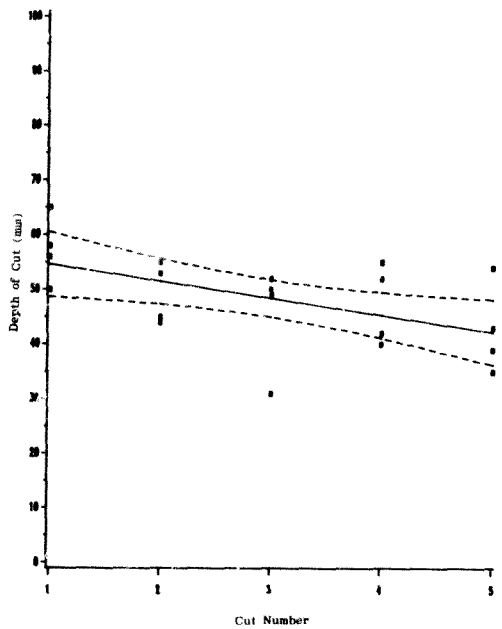


Figure 6.24 : Effect of Cut Number (number of times the abrasive is re-used) on Depth of Cut in Norite, Using Quartzite Abrasive

$$DOC = 57,70 - 3,10\ Cutno$$

A test was undertaken to detect any curve in the data but none was found. Therefore the linear regression model was accepted as being the most acceptable with the available data.

Figure 6.24 shows a plot of the data with the model and 95% confidence limits and Table 7, Appendix 5 contains the sieve analysis.

An amount of 3,1 mm depth of cut is lost per cycle, and though this value is small, it is found to be significant (>98%). The 95% confidence limits for this value are 0,7 mm and 5,5 mm loss in depth of cut per cycle.

Iron grit E5 abrasive

A linear regression model showed that depth of cut increased significantly (>99,99%) with cut number. It was hypothesised that it was unlikely that the depth of cut would increase indefinitely, but was more likely to reach a maximum at a certain cut number, and then start to decrease. Hence a quadratic model of the form:

$$DOC = A + B\ Cutno + C\ Cutno^2$$

was postulated, where A is the intercept value, and B and C are the coefficients of Cutno and $Cutno^2$ respectively.

Table 12, Appendix 4, shows the computer output from the quadratic regression, giving a best estimate of the model of :

$$DOC = 69,24 + 5,4983\ Cutno - 0,2442\ Cutno^2$$

The model was found to be highly significant (>99,99%).

A t test (one-sided) was performed on the Cutno^2 parameter estimate to test the hypothesis that the coefficient was not significantly different from zero, against the alternative that it was less than zero. The result was that the parameter estimate is significantly less than zero at the 95% level. Therefore the levelling off effect on the upward slope is found to be significant. This is shown graphically in Figure 6.25.

An estimate of the cut number where the maximum depth of cut occurs can be made by differentiating the above equation with respect to Cutno, equating to zero, and solving for Cutno :

$$\frac{d(DOC)}{d(Cutno)} = 5,4983 - (0,2442) \times 2 \times Cutno$$

$$= 0$$

$$Cutno = \frac{-5,4983}{-0,2442 \times 2}$$

$$= 11,26$$

The maximum depth of cut is therefore estimated to occur between the 11th and 12th cycle. The lower 95% confidence limit for Cutno at the maximum depth of cut is not well estimated but is thought to be between the 7th and 8th cycle. The upper 95% confidence limit is indeterminate, but is thought to be around the 30th cycle.

Part of the reason for the confidence limits for the maximum being poorly determined is that there is no data for values of Cutno greater than 11. For the maximum to be well established, data for cut numbers much greater than 11 would need to be available.

The value of the maximum depth of cut can be estimated by substituting the value of 11,26 for Cutno into the depth of cut equation, giving 100,19 mm.

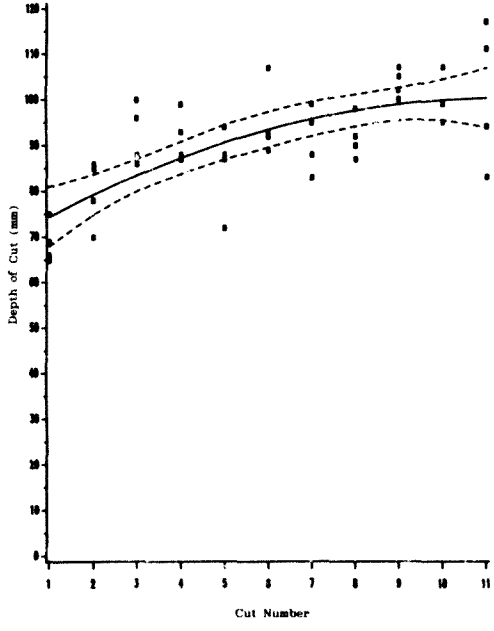


Figure 6.25 : Effect of Cut Number (number of times the abrasive is re-used) on Depth of Cut in Norite, Using Iron Based Abrasive



Figure 6.26 : BS Iron Grit Before Cutting (magnified 10 times)

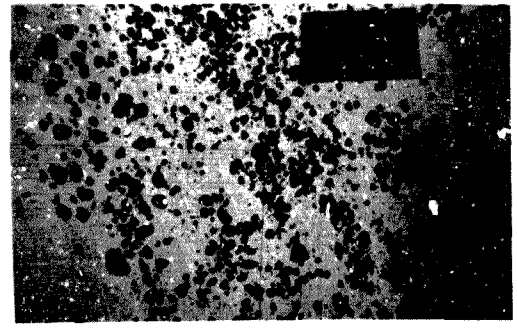


Figure 6.27 : BS Iron Grit After 11 Cuts (magnified 10 times)

Although Slurry-Jet Experiment No's 1 and 2, identified slurry abrasive jet cutting to be more efficient than dry abrasive jet cutting, it also highlighted the fact that in the slurry cutting mode, significantly more abrasive is required. Therefore, for slurry abrasive jet cutting to be practicable in the underground mining environment, a means of reducing abrasive consumption is a pre-requisite.

Although chromite and quartzite abrasives both lost depth of cut with successive recycling numbers, by far the most interesting and important result was achieved with the iron based abrasive, E5 iron grit. In the dry abrasive jet cutting mode, abrasive recycling tests indicated that abrasive consumption could be reduced, with the attendant loss in cut depth, Section 6.1.4. Based on these results and observations made during the initial slurry abrasive jet cutting investigation, it was postulated that the rate of particle degradation of an iron based abrasive should be less in the slurry cutting mode than in the dry cutting mode. This would further extend the "cutting life" of an iron based abrasive.

This hypothesis is based on the relationship between jet velocity and jet pressure. Slurry abrasive and dry abrasive cutting are carried out at jet pressures of less than 40 MPa and more than 220 MPa respectively.

It is not unreasonable to assume that particle degradation is directly related to jet velocity, the higher the jet pressure the higher the jet velocity and the greater the damage caused to the abrasive particle on impact.

The results of the E5 iron grit recycling tests verified the abovementioned hypothesis. The mass distribution by size for successive cutting cycles using recycled E5 iron grit is presented in Appendix 5, which indicates no significant difference in mean particle size between unused and "11 cycle old" abrasive. Indeed, the difference in mean particle size, discounting the first two cycles, is negligible.

When cutting in the dry abrasive recycling mode, a clear downward trend in mean particle size with successive cutting cycles was observed, Figure 6.16. It appears, therefore, that the abrasive particles suffer less damage in the slurry cutting mode.

Figure 6.25 shows that cut depth actually increases with successive cutting cycles. This result was unexpected, because firstly, this phenomenon does not occur in the dry abrasive cutting mode, and secondly, if the mean particle size remains unchanged, there is no reason to expect an increase in depth of cut.

Two theories were proposed to explain this apparent anomaly, namely, an increase in particle hardness (work hardening effect) or a change in particle shape from an angular to a more rounded configuration. Particle hardness tests were conducted in the University of the Witwatersrand's micro-indentation facility.

The average hardness of the unused and 11 cycle old abrasive samples were 777 and 801 respectively on the Vickers hardness scale.

While the difference in hardness is not particularly significant, it does support the kinematic model, **Splaine et al** [70] (developed to describe the behaviour of a dry abrasive entrained water jet, but not applicable to slurry abrasive jet cutting), which predicts an increase in cut depth with increasing particle hardness.

Of the abovementioned theories, it is more likely that a change in particle shape is responsible for the phenomenon observed while cutting in the slurry abrasive recycling mode. The most desirable properties of an abrasive, Sylaine et al [70], suggests that large particle size and high density are important characteristics. A spherical shaped abrasive, by virtue of the fact that maximum mass is contained within minimum surface area, ameliorates these characteristics. Previous dry abrasive recycling work, (Section 6.1.4), has shown that iron shot of a similar nominal size to that of iron grit gives a greater depth of cut, which supports the theory that rounded particles are more effective than angular shaped particles. Iron grit, due to the nature of its manufacturing process, contains inherent micro-fracture systems. Failure along planes of weakness probably occurs during the first few cutting cycles and the particles tend thereafter to adopt a more spherical configuration. This is illustrated for E5 iron grit in Figures 6.26 and 6.27.

It should be noted that E5 abrasive in grit form as opposed to shot form was used, because it was the only readily available iron based abrasive that could be accommodated by the prototype cutting unit. Furthermore, it does not possess the optimum mean particle size required for maximum effectiveness (it is too small). This explains why the initial depth of cut obtained with E5 iron grit is less than that obtained using chromite and quartzite.

The smaller depth of cut achieved using E5 iron grit should not detract from the implications associated with slurry abrasive recycling. It is felt that even better results would be obtained by optimising the iron abrasive particle size using it in shot as opposed to grit form.

Abrasive recycling could solve the abrasive logistic problems associated with the slurry abrasive jet cutting concept.

Replenishment of abrasive with slurry-jet cutting

The replenishment test work was carried out using iron based abrasive, E5 grit. The replenishment tests were conducted at fixed values of pressure, stand-off distance, abrasive mass flow ratio and nozzle orifice, all within one block of norite, using iron grit E5 abrasive, Table 16 (Appendix 1).

After each slot was cut and the depth of cut measured, the abrasive was recovered, dried, made up to the original start mass by adding fresh abrasive (replenished) and then the next slot was cut. After the second slot was cut, the mass of the used abrasive was halved and made up to half the original mass. This helped reduce the time required for abrasive preparation before the next slot could be cut, and so more slots could be cut in the available time.

A linear regression model showed that depth of cut increased significantly (>99,9%) with the number of replenishments. It was hypothesised that it was unlikely that the depth of cut would increase indefinitely, but was more likely to approach an assymptote as the condition of the abrasive approached a steady state.

A statistical test was conducted on the data to find whether there was any tendency for the upward sloping line to level off.

The test showed that this effect was just significant at the 95% level.

An inverse negative exponential model of the form :

$$DOC = A + B\,(1 - e^{(C \times \text{Replenishment No.})})$$

was postulated, where :

DOC is the depth of cut in mm,

A is the intercept value (i.e. the depth of cut at zero Replenishment No. (fresh abrasive)),

B is the coefficient of the inverse negative exponential term,

C is the coefficient of Replenishment No., which is expected to be negative,

The SAS NLIN procedure produced the output shown in Table 13, Appendix 4. The model was found to be highly significant (>99,99%) and the output shows that the best estimate of the model is :

$$DOC = 91,70 + 16,07(1 - e^{-0\ 3657\ \text{Replenishment No.}})$$

Figure 6.28 shows a plot of the data and the above model.

As Replenishment No. becomes large then the exponential term approaches zero, and the estimate of the assymptote is 91,70 + 16,07 = 107,77 mm

By substitution into the depth of cut equation, the model estimate of depth of cut at the 12th replenishment is 107,57 mm, which is :

$$\frac{107,57}{107,77} \times 100\% = 99,81\%$$

of the estimate of the assymptote. Therefore it is argued that at the 12th replenishment the depth of cut is approaching the assymptote.

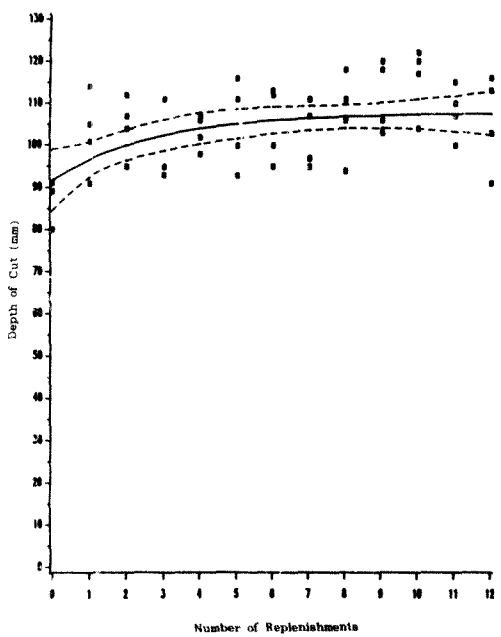


Figure 6.28 : **Effect of Abrasive Replenishment with Abrasive Recycling on Depth of Cut in Norite**

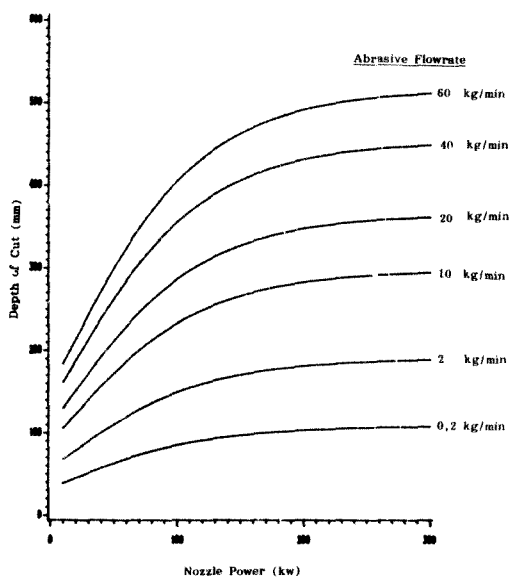


Figure 6.29 : **Depth of Cut, for Slurry Cutting, Modelled in Terms of Nozzle Power and Abrasive Flowrate**

Consequently the confidence limits for the model at the 12th replenishment can be used as the approximate confidence limits for the assymptote. Hence the approximate 95% confidence limits for the assymptote of 107,77 mm are found to be 103,3 mm and 112,3 mm.

It is inevitable that in the production orientated abrasive recycling situation, not all the abrasive would be recoverable. Consequently the abrasive supply would need to be continually replenished or "topped-up". For an average abrasive collection rate of 90% (hence an average replenishment rate of 10%), the cut depth actually increases with successive cutting cycles, Figure 6.28, although the rate of increase is not as great as that recorded during the recycling tests, Figure 6.25. This confirms the findings that with an iron grit abrasive you would get an increase in depth of cut, due to rounding of the abrasive particles and possible work hardening. In future it is likely that the abrasive used will be optimised and hence no increase in depth of cut will be observed.

Although the rate of increase in cut depth is different when operating in the abrasive recycling and replenishing modes, under steady state conditions, the maximum cut depth achieved is similar.

In fact in the abrasive replenishing mode the maximum cut depth is greater. This indicates that a 10% abrasive replenishment rate will not adversely effect cutting performance. This significant reduction in abrasive consumption alleviates one of the major disadvantages associated with the implementation of slurry abrasive jet cutting underground.

6.2.8 A depth of cut model for slurry cutting

In an attempt to create a depth of cut model for slurry cutting similar to the one produced for dry abrasive waterjet cutting (Section 6.1.1), results from the slurry investigation and previous dry abrasive work were analysed.

On examination of the combined data, a trend of increase in depth of cut with nozzle power and abrasive flowrate was observed.

From experience, the data appeared to fit curves of the form:

$$\text{Ln } Y = A(1-e^{Bx}) + C$$

Hence, the following depth of cut model was proposed:

$$\text{Ln Depth of Cut} = A\,[1-e^{BP}] + CF^{D}$$

where nozzle power P and abrasive flowrate F are input values and

A = 1,21, B = 0,02, C = 3,86 and D = 0,06 are constants.

Based on the above depth of cut model, a suite of curves, at varying abrasive flowrates, is presented in Figure 6.29 (the data points, from Appendix 1, have been omitted to help clarify the graph). The model was found to be significant at the 95% confidence level. Comparing this model with the one produced for dry abrasive cutting, Section 6.1.1, shows that for the same cutting power slurry cutting gives approximately twice the depth of cut.

The main assumption of the model is that slurry and dry abrasive data can be grouped together. This implies that slurry and dry abrasive waterjet cutting are a similar process, i.e. erosion by abrasive jet stream.

6.3 Diamond Saw Cutting

During preliminary sawing tests, a variety of wear patterns were observed, which included polishing of the segments, normal wear and diamond loss.

These wear patterns are indicative of different problems and their monitoring led to the determination of the necessary variation in cutting parameters.

Water flushing of the blade is considered a major factor in the cutting process and was constantly monitored. A water flow of approximately 10 l/min resulted in satisfactory cutting debris removal, with minimal fines remaining in the slot after a cut.

Throughout these initial trials the up-cutting mode was utilised (see Figure 6.30).

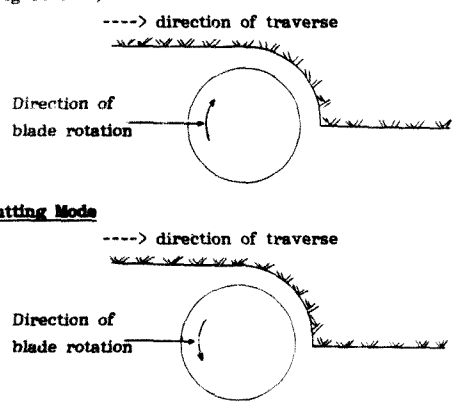


Figure 6.30: Schematic Illustration of Diamond Circular Saw Cutting Modes

Rig stability is one of the most important factors when cutting with Diamond Circular saws. It is understandable that, for good sawing conditions to prevail, the rig must be as stable as possible.

6.3.1 600 mm diameter blade

During the 600 mm diameter JKM saw blade tests, a total of 14,0 m^2 was cut. In achieving this, the mean segment height was reduced from 9,50 mm to 1,55 mm.

Because of polishing of the blade, due to the incorrect cutting parameters at stages during the blades life, the blade was also redressed three times with a resulting segment height loss of 1,15 mm (redressing the blade, wears away the matrix and exposes the diamonds).

As this would not occur when the blade is continually monitored underground, to ensure the correct cutting parameters, the blade wear rate can then be expressed as follows:

absolute wear = segment height - remaining segment height - redressing height

absolute wear = 9,50 - 1,55 - 1,15 = 6,80 mm

wear rate : $\frac{6,80}{14,0}$ = 0,486 mm/m^2 (for 600/JKM blade).

At the end of the trial period, a satisfactory cutting performance was achieved with the blade completely bedded into the face for maximum depth of cut. Due to the uneven shape of the sidewall being cut, it was impossible to achieve a constant depth of cut. Depths of over 100mm were regularly achieved, with a maximum mean value of 148mm over a single pass.

The acceptable ranges of cutting parameters were defined as follows for the maximum depth of cut:

Peripheral speed : 27,3 to 30,2 m/s.
Traverse speed : 320 to 370 mm/min

The maximum depth of cut obtainable from a blade is usually accepted as being equal to one third of its diameter. Deeper cuts were however obtained during underground trials, the maximum physically possible being 240mm for a 600mm diameter blade. Smaller than 600 mm diameter blades were not investigated due to practical considerations. These were; that a minimum depth of cut was required to intersect the vertical stress fractures ahead of the stope face and a reasonable advance per mining cycle was required, Section 7.

Based on the above results, the following cost can be derived.

The present cost for a 600/JKM blade is R 1 663 (inclusive of GST) for a blade featuring 10mm segments. Hence, the sawing cost is:

$$\frac{1663}{10} \times 0{,}486 = 81 \text{ R/m}^2 \text{ cut.}$$

New technologies make it possible to use the full segment height for cutting and this has been taken into account for the above cost calculation.

The optimum cutting parameters mentioned above do not necessarily reflect the cheapest cutting rate. Practical problems arise when the best possible parameters are not used, the reason being that the blade becomes increasingly more ineffective with shallower depths of cut.

This results in glazing or polishing of the blade segments and would require redressing before effective cutting can continue.

Redressing of a blade results in segment height loss. This is an expensive operation as 1 mm of total segment height can be assumed to cost one tenth of the total blade cost, i.e. R166, for a blade featuring 10mm segments.

6.3.2 800 mm diameter blade

The 800/JKM blade achieved 15,56 m² of cut. The blade was redressed once*. The average segment height varied as follows:

Initial height		7,22 mm
- redressing height	-	0,65 mm
- remaining height	-	1,62 mm
Segment height used	=	4,95 mm

Hence, the wear rate is $\frac{4,95}{15,56}$ = 0,32 mm/m²

* For this blade, the cost associated with dressing is R 250 per mm of segment height loss.

The cutting parameters for the 800/JKM blade were found to be:

peripheral speed:	20 to 23 m/s
traverse speed:	250 mm/min.

The 800/JKM blade obtained from Boart presently costs R2 221 (inclusive of GST).

For a blade initially supplied with 8,9mm height segments, the blade cost per m² cut can be calculated as follows:

$\frac{2\ 221}{8,9}$ x 0,32 = R 79,8 per m² cut

As with the 600mm blade, jamming problems were experienced when sawing through friable ground. Removal of the jammed blade from the slot sometimes resulted in lost or damaged segments. It was however noticed that this did not lead to a noticeable variation in blade performance. This specific feature will be investigated as the volume of the diamond impregnated segments (hence their number), is a major contributor to the total blade cost. Reducing the number of segments or their individual length, could lead to a significant cost reduction, not necessarily proportional to a loss in blade performance. Hence, an optimum cost/performance ratio could be derived.

After sawing 8,7m², it was noticed that the saw blade started to deviate from the horizontal plane, resulting in a slot curved downwards. Vertical deviation measurements were as high as 25mm over a horizontal distance of 3m.

The following reasons for this behaviour were proposed:

1. Loss of Kerf Profile - Basic cause due to:

   a) poor diamond distribution
   b) bond density differs across segment width
   c) saw blade tension loss
   d) excessive pressure on diamond segments

2. Diamond Polishing - Basic cause due to.

   a) impact resistance of diamonds too high
   b) diamond size too large
   c) diamond concentration too high
   d) insufficient work load on diamonds

3. Deviation of Saw Blade - Basic cause due to:

a) saw blade tension loss
b) saw blank thickness insufficient (especially for deep sawing operations, i.e. over 100mm depth of cut per pass)
c) glazing of segments, diamond polishing

The blade was re-tensioned and redressed, but when it was reinstalled on the saw, the same behaviour occurred. Hence, causes 1c, 2a,b,c, and d, 3a and c, can be eliminated as being the reason for the blade deviation.

It was then decided to investigate this phenomenon further by turning the blade over on the saw. This resulted in very high initial wear rate when resuming sawing operations, due to "diamond reshaping" in the other direction, the relative direction of rotation being, in fact, reversed. The blade still deviated in the slot, but now in an upwards direction.

After a while, however, this phenomenon disappeared. This suggests that this behaviour could be caused by a loss of kerf profile, possibly due to excessive pressure, coupled with an insufficient blank thickness.

Due to the irregular shape of the sidewall being cut, only occasionally was a cut depth of more than 250mm achieved (300mm being achieved once in a single pass). It is felt, however, that for deeper cuts, the blade will be more effective in terms of mm of segment wear per m^2 cut. This assumption will need to be verified during future tests. The maximum depth of cut physically achievable with the 800mm blade used is 340mm.

6.3.3 Comparison of 600 mm and 800 mm diameter blades

The differences between the two blades tested to date, as well as their performance, are summarised in Table 6.9.

Table 6.9 : Comparison of 600 mm and 800 mm Diameter Blades

DESCRIPTION		BLADE DIAMETER	
		600mm ϕ	800mm ϕ
Matrix		JKM	JKM
Number of segments		36	46
Total segment length	(mm)	1 440	1 840
Segment height	(mm)	10,00	8,90
Segment width	(mm)	4,27	5,57
Blank width	(mm)	3,44	4,48
Wear rate	(mm/m^2)	0,49	0,32
Cost	(R)	1 663	2 221
Sawing cost	(R/m^2)	81,00	79,80
Best peripheral speed	(m/s)	27-30	20-23
Best traverse speed	(mm/min.)	320-370	250
Best average depth of cut	(mm)	148	233

It can be seen from Table 6.9 that the decrease in wear rate (35%) featured by the 800mm blade, is offset by a 34% increase in blade cost. This results in sawing costs, in terms of R/m^2 cut, being only 1% lower.

The reduction in traverse and peripheral speeds can possibly be explained by the increase in segment width, resulting in a wider slot being cut. In addition, the cuts achieved with the 800mm blades were, on average, deeper than those achieved with the 600 mm blade.

Author Dunn Paul Gregory
Name of thesis The Non-explosive Mechanisation Of The South African Gold Mine Stoping Operation. 1989

PUBLISHER:
University of the Witwatersrand, Johannesburg
©2013

LEGAL NOTICES:

Copyright Notice: All materials on the University of the Witwatersrand, Johannesburg Library website are protected by South African copyright law and may not be distributed, transmitted, displayed, or otherwise published in any format, without the prior written permission of the copyright owner.

Disclaimer and Terms of Use: Provided that you maintain all copyright and other notices contained therein, you may download material (one machine readable copy and one print copy per page) for your personal and/or educational non-commercial use only.

The University of the Witwatersrand, Johannesburg, is not responsible for any errors or omissions and excludes any and all liability for any errors in or omissions from the information on the Library website.